U.S. DEPARTMENT OF COMMERCE

PB80-175037

Pilot-Scale Field Tests of High-Gradient Magnetic Filtration

Research Triangle Inst.
Research Triangle Park, NC

Prepared for

Industrial Environmental Research Lab.
Research Triangle Park, NC

Mar 80

U.S. Department of Commerce
National Technical Information Service
NTIS

PB80-175037

United States
Environmental Protection
Agency

Industrial Environmental Research
Laboratory
Research Triangle Park NC 27711

EPA-600/7-80-037
March 1980

EPA

Pilot-scale Field Tests of High-gradient Magnetic Filtration

Interagency Energy/Environment R&D Program Report

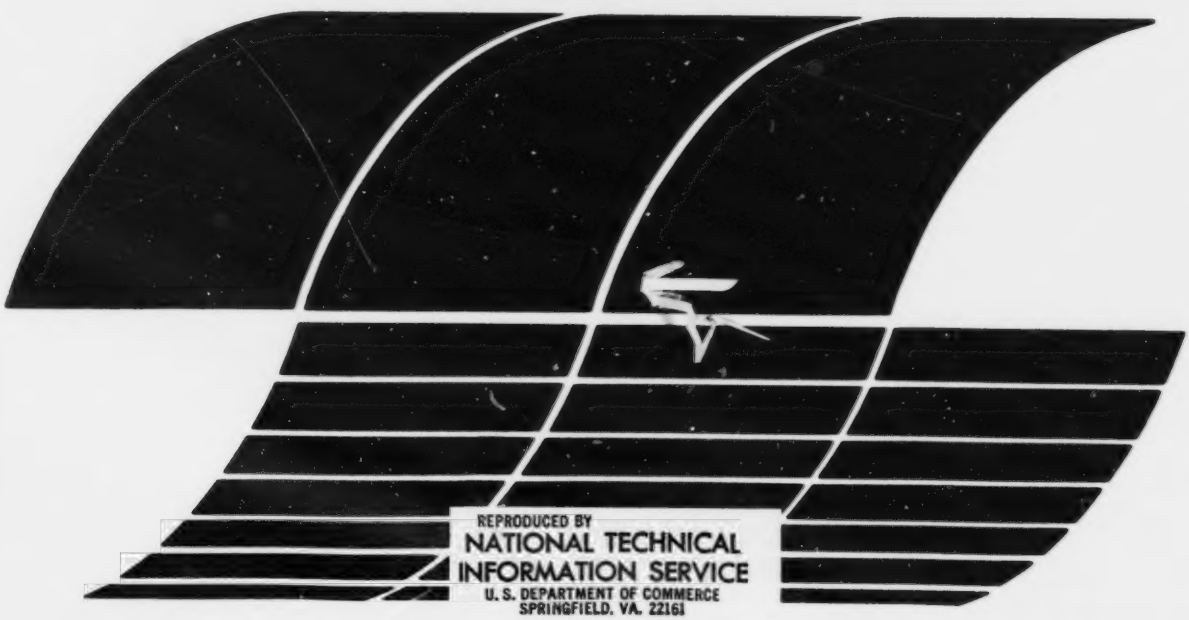

REPRODUCED BY
NATIONAL TECHNICAL
INFORMATION SERVICE
U. S. DEPARTMENT OF COMMERCE
SPRINGFIELD, VA. 22161

RESEARCH REPORTING SERIES

Research reports of the Office of Research and Development, U.S. Environmental Protection Agency, have been grouped into nine series. These nine broad categories were established to facilitate further development and application of environmental technology. Elimination of traditional grouping was consciously planned to foster technology transfer and a maximum interface in related fields. The nine series are:

1. Environmental Health Effects Research
2. Environmental Protection Technology
3. Ecological Research
4. Environmental Monitoring
5. Socioeconomic Environmental Studies
6. Scientific and Technical Assessment Reports (STAR)
7. Interagency Energy-Environment Research and Development
8. "Special" Reports
9. Miscellaneous Reports

This report has been assigned to the INTERAGENCY ENERGY-ENVIRONMENT RESEARCH AND DEVELOPMENT series. Reports in this series result from the effort funded under the 17-agency Federal Energy/Environment Research and Development Program. These studies relate to EPA's mission to protect the public health and welfare from adverse effects of pollutants associated with energy systems. The goal of the Program is to assure the rapid development of domestic energy supplies in an environmentally-compatible manner by providing the necessary environmental data and control technology. Investigations include analyses of the transport of energy-related pollutants and their health and ecological effects; assessments of, and development of, control technologies for energy systems; and integrated assessments of a wide range of energy-related environmental issues.

EPA REVIEW NOTICE

This report has been reviewed by the participating Federal Agencies, and approved for publication. Approval does not signify that the contents necessarily reflect the views and policies of the Government, nor does mention of trade names or commercial products constitute endorsement or recommendation for use.

This document is available to the public through the National Technical Information Service, Springfield, Virginia 22161.

TECHNICAL REPORT DATA
(Please read Instructions on the reverse before completing)

1. REPORT NO. EPA-600/7-80-037	2.
3. RECIPIENT'S ACCESSION NO. PB80-175037	
4. TITLE AND SUBTITLE Pilot-scale Field Tests of High-gradient Magnetic Filtration	5. REPORT DATE March 1980
	6. PERFORMING ORGANIZATION CODE
7. AUTHOR(S) Charles H. Gooding	8. PERFORMING ORGANIZATION REPORT NO.
9. PERFORMING ORGANIZATION NAME AND ADDRESS Research Triangle Institute, P.O. Box 12194, Research Triangle Park, North Carolina 27709	10. PROGRAM ELEMENT NO. EHE624A
	11. CONTRACT/GRANT NO. 68-02-2650
12. SPONSORING AGENCY NAME AND ADDRESS EPA, Office of Research and Development, Industrial Environmental Research Laboratory, Research Triangle Park, NC 27711	13. TYPE OF REPORT AND PERIOD COVERED Final; 9/77 - 12/79
	14. SPONSORING AGENCY CODE EPA/600/13

15. SUPPLEMENTARY NOTES IERL-RTP project officer is Dennis C. Drehmel, Mail Drop 61, 919/541-2925.

16. ABSTRACT The report gives results of using a 5100 cu m/hr mobile pilot plant to evaluate the effectiveness and economics of applying high-gradient magnetic filtration (HGMF) to particulate emission control. A 4-1/2 month test program was conducted at a Pennsylvania sintering plant to characterize the performance of the pilot plant and to demonstrate its practicality under long-term operation. The pilot plant collected approximately 90% of the iron-bearing particulate under practical operating conditions but achieved lower overall collection because the windbox gas contained an unexpectedly high concentration of fine alkali-chloride aerosol. To collect the nonmagnetic aerosol, a finer filter had to be used under conditions that were conducive to plugging. Under the practical conditions, the pilot plant operated over 450 hours without significant problems. Analysis of the results indicates that high-efficiency collection can be achieved economically if HGMF is applied to steel industry dusts that are more homogeneous and more strongly magnetic than the tested sinter dust. The report describes laboratory pilot-plant work that demonstrated collection efficiencies greater than 99% with basic oxygen furnace and electric arc furnace dusts. The development of a filter cleaning system and the design and construction of the pilot plant are discussed. Experimental data are reported.

17. KEY WORDS AND DOCUMENT ANALYSIS

a. DESCRIPTORS		b. IDENTIFIERS/OPEN ENDED TERMS	c. COSATI Field/Group	
Pollution	Aerosols	Pollution Control	13B	
Filtration	Sintering Furnaces	Stationary Sources	07D	13A
Magnetic Properties	Iron and Steel Industry	High-gradient Magnetic Filtration	20C	
Magnetic Separators			13I	11F
Testing		Particulate	14B	
Dust			11G	

18. DISTRIBUTION STATEMENT Release to Public	19. SECURITY CLASS *(This Report)* Unclassified	21. NO. OF PAGES
	20. SECURITY CLASS *(This page)* Unclassified	22. PRICE

EPA Form 2220-1 (9-73)

EPA-600/7-80-037

March 1980

Pilot-scale Field Tests of High-gradient Magnetic Filtration

by

Charles H. Gooding

Research Triangle Institute
P.O. Box 12194
Research Triangle Park, North Carolina 27709

Contract No. 68-02-2650
Program Element No. EHE624A

EPA Project Officer: Dennis C. Drehmel

Industrial Environmental Research Laboratory
Office of Environmental Engineering and Technology
Research Triangle Park, NC 27711

Prepared for

U.S. ENVIRONMENTAL PROTECTION AGENCY
Office of Research and Development
Washington, DC 20460

ABSTRACT

A 5100 m^3/hr mobile pilot plant was designed and built to evaluate the effectiveness and economics of applying high-gradient magnetic filtration (HGMF) to particulate emission control. A 4 1/2-month test program was conducted at a Pennsylvania sintering plant to characterize the performance of the pilot plant and to demonstrate its practicality under long-term operation.

The pilot plant collected approximately 90 percent of the iron-bearing particulate under practical operating conditions, but the overall mass efficiency was lower than expected because the windbox gas contained a high concentration of a fine alkali-chloride aerosol.* To collect the non-magnetic aerosol, a finer filter had to be used under conditions that were conducive to plugging. Under the practical conditions the pilot plant was operated for over 450 hours with no significant problems. Analysis of the results indicates that high-efficiency collection can be achieved economically if HGMF is applied to steel industry dusts that are more homogeneous and more strongly magnetic than the sinter dust tested.

The report describes laboratory pilot-plant work that demonstrated collection efficiencies of greater than 99 percent with basic oxygen furnace and electric arc furnace dusts. The development of a filter cleaning system and the design and construction of the mobile pilot plant are discussed. The field start-up, performance characterization, and long-term operation are discussed in detail, and experimental data are reported. The final section presents an analysis of the field results and an economic evaluation of the HGMF process. The development of a mathematical model in conjunction with the laboratory pilot plant work is included as an Appendix.

---

*It should be noted that the slipstream for the HGMF pilot plant was drawn from the plant duct upstream of the plants' air pollution control devices. No testing was conducted on the plant stack; hence the data contained in this report should not be construed to contain any implications about the actual plant emissions or plant compliance with relevant emission standards at the time of the test program.

TABLE OF CONTENTS

		Page
Abstract		iii
List of Figures		vi
List of Tables		ix
Acknowledgments		x
Section 1.	Summary	1
Section 2.	Conclusions	3
Section 3.	Recommendations	4
Section 4.	Background	5
	Basic Concept of the HGMF Process	5
	Process Development and Applications	8
	Potential Applications to Particulate Emission Control	8
Section 5.	Preliminary Design and Development	12
	Laboratory Pilot Testing	12
	Mathematical Modeling of Preliminary Results	18
	Site Selection for Field Tests	27
	Development of Filter Cleaning System	30
Section 6.	Detailed Design and Construction of the Mobile Pilot Plant	34
Section 7.	Field Operations	42
	Description of the Sinter Plant	42
	Installation and Startup of the Pilot Plant	44
	Temperature Control	44
	Blower Noise	45
	Filter Construction and Cleaning	45
	Magnet Operation	46
	Flow Measurement and Control	46
	Final Site Setup	47
	Performance Characterization	49
	Long-term Testing	62
	Additional Tests with Coarse Grade Steel Wool	70

TABLE OF CONTENTS (continue)

		Page
Section 8.	Discussion and Application of Results.	75
	Chemical and Magnetic Analysis of Sinter Dust.	75
	Transient Emissions During Filter Cleaning	83
	Projected Applications: Economics and Effectiveness .	85
	Discussion of Potential Candidates for Application.	86
	Full-Scale Design Considerations.	86
	Efficiency and Economic Calculations.	90
Section 9.	References	98
Appendix A	Tabulation of Experimental Conditions and Results from Laboratory Pilot Plant Tests.	102
Appendix B.	Mathematical Model of HGMF	114

LIST OF FIGURES

Page

Figure 1. Conceptual illustration of a high gradient magnetic collector. 6

Figure 2. Schematic representation of a high gradient magnetic filter 7

Figure 3. Schematic diagram of the HGMF laboratory pilot plant . 13

Figure 4. Magnetization curves of the two industrial dusts used in the preliminary experiments 14

Figure 5. Effect of filter loading on BOF dust collection efficiency and filter pressure drop. 16

Figure 6. Effect of filter loading on EAF dust collection efficiency and filter pressure drop. 17

Figure 7. Replicate data from lab pilot plant experiments showing 95 percent confidence intervals on the true mean efficiency and corrected model predictions. . . . 19

Figure 8. Collection of BOF and EAF dusts under identical operating conditions 21

Figure 9. Effect of applied magnetic field on collection efficiency 22

Figure 10. Effect of filter packing density on collection efficiency 23

Figure 11. Effect of filter depth on collection efficiency. . . . 24

Figure 12. Effect of superficial gas velocity on collection efficiency 25

Figure 13. Results of sinter dust tests conducted in the lab pilot plant. 29

Figure 14. Comparison of forces exerted on collected particles. . 31

Figure 15. Flow schematic of HGMF mobile pilot plant. 35

Figure 16. View of the pilot plant from the rear interior of the trailer. 37

LIST OF FIGURES (continue)

Page

Figure 17. View of the pilot plant from the front interior of the trailer. 38

Figure 18. Flow control diagram 40

Figure 19. Layout of the sinter strand and the HGMF pilot plant . 43

Figure 20. HGMF mobile pilot plant setup at the sintering plant . 48

Figure 21. Side entrance of mobile pilot plant. 48

Figure 22. Clean side piping and stack. 50

Figure 23. View from rear of pilot plant. 50

Figure 24. Size distributions from test nos. 08042, 08041, 08031, and 08062 53

Figure 25. Size distributions from test nos. 08051, 08061, 08082, and 08183. 54

Figure 26. Size distributions from test nos. 08182, 08181, 08231, and 08222. 55

Figure 27. Size distributions from test nos. 08291, 08282, 08281, and 08292. 56

Figure 28. Size distributions from test nos. 08301, 09201, 08302, and 09013. 57

Figure 29. Size distributions from test nos. 09012, 09031, 09032, and 09033. 58

Figure 30. Fractional efficiency curves from tests conducted on filter nos. 1 and 3. 59

Figure 31. Fractional efficiency curves from tests conducted on filter nos. 2 and 4. 60

Figure 32. Outlet particle size distributions obtained during total mass sampling. 69

Figure 33. Cumulative size distributions for test nos. 10231 through 10271. 72

Figure 34. Fractional collection efficiency curves for test nos. 10231 through 10271. 73

LIST OF FIGURES (continue)

Page

Figure 35. Magnetic analysis of dust samples from HGMF pilot plant tests. 78

Figure 36. Transient emission levels during a single cycle of operation. 84

Figure 37. Schematic layout of the SALA-HGMS® 480 Series Carousel. 89

Figure 38. Predicted HGMF collection efficiency for three dust categories at typical operating conditions 93

Figure 39. Pressure drop-flow correlation for coarse steel wool . 95

Figure B1. Illustration of particle capture by a single wire. . . 115

Figure B2. Geometric basis of HGMF trajectory model 116

Figure B3. Contour map of collision radius as a function of W and K (A=1, G=0) 123

Figure B4. Comparison of experimental data to the uncorrected theoretical prediction and to two corrected models . . 125

Figure B5. Illustration of the particle bounce reentrainment model. 126

LIST OF TABLES

		Page
Table 1.	Reports of application-oriented experimental investigations of HGMF.	9
Table 2.	Expected characteristics of uncontrolled gas streams from several processes.	10
Table 3.	Results of performance characterization with medium grade steel wool.	52
Table 4.	Operating log of the long-term test period.	63
Table 5.	Efficiency testing during long-term operation	68
Table 6.	Additional testing with coarse grade steel wool (filter #8)	71
Table 7.	Chemical analysis of dust samples from HGMF pilot plant tests	76
Table 8.	Component mass balances based on chemical analysis. . .	80
Table 9.	Illustration of filter loading times.	87
Table 10.	HGMF operating parameters used for economic calculations	92
Table 11.	Pressure drop characterization of coarse steel wool . .	94
Table A1.	Ranges of experimental parameters	102
Table A2.	Experimental data on clean filter pressure drop	103
Table A3.	Conditions and results of laboratory pilot-plant experiments	106
Table B1.	Correlation of reentrainment correction	129

ACKNOWLEDGMENTS

The author wishes to acknowledge the assistance and support of the following individuals in various segments of this work.

Dr. Dennis C. Drehmel, EPA Project Officer, provided overall direction and many helpful suggestions during the course of the project.

The field work described in this report was conducted at U.S. Steel Corporation's Saxonburg Sintering Plant near Butler, Pennsylvania. The author would like to express his sincere appreciation to U.S. Steel for their participation in the project. In particular, Mr. John Turnage of the Research Laboratory was most helpful in planning and coordinating the work, and Mr. George Frye, Superintendent of the Saxonburg Plant, provided invaluable assistance and support throughout the field program.

Dr. Herbert Hacker, Jr. of Duke University conducted the experimental measurements of particle magnetization.

From RTI, Carlos Pareja assisted in the latter stages of the design and in the construction of the mobile pilot plant and served as field engineer during the tests at the sinter plant. Douglas VanOsdell was particularly helpful in several portions of the engineering design and construction of the pilot plant and in the field startup. Technicians John Sauerbier and Daryl Smith were key participants in the construction, field operation and testing of the pilot plant. Several speciality items for the sampling trains were fabricated by RTI's master machinist, Fred Schwarz. David Carter assisted with the EPA Method 5 testing, and Peter Grohse coordinated the chemical analysis of sinter dust samples.

SECTION 1

SUMMARY

High-gradient magnetic filtration (HGMF) has been gaining recognition as an effective and versatile separation technique since its commercialization in the clay industry 10 years ago. The strength of the process lies in its ability to separate fine, weakly magnetic particles from fluids at flow rates over 100 times the flow rates achievable in other filtration processes. An experimental project conducted by RTI from 1975 to 1977 under funding from the U.S. Environmental Protection Agency established that HGMF could be applied to particle-gas separations of practical interest to air pollution control. Several sources of submicron, magnetic particles were identified among iron and steel industry processes, and high-efficiency filtration of two of the dusts was demonstrated in a laboratory pilot plant. The objective of the subsequent work described in this report was to demonstrate the practical operation of an HGMF pilot plant in a field application.

To begin the work, additional tests were run in the laboratory pilot plant with the basic oxygen furnace (BOF) and electric arc furnace (EAF) dusts used in the original tests. Sufficient data were obtained to verify the achievement of high collection efficiencies and to identify the effects of important operating variables. A mathematical model was developed to correlate the experimental results and to aid in the design of the field pilot plant.

A presentation was made to the American Iron and Steel Institute's Technical Committee on Environmental Quality Control in December, 1977, describing the prior work with HGMF and the objectives of the field program. Following discussions with several steel companies, an agreement was reached to test the pilot plant at a Pennsylvania sintering plant. A limited series of tests was run in the laboratory pilot plant with dust obtained from the sintering plant to obtain final data for the design of the magnetic filter and for the design of a practical filter cleaning system.

Over the next 12 months the design details were implemented, and the pilot plant was constructed. The cyclic system, incorporating two parallel filters, each with a flow capacity of 5100 m^3/hr (3000 cfm), was housed in a mobile trailer. A pulsed air filter-cleaning system was developed, and valving was installed to allow continuous filtration as each filter was cleaned in turn. Instrumentation and test equipment were provided to monitor the operation and efficiency of the process.

In June, 1979 the pilot plant was transported to the sinter plant and connected to draw a slipstream from the windbox exhaust of the #1 sinter strand. After the startup and debugging procedures were completed, a performance characterization was conducted to determine the effects of applied magnetic field, filter density and depth, and gas throughput on fractional collection efficiency. Optimal operating conditions were identified from the results of the performance characterization, and a 500-hour operational test was initiated. During the long-term testing, the pilot plant was shut down only to correct malfunctions, to accommodate sinter plant interruptions, or to change operating conditions. Total mass and fractional efficiency tests were conducted, and periodic opacity observations were made. Samples of dust entering the pilot plant, exiting the pilot plant, and collected by the pilot plant were obtained for magnetic and chemical analyses.

The results of the field tests were used to make a technical and economic assessment of the application of HGMF to sinter plants as well as to other iron and steel industry processes. The experience gained from the field operations demonstrates the practicality of applying HGMF to particulate emission control while providing the basis for several recommended design improvements.

The following sections of this report state conclusions and recommendations drawn from the results of the field tests and the earlier laboratory work. A background description of the HGMF process development is then presented, followed by details of the laboratory pilot plant work, the mathematical model development, the design, construction, and field operation of the pilot plant, and an analysis of the field-test results with respect to potential applications of HGMF.

SECTION 2

CONCLUSIONS

The following conclusions were drawn from field operation of the HGMF pilot plant and from the laboratory work that preceded the design of the mobile unit.

(1) High gradient magnetic filtration can be applied under practical operating conditions to collect fine magnetic dust particles with high efficiency.

(2) For HGMF to be applied successfully to an industrial source, non-magnetic dust components that appear in significant concentrations must be physically or chemically bound to ferrous particles. Emissions from most basic oxygen furnaces, electric arc furnaces, and scarfing operations are believed to meet this criterion. More complete dust characterization data are needed to determine whether blast furnaces and some sinter plants might be suitable for HGMF application.

(3) A generalized economic analysis indicates that HGMF can be economically competitive with conventional particulate control methods in terms of primary equipment cost and energy requirements. The high gas velocities demonstrated in the experimental work indicate much smaller space requirements than either electrostatic precipitators or baghouses, which could lead to a substantial reduction in total installed equipment costs. Since HGMF collects the dust in a dry form, it avoids the problems of sludge dewatering and liquid waste treatment that a scrubber entails.

SECTION 3

RECOMMENDATIONS

The development of high gradient magnetic filtration as an alternate method of particulate emission control should be continued. To maximize the potential for a successful field demonstration on an appropriate industrial source, the following points are recommended.

(1) The pilot plant should be converted from cyclic to continuous operation so that it can be applied to continuous industrial process that produce high dust concentrations. For lower concentrations or intermittent industrial processes the results will still be applicable to the cyclic approach if that proves to be more suitable.

(2) The filter cleaning system should be modified to eliminate the emission puffs associated with the cleaning air pulse.

(3) More complete and reliable information should be gathered on operating and dust characteristics of the iron and steel industry processes that are potential candidates for HGMF application. Before the next field test, representative dust samples should be collected at the proposed point of application and analyzed to provide data on dust concentration, size distribution, composition, and magnetization.

SECTION 4

BACKGROUND

BASIC CONCEPT OF THE HGMF PROCESS

The basis of high-gradient magnetic filtration is the interaction of a small paramagnetic or ferrimagnetic particle with a ferromagnetic wire in the presence of a strong background magnetic field. The phenomenon is illustrated in Figure 1, with the field applied perpendicular to the axis of a cylindrical wire. The applied field magnetizes the wire and induces a magnetic dipole in the particle. The convergence of the applied field near the wire produces a region of highly nonuniform field intensity that attracts the dipolar particle toward the wire, much like a bar magnet attracts iron filings toward its poles. Depending on the physical characteristics of the system, inertial, viscous, and gravitational forces may also act on the particle in the vicinity of the wire.

In its simplest form, the high gradient magnetic filter consists of a canister loosely packed with a fibrous, ferromagnetic material such as AISI Type 430 stainless steel wool (Figure 2). The canister is placed in a magnetic field that is customarily generated by a solenoid, and the resulting attractive magnetic force provides high-efficiency filtration of particles as the fluid passes through the canister. Because of the high porosity of the filter, particle capture is actually a particle-wire phenomenon as opposed to the cake collection mechanism that normally dominates conventional fabric filters. Filtration may be continued until the pressure drop through the canister becomes prohibitively high due to the decreased size of the interstitial flow paths or until heavy loading on the wires decreases the efficiency of particle capture. To regenerate the filter, the magnetic field is removed and the canister is backflushed with clean fluid. Continuous filtration may be achieved by using a system of several parallel modules, with each module providing filtration for a predetermined time interval. When the flow is diverted from a module, the magnetic field of the loaded module is deenergized, the filter is cleaned, the filter is reenergized, and the module is ready for reuse. An alternative scheme that results in zero downtime of the magnet is to construct the magnet and canister so that the loaded filter

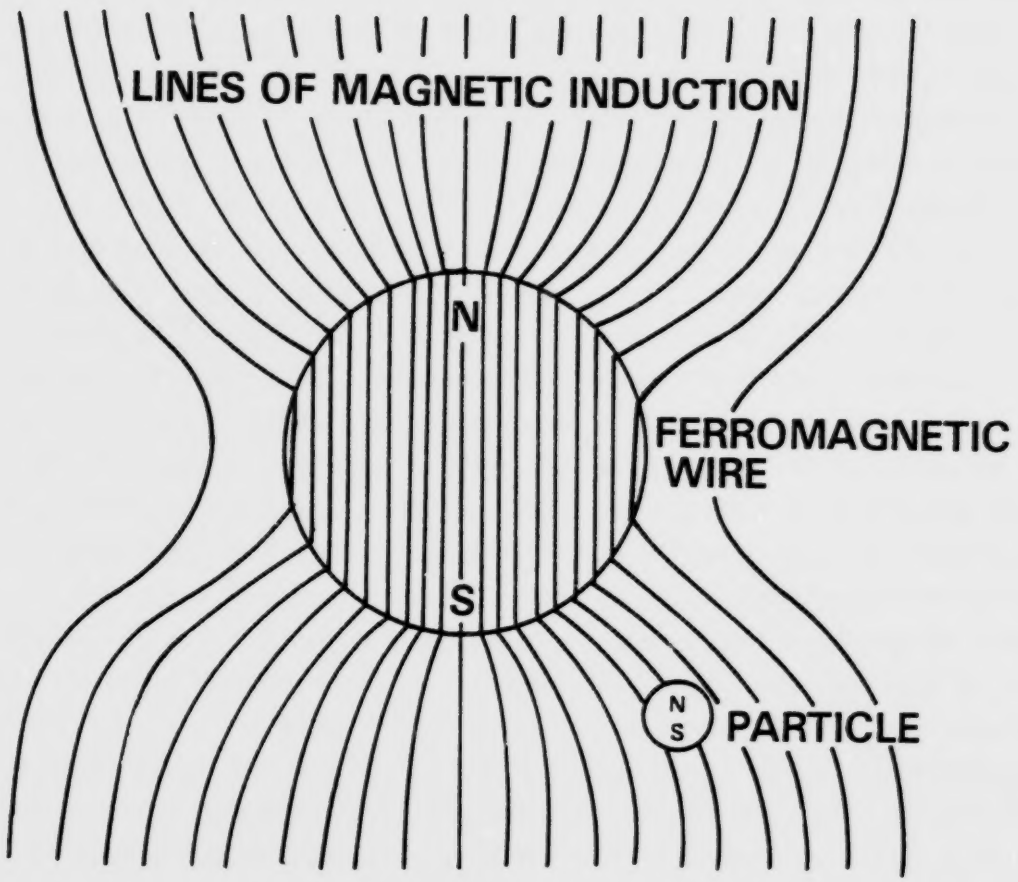

Figure 1. Conceptual illustration of a high gradient magnetic collector.

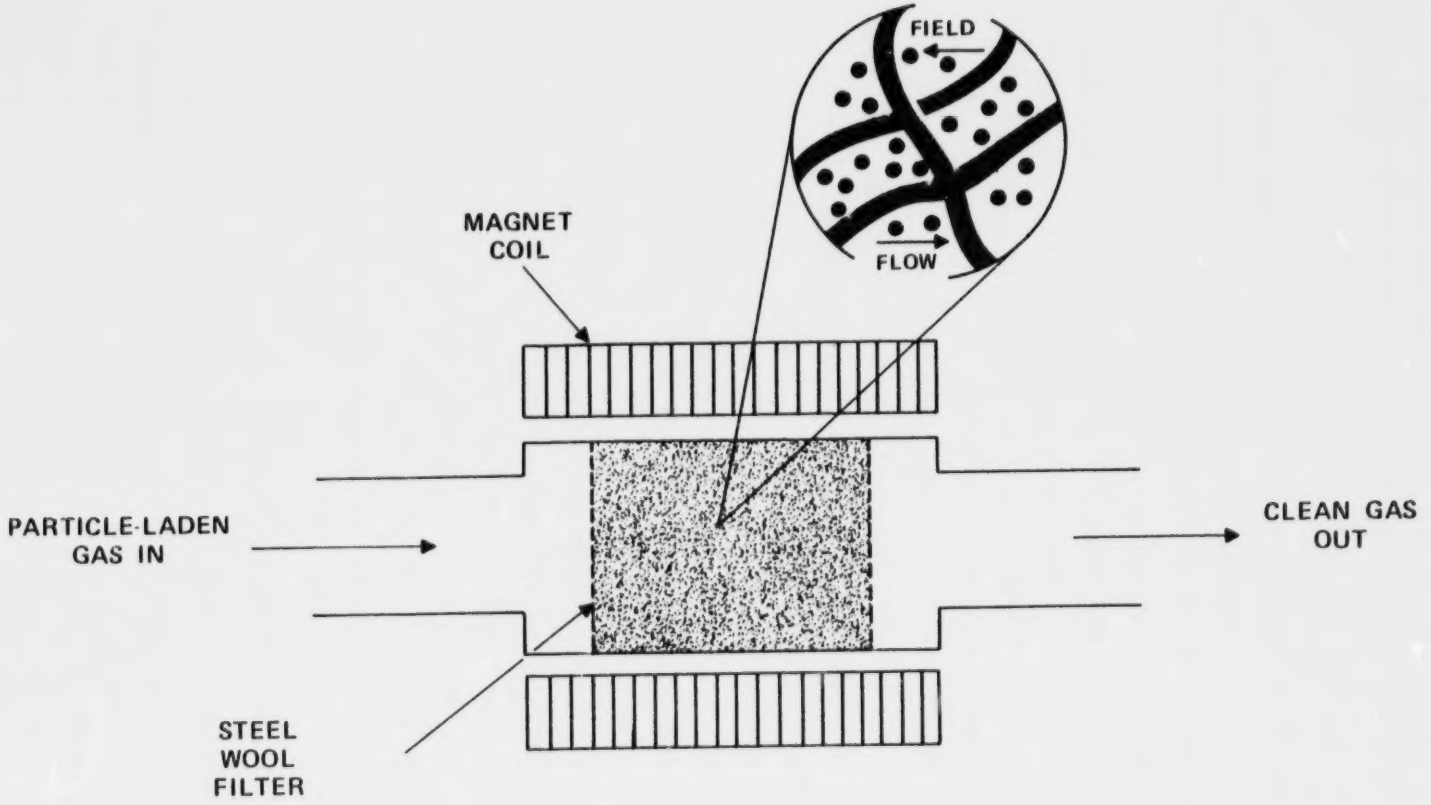

Figure 2. Schematic representation of a high gradient magnetic filter.

can be continuously or intermittently removed from the magnetized region and replaced by a clean filter without interrupting the filtration process. Both cyclic and continuous systems are commercially available.

PROCESS DEVELOPMENT AND APPLICATIONS

With the exception of the EPA-sponsored development that began in 1975, nearly all of the experimental work in high-gradient magnetics has involved the separation of different types of particles in a slurry according to their magnetic susceptibility. Oberteuffer (1974), Kolm, et al. (1975), Oder (1976), and Iannicelli (1976) have published complementary reviews that provide an excellent introduction to the process and its chronological development. The most extensive commercial development has occurred within the last decade in the clay industry where HGMF is used to remove fine, paramagnetic color-bodies from kaolin. Oder (1976) estimated three years ago that installed commercial units already had the capability to process 75 percent of the world production of coating-quality kaolin.

The successful demonstration of HGMF in the clay industry catalyzed experimental investigations of the new separation process for many other applications. Well over 100 patents, reports, and technical papers have been published in the last decade, describing projects conducted throughout the world. Table 1 lists a representative sample of published references in the reported areas of experimental work. In August 1978, the Engineering Foundation sponsored an International Conference on Industrial Applications of Magnetic Separation that was dominated by papers and discussions of HGMF, including reports of emerging commercial applications for boiler water polishing in West Germany and steel mill wastewater treatment in Japan (Liu, 1979).

POTENTIAL APPLICATIONS TO PARTICULATE EMISSION CONTROL

Although most of the experimental investigations reported in the open literature involve the separation of particles from liquid streams, HGMF can be applied successfully in gas streams as well. Table 2 lists waste gas characteristics of several processes that are widely used in the iron and steel and ferroalloy industries. In the production of iron,

Table 1. Reports of application-oriented experimental investigations of HGMF.

Application	References
Mineral beneficiation-general	Kelland, 1973 Murray, 1976
Taconite beneficiation	Kelland and Maxwell, 1975
Coal deashing and desulfurization	Ergun and Bean, 1968 Trindade and Kolm, 1973 Vives, et al., 1976 Maxwell, et al., 1976 Maxwell, et al., 1977 Liu, et al., 1978 Maxwell and Kelland, 1978
Wastewater treatment-general	Mitchell, et al., 1975 Petrakis and Ahner, 1978
Steel mill wastewater treatment	Oberteuffer, et al., 1975 Harland, et al., 1976
Municipal wastewater treatment	deLatour and Kolm, 1975 Yadidia, et al., 1977
Blood component separation	Melville, et al., 1975
Catalyst recovery	Whitesides, et al., 1976

sintering is used to combine iron ore fines with flux in the form of limestone or dolomite and with other iron-bearing materials such as flue dust, mill scale, turnings, and borings, to form a blast furnace feed material of appropriate composition and size. The blast furnace then reduces iron ore and pellets as well as the sinter. The iron is refined to steels of various composition in basic oxygen, electric arc, or open hearth furnaces. Scarfing is a surface improvement process in which a thin layer of the hot steel slab or bloom is volatilized by blasting it with oxygen. In each of these processes, the combustion air or oxygen entrains a substantial concentration of iron-bearing dust particles that would be emitted to the atmosphere if the emissions were not properly controlled. Cyclones, baghouses, wet scrubbers and electrostatic precipitators are currently employed to control the emissions with varying degrees of success.

Table 2. Expected characteristics of uncontrolled gas streams from several processes.*

Process	Dust Concentration g/m^3	Mass Median Diameter μm	Iron Composition % Total Fe	Noteworthy Gas Characteristics
Sinter Machine				
Windbox	1-2	10	25-50	5-15% H_2O, Hydrocarbons, Fluorides, SO_x, 120-180°C
Discharge End	5-12	10	25-50	120-180°C
Blast Furnace	10-25	20	35-50	20-40 % CO, 2-6% H_2, 200-300°C
Basic Oxygen Furnace				
Open System	10-25	1	55-70	250-300°C
Closed System	40-70	2	55-70	75% CO, 250-300°C
Electric Arc Furnace	0.2-7	1	15-40	40-120°C
Open Hearth Furnace	4-7	5	55-70	7-15% H_2O, 250-350°C
Scarfing Machine	0.5-1	0.5	50-70	H_2O Saturated, 50-60°C

*Compiled from numerous references including Hardison and Greathouse (1972), Dulaney (1974), Steiner (1976), Jaasund (1977), and Whitehead (1977).

With current magnet technology the capital costs and power requirements of large solenoids make HGMF potentially competitive with other particulate control methods. Since the filtration process is enhanced by magnetic forces, the void volume of the collection matrix can be much larger than in a conventional filter, allowing very high gas velocities at relatively low pressure drops. This combination translates into a potential reduction in energy requirements compared to conventional particulate control techniques, even though production of the magnetic field requires some energy. High operating velocities help to reduce both the capital costs and space requirements of the equipment. Furthermore, if air is used as the backflush fluid, the process can be applied completely dry to avoid the water pollution problems associated with some scrubber installations. Magnetic stainless steels of the 400 series are compatible with both high temperature and corrosive enviroments and the absence of any sparking mechanism in the collection process should allow its application in combustible gas streams. In brief, all of the processes listed in Table 2 should be considered as potential candidates for HGMF fine particle control subject to more complete evaluation based on experimental testing.

SECTION 5

PRELIMINARY DESIGN AND DEVELOPMENT

LABORATORY PILOT TESTING

In work conducted by Research Triangle Institute for EPA from 1975 to 1977, a laboratory pilot plant was constructed and operated to obtain data sufficient to demonstrate that HGMF could be used to remove fine magnetic dusts from an air stream with high collection efficiency. The design and operating procedures of the lab pilot plant are described in detail in a prior report (Gooding, et al., 1977). The same pilot plant was used in this project to obtain verification data needed to design the mobile pilot plant. This preliminary work is described in the following paragraphs.

A schematic of the lab pilot plant is shown in Figure 3. The 30-cm diameter filter was operated with flow rates up to 3100 m^3/hr from a slipstream off an existing wind tunnel. Two types of industrial dust were obtained from a major steel corporation for use in the experiments. Most of the tests were run with dust collected from the hoppers of an electrostatic precipitator that controls emissions from a basic oxygen furnace (BOF dust). To provide further evaluation of the effects of dust characteristics, a limited number of tests was run with dust obtained from the hoppers of a roof-system baghouse that controls emissions from an electric arc furnace shop (EAF dust). Experimentally determined magnetization curves for the two dusts are shown in Figure 4. Atomic absorption measurements indicated the iron contents to be 76 percent and 41 percent in the BOF and EAF dust, respectively. Both of these are slightly above the general ranges reported in Table 2.

The dusts were dispersed in a room-temperature air stream by means of a fluidized-bed dust generator. Since the concentration of dust in the slipstream was normally only 50 to 100 mg/Nm^3, the filter could be operated without cleaning for the two hours required for sampling. Between tests the filter was either replaced or cleaned in situ by backflushing with pressurized air routed to a set of perforated rings mounted in the filter canister. A vibrator attached to the filter assembly was also operated concurrently with the backflushing operation to assist the cleaning.

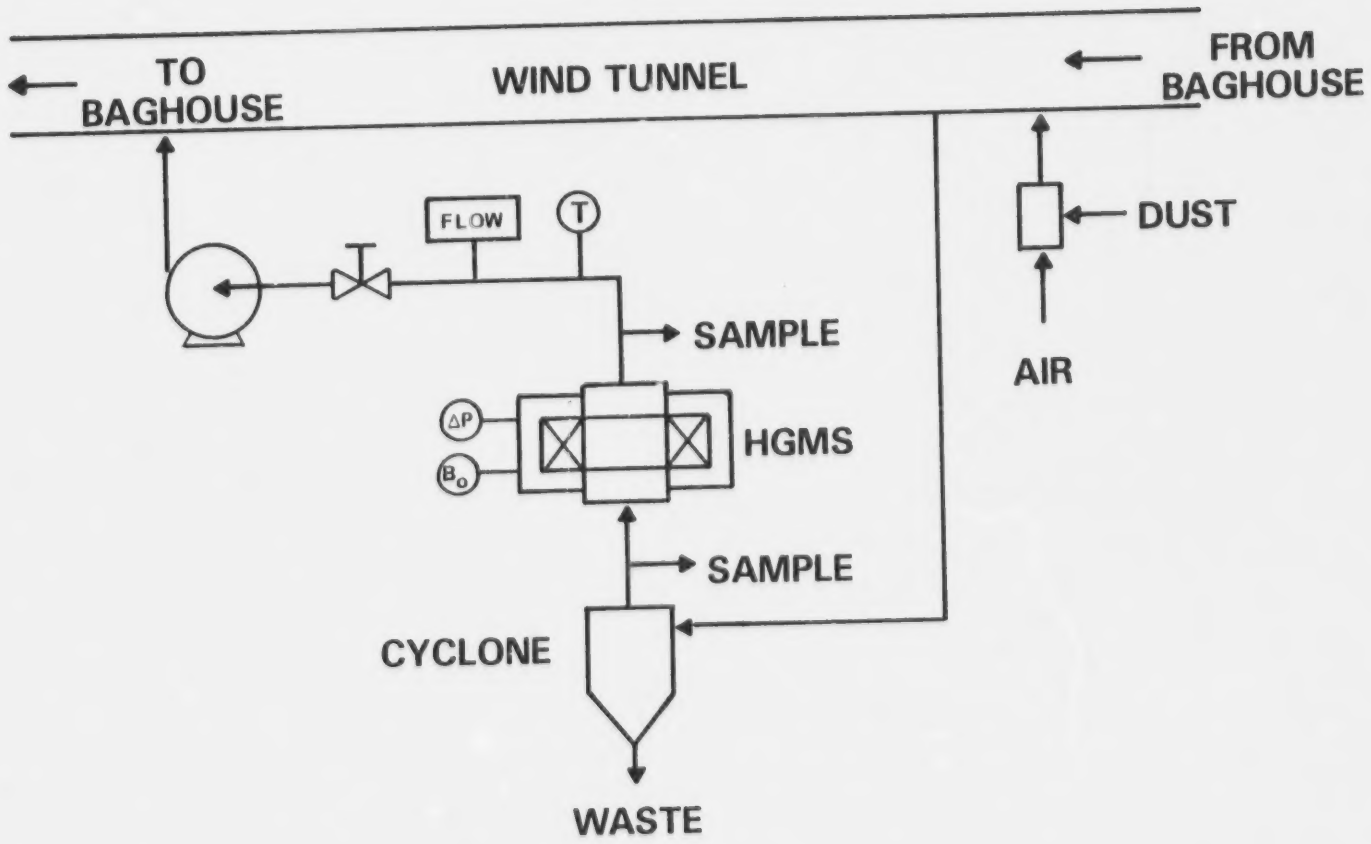

Figure 3. Schematic diagram of the HGMF laboratory pilot plant.

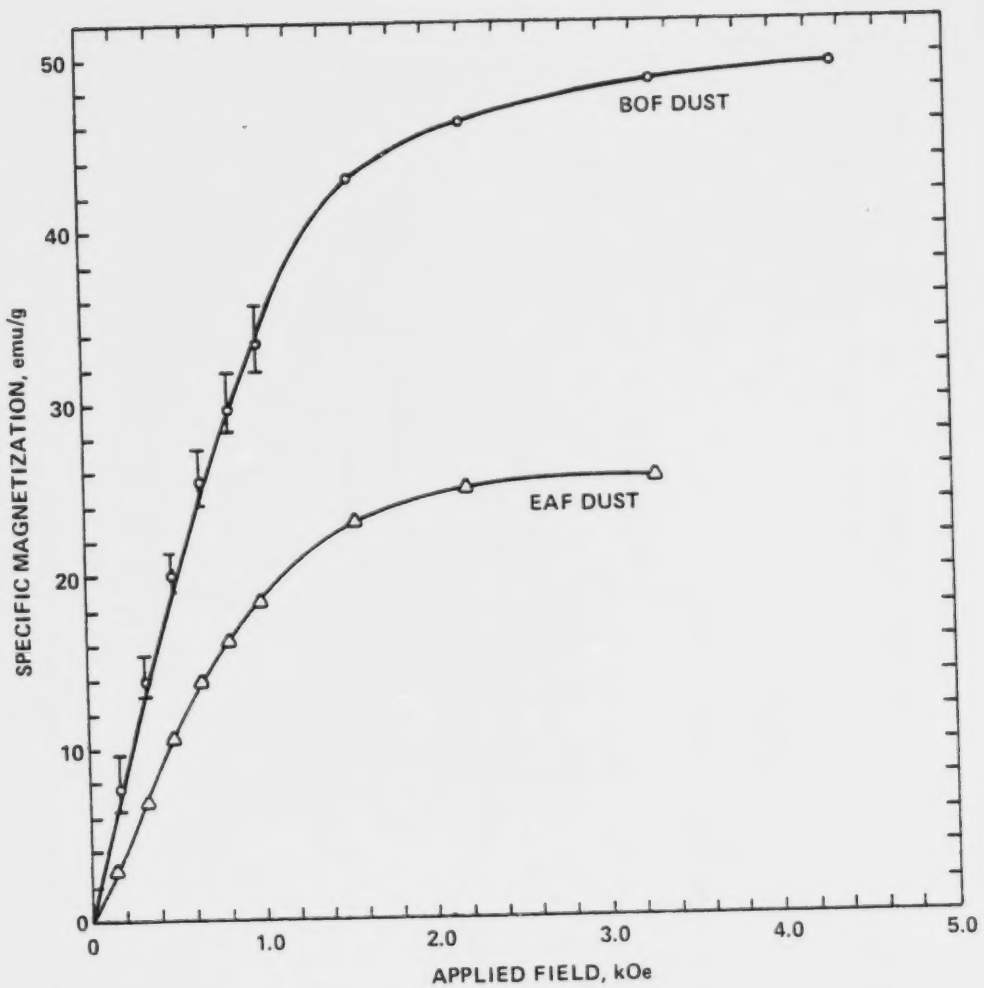

Figure 4. Magnetization curves of the two industrial dusts used in the preliminary experiments.

Numerous tests were run in the laboratory pilot plant to demonstrate the achievement of high collection efficiencies and to study the effects of operating parameters. Variations were made in the depth of the steel wool filter, the density of the filter, the strength of the applied magnetic field, and the gas velocity through the filter. In each experiment the particle size distribution and concentration were determined upstream and downstream of the filter from samples obtained with MRI Model 1502 impactors manufactured by Meteorology Research, Inc., Altadena, CA. In accordance with EPA's recommended procedures (Harris, 1977) the impactor substrates were coated with Apiezon L grease (James G. Biddle Co., Plymouth Meeting, PA) prior to use. Clean filter pressure drop tests were also obtained with several different combinations of filter depth and density.

Fractional collection efficiencies exceeding 99 percent were achieved with filtration velocities as high as 10 m/s, confirming the potential practicality of applying HGMF to particulate emission control in the iron and steel industry. The complete results of the laboratory pilot plant tests are presented in Appendix A.

Figures 5 and 6 show the effects of filter loading on collection efficiency and pressure drop for each of the dusts, starting with a clean, 420-g filter at time zero. The efficiency data were obtained with a Climet Model 208A optical particle analyzer (Climet Instruments Co., Redlands, CA). The BOF data show no deterioration in efficiency during the test period despite a dust accumulation of 800 g. Apparently the highly magnetic dust particles accumulating on the wires distorted the magnetic field sufficiently to act as new collection sites, rather than simply filling the gradient region as an inert material. This result implies that with a strongly magnetic dust increasing pressure drop rather than deteriorating efficiency will most likely determine the allowable filtration time between cleanings. In contrast, the EAF dust, which had a lower specific magnetization than the BOF dust, showed a deterioration in efficiency as the filter loaded. The total accumulation was 1270 g at the end of the test. Under the latter circumstances, the cleaning cycle would be determined by the minimum acceptable collection efficiency.

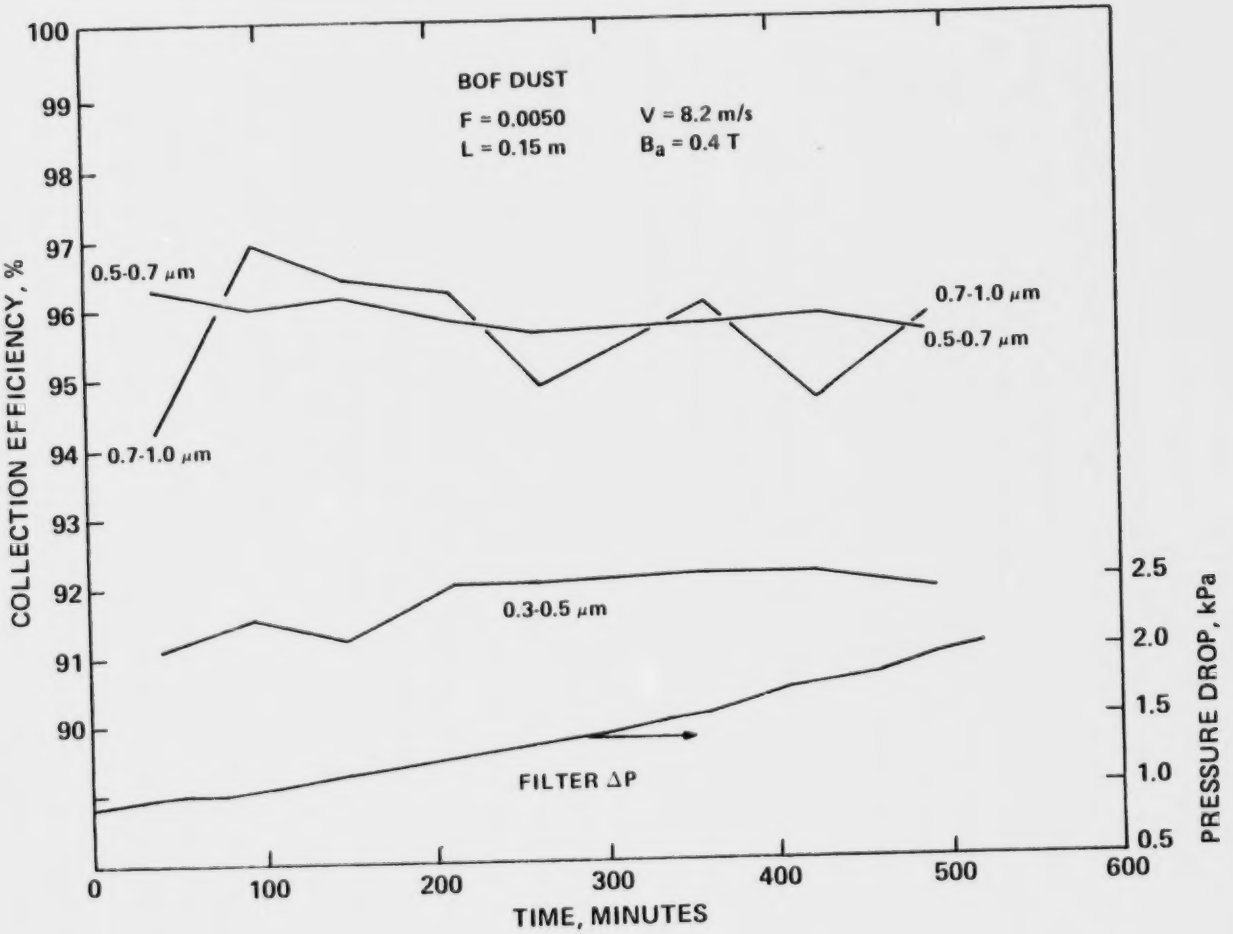

Figure 5. Effect of filter loading on BOF dust collection efficiency and filter pressure drop.

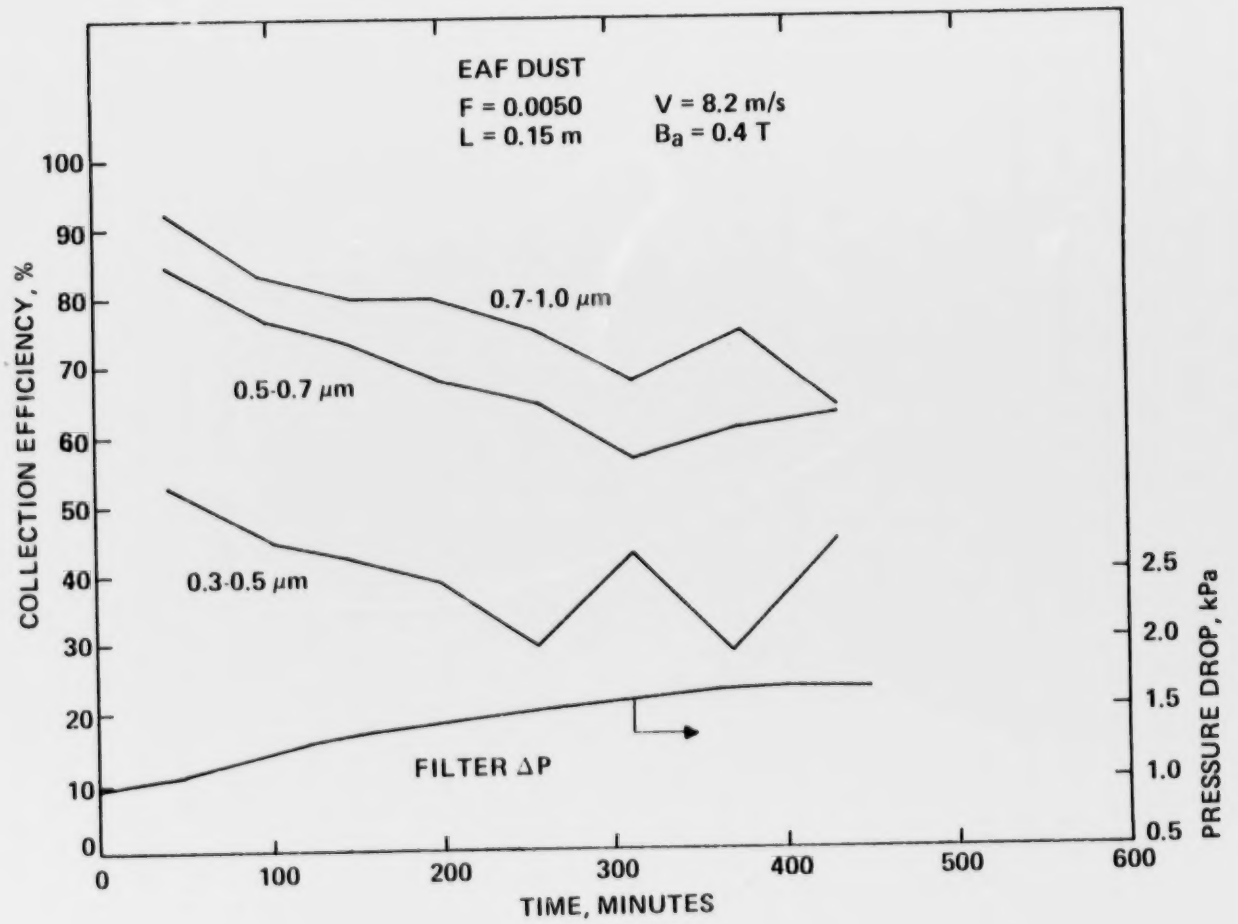

Figure 6. Effect of filter loading on EAF dust collection efficiency and filter pressure drop.

MATHEMATICAL MODELING OF PRELIMINARY RESULTS

A mathematical model of the HGMF process was developed in conjunction with the laboratory pilot plant work to give a better understanding of the effects of various design parameters. Like the common theoretical approach to conventional filtration, the model is based on the calculation of particle trajectories near the ferromagnetic wires, taking into account inertial, viscous, and magnetic forces. The development of the model is presented in detail in Appendix B. The final predictive equation for fractional collection efficiency is

$$E = 1 - \exp\left[-\frac{4FLY_c p}{\pi^2 s(1-F)^2}\right] \qquad (1)$$

where E = fractional collection efficiency, dimensionless;

F = filter packing density (actual volume of steel wires/volume occupied by filter), dimensionless;

L = filter depth, m;

s = wire radius, m;

Y_c = single wire collision radius, dimensionless; and

p = probability of particle adhesion, dimensionless.

The trajectory calculations lead to a theoretical correlation of Y_c in terms of two dimensionless groups, the familiar Stokes number and an unnamed magnetic parameter (see Appendix B). Each of these may be calculated from operating parameters of the system and physical properties of the dust and the gas stream. Comparison of the theoretical predictions of collection efficiency to experimental data revealed that the model agreed well with small particle data but underestimated the penetration of large particles through the filter. Two theoretical reentrainment models were investigated but neither proved to be satisfactory. To reconcile the discrepancy between the uncorrected theory and the experimental data, an empirical correlation was developed for the probability of particle adhesion in terms of the same two dimensionless groups used to predict Y_c. The agreement between the corrected model and the data is illustrated in Figure 7, which also demonstrates the high collection efficiency attainable with BOF dust.

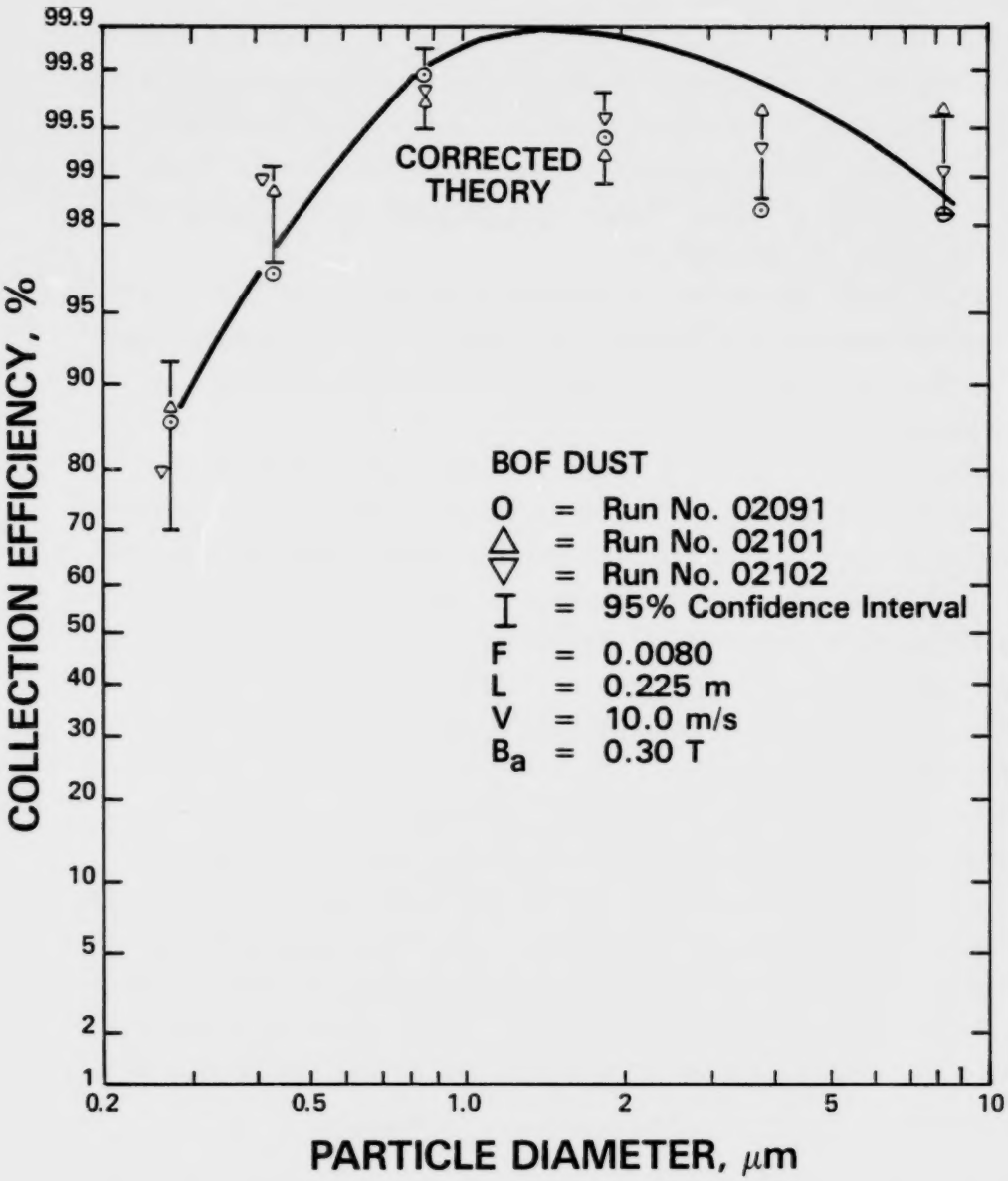

Figure 7. Replicate data from lab pilot plant experiments showing 95 percent confidence intervals on the true mean efficiency and corrected model predictions.

The next five figures illustrate the effects of different operating parameters on collection efficiency. The curves in each case were generated by the corrected theoretical model [Equation (1)] with the empirically determined adhesion probability; hence they reflect the experimental behavior of the process in the lab pilot plant. Figure 8 compares collection of the two dusts under identical operating conditions. The BOF dust, which had roughly twice the specific magnetization of the EAF dust at any field, was collected with significantly higher efficiency. The EAF dust could be collected with a peak efficiency above 99 percent, but a higher field and deeper filter were required to accomplish this (see Run No. 11151 in Appendix A).

Figure 9 shows the effect of applied field on the collection of BOF dust. The improvement in efficiency provided by the increased magnetic force is clear, but the return is diminished as the dust particles approach magnetic saturation.

Figures 10 and 11 show the effects on collection efficiency of filter packing density and filter depth, respectively. The effects of these two parameters are identical. One can deduce from Equation (1) that doubling either the packing density or the filter depth squares the fractional particle penetration. For example, in Figure 10 the collection efficiency at 6 μm goes from 95 percent to 99.75 percent [$0.0025 = (0.05)^2$] when the packing density is doubled from 0.005 to 0.01.

Figure 12 shows the typical effect of gas velocity on collection efficiency. Theoretically, the role of velocity is a complicated one. As a component of particle inertia, increasing velocity can be beneficial or detrimental to particle collection depending on the value of other physical properties and conditions. But increasing velocity always reduces the probability of particle adherence, so the net result is usually the relatively weak detrimental effect shown in Figure 12. Appendix B includes a more detailed discussion of the theoretical effect of velocity.

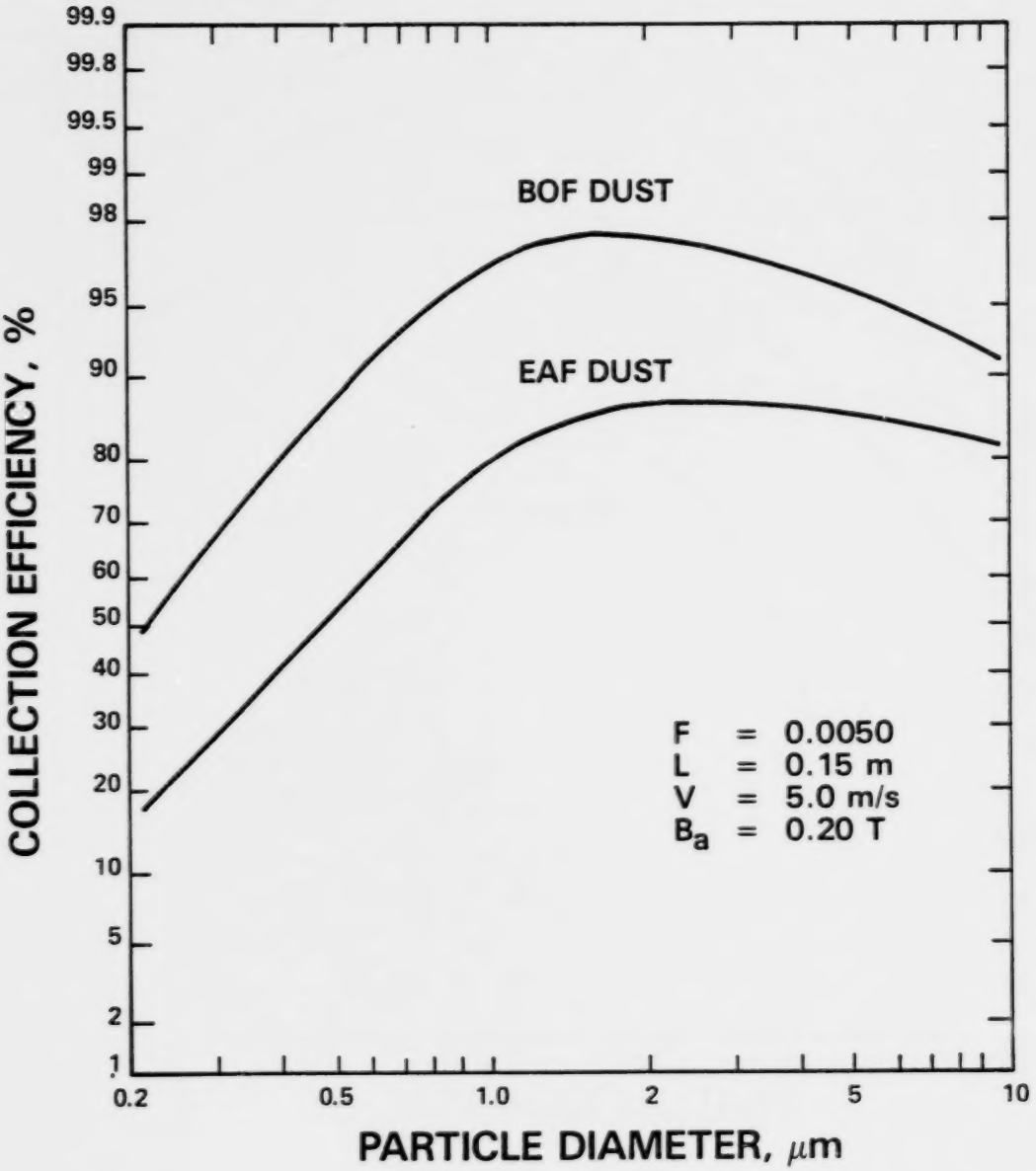

Figure 8. Collection of BOF and EAF dusts under identical operating conditions.

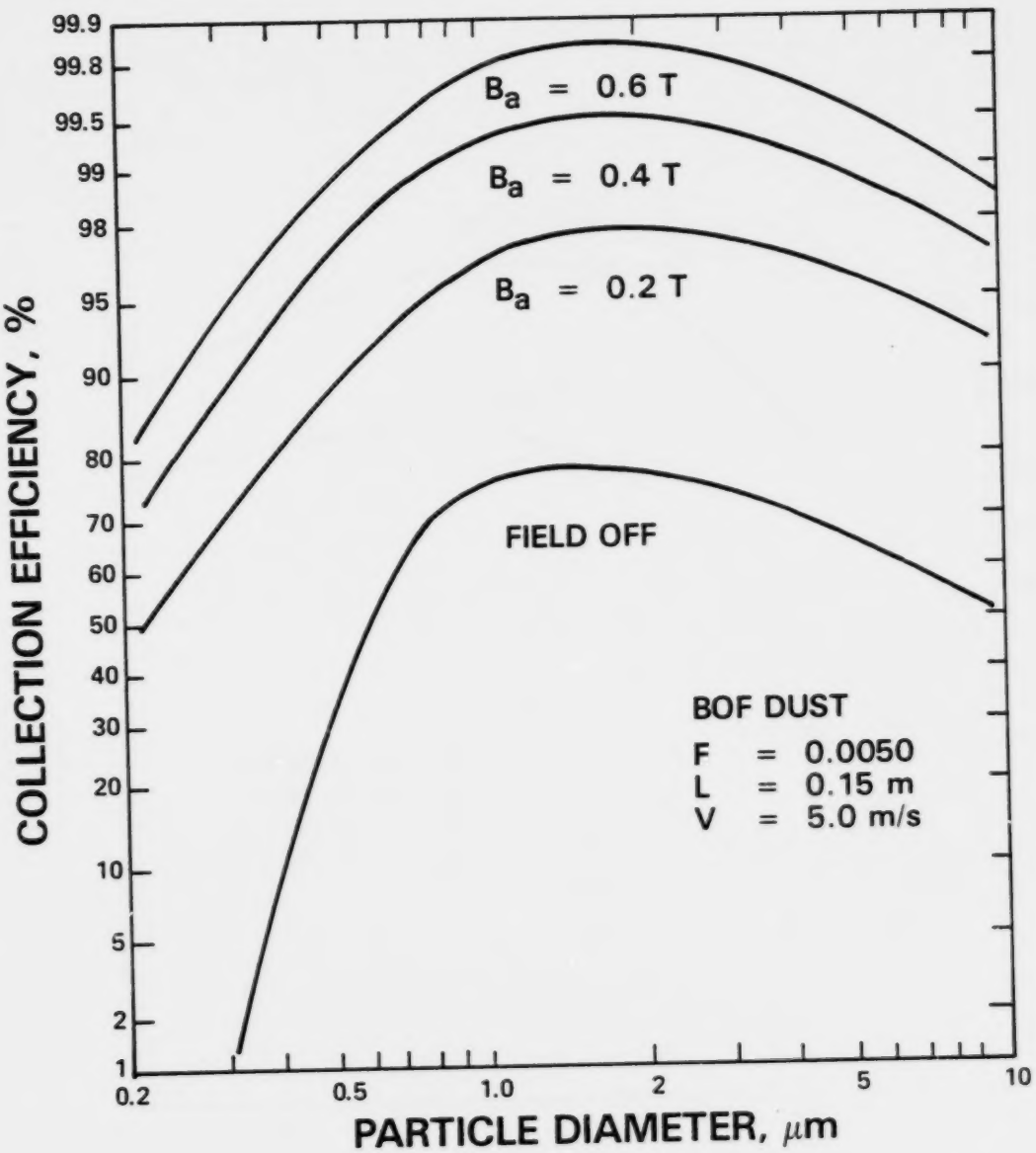

Figure 9. Effect of applied magnetic field on collection efficiency.

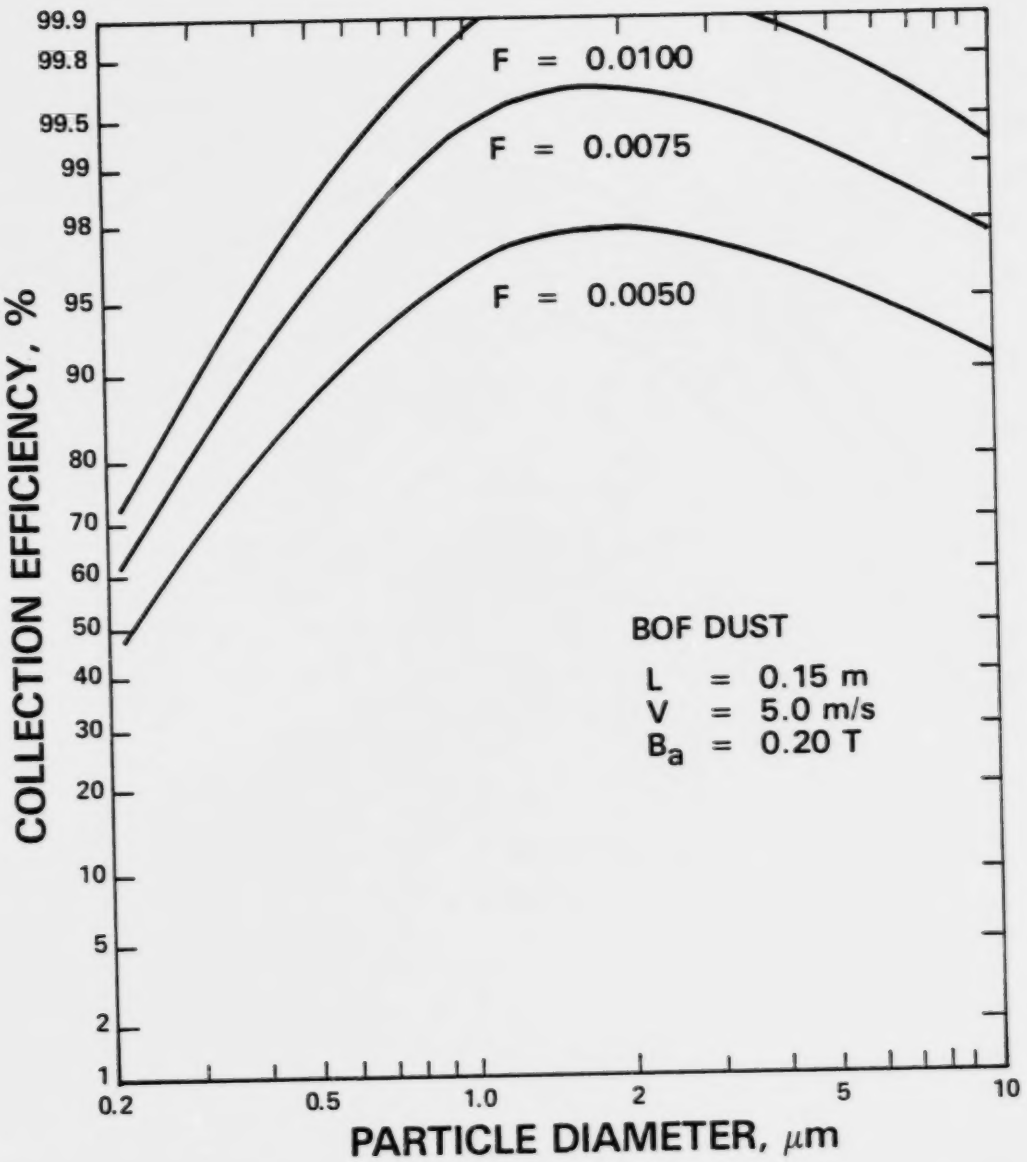

Figure 10. Effect of filter packing density on collection efficiency.

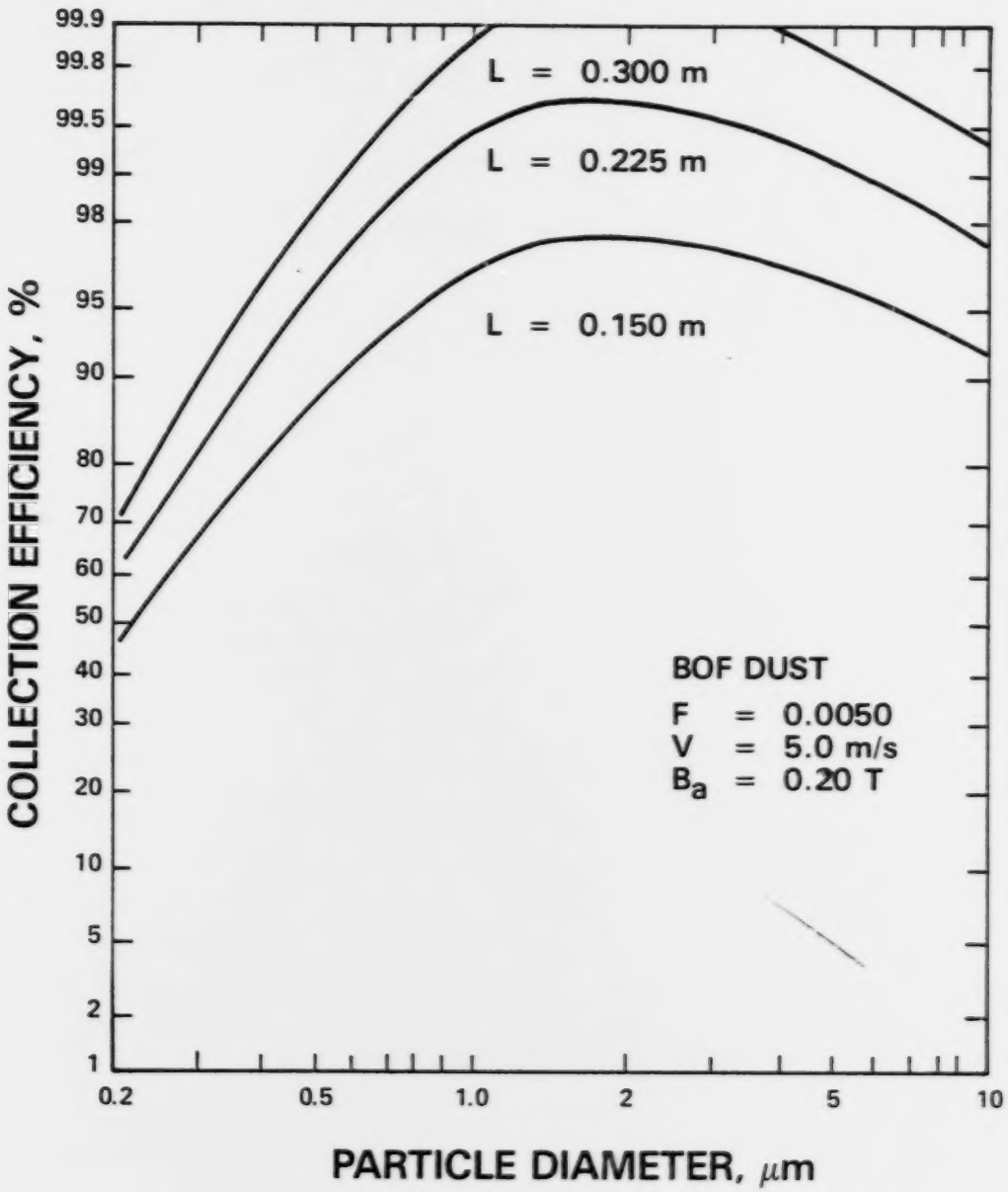

Figure 11. Effect of filter depth on collection efficiency.

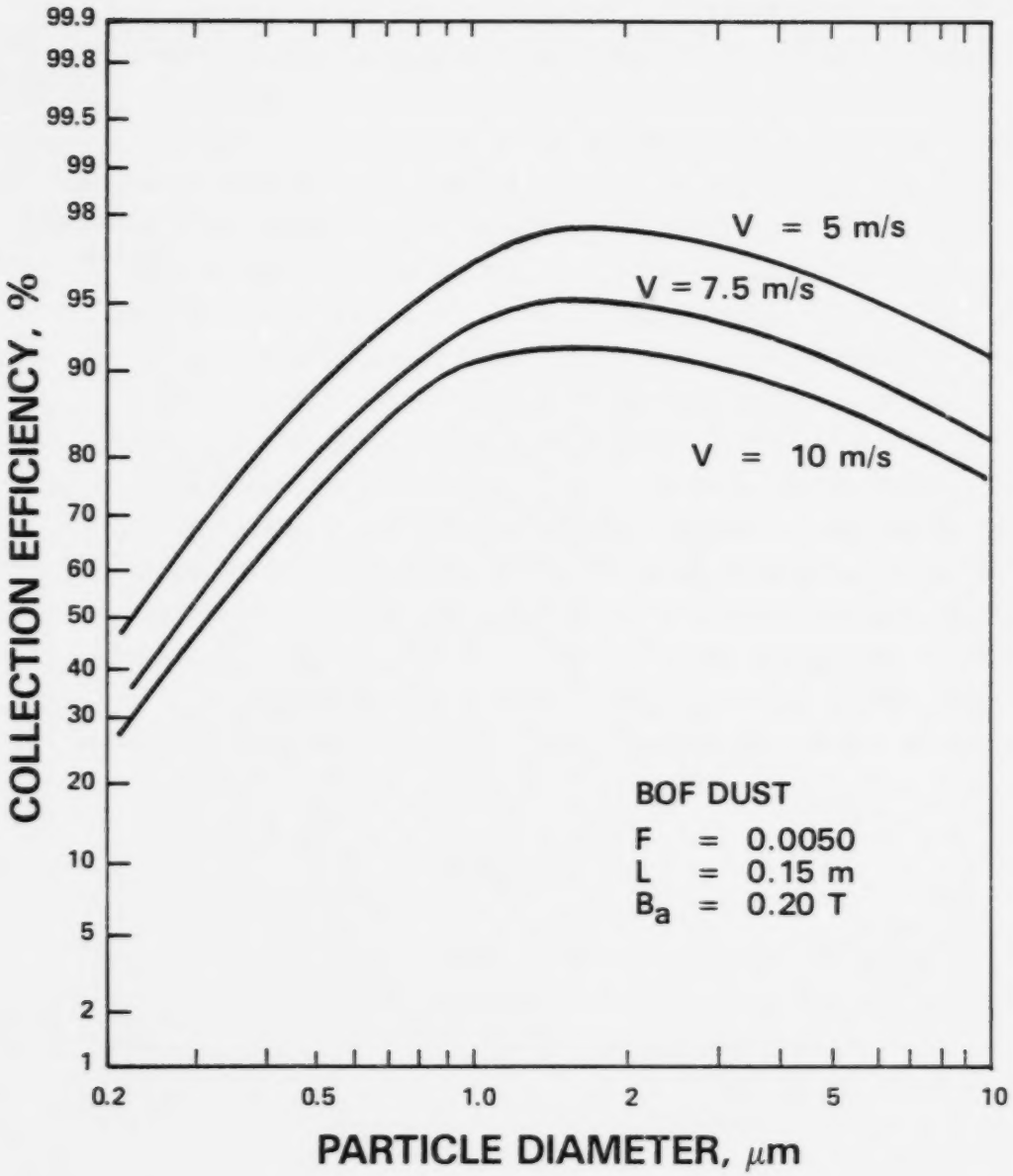

Figure 12. Effect of superficial gas velocity on collection efficiency.

It can be noted that all of the curves show a peak in collection efficiency in the 1 to 2 μm particle size range. This prediction, which accurately reflects the observed experimental system behavior, is clearly a consequence of the reentrainment phenomenon. The uncorrected model predicts a monotonic increase in collection efficiency with particle size up to at least 5 μm, above which the efficiency may level off but does not decrease. The empirical correlation does not reveal whether reentrainment is caused by particle bounce, drag forces on collected particles, or a combination of these and perhaps other phenomena, but the results clearly indicate that reentrainment is an important factor in determining collection efficiency under the experimental conditions of interest to air pollution control applications of HGMF.

One other factor of particular interest to air pollution control applications is the effect of operating temperature. Theoretically, increasing temperature exerts a detrimental effect in two ways--by increasing the gas viscosity and by decreasing the magnetization of the wire and the particles. Thus the drag force tending to keep the particles entrained in the gas increases, and the magnetic force decreases, but neither of these effects is prohibitive to operation until the Curie point of the magnetic materials is reached. The Curie point of the most commonly used filter material, AISI Type 430 stainless steel, is approximately 680°C (Bozorth, 1951). Above that temperature the material loses its ferromagnetism. Below the Curie point the saturation magnetization obeys the relationship

$$M_s/M_o = \tanh \frac{M_s/M_o}{T/T_c} \qquad (2)$$

where M_s = saturation magnetization at T, A/m;
M_o = saturation magnetization at absolute zero, A/m;
T = absolute temperature, °K; and
T_c = Curie point, °K.

Equation (2) indicates that the saturation magnetization of 430 stainless steel at 310°C is 90 percent of its value at 25°C. At 500°C it is still 70 percent of the 25°C value. Ferromagnetic dust particles could be expected to exhibit roughly the same behavior. Viscosity of air is approximately proportional to absolute temperature raised to the 0.7 power. Thus, an increase in temperature from 25°C to 550°C causes a doubling of viscosity. This theoretical analysis reveals that HGMF should certainly be applicable at temperatures of 500 to 600°C although the filtration of particles will be somewhat more difficult than at lower temperatures.

The corrected theoretical model of HGMF developed in conjunction with the lab pilot plant work provided a valuable tool for the design of the mobile pilot plant and the field experiment. The model can also be used in conjunction with economic estimates when one must compare alternative operating conditions. In its present form the model has four significant limitations:

(1) It is based on a clean wire assumption, so it is not valid under conditions in which the filter loading significantly affects collection efficiency;

(2) The effect of wire size has not been confirmed experimentally, and the method of estimating wire size for model calculations is subject to error because it ignores possible influences of shape and surface irregularities and wire-size distributions (see Appendix A);

(3) The effect of gas temperature has not been evaluated experimentally; and

(4) The reentrainment correction contains empirical constants that most probably vary with dust properties.

SITE SELECTION FOR FIELD TESTS

Having demonstrated the attainment of high collection efficiency with two steel industry dusts, RTI approached the American Iron and Steel Institute to solicit their assistance in finding a suitable site for field tests. In December, 1977, a presentation was made before the AISI Technical Committee on Environmental Quality Control to describe the lab pilot plant work and to introduce the objectives of the field program.

Subsequent discussions were held with several individual companies until one company expressed a definite interest in testing the HGMF process at a sintering plant. Sinter dust was not the obvious choice for a first evaluation of HGMF because it was anticipated to have a relatively low magnetization, but the sintering process is one of the more difficult environmental control problems presently facing the steel industry; hence the opportunity is greatest for the application of a new concept.

In April, 1978, a drum of dust was received from the sintering plant that had been tentatively chosen for the field tests. The dust was obtained from the hoppers of the electrostatic precipitators that presently control windbox emissions. The magnetization curve of the bulk dust was similar in curvature to those of the BOF and EAF dust (Figure 4), but the saturation value was only 9 emu/g. The dust was quite coarse in appearance, containing some particles as large as 3 mm. The average particle density was determined by pycnometer measurements to be 3.9 g/cm^3.

A series of tests was initiated with the sinter dust in the laboratory pilot plant, but the number of runs was limited by severe problems feeding the coarse dust into the dust generator. Because of difficulty entraining the large dust, the particle stream entering the HGMF had a mass median diameter of approximately 6 μm (aerodynamic) and a dust concentration of only 10 to 40 mg/Nm^3. The pilot plant gas conditions were adjusted to approximately 130°C and 5 percent moisture to simulate actual windbox conditions. The experimental results of the sinter runs are shown in Figure 13. All of the runs were made with an applied flux density of 0.5 T. In comparison to the theoretical model, the data actually showed somewhat better small-particle collection than was expected and not quite as good as expected with the larger particles. The test series was too limited to draw any conclusions about optimal operating conditions, but the results were sufficiently promising to move ahead with plans for the field work.

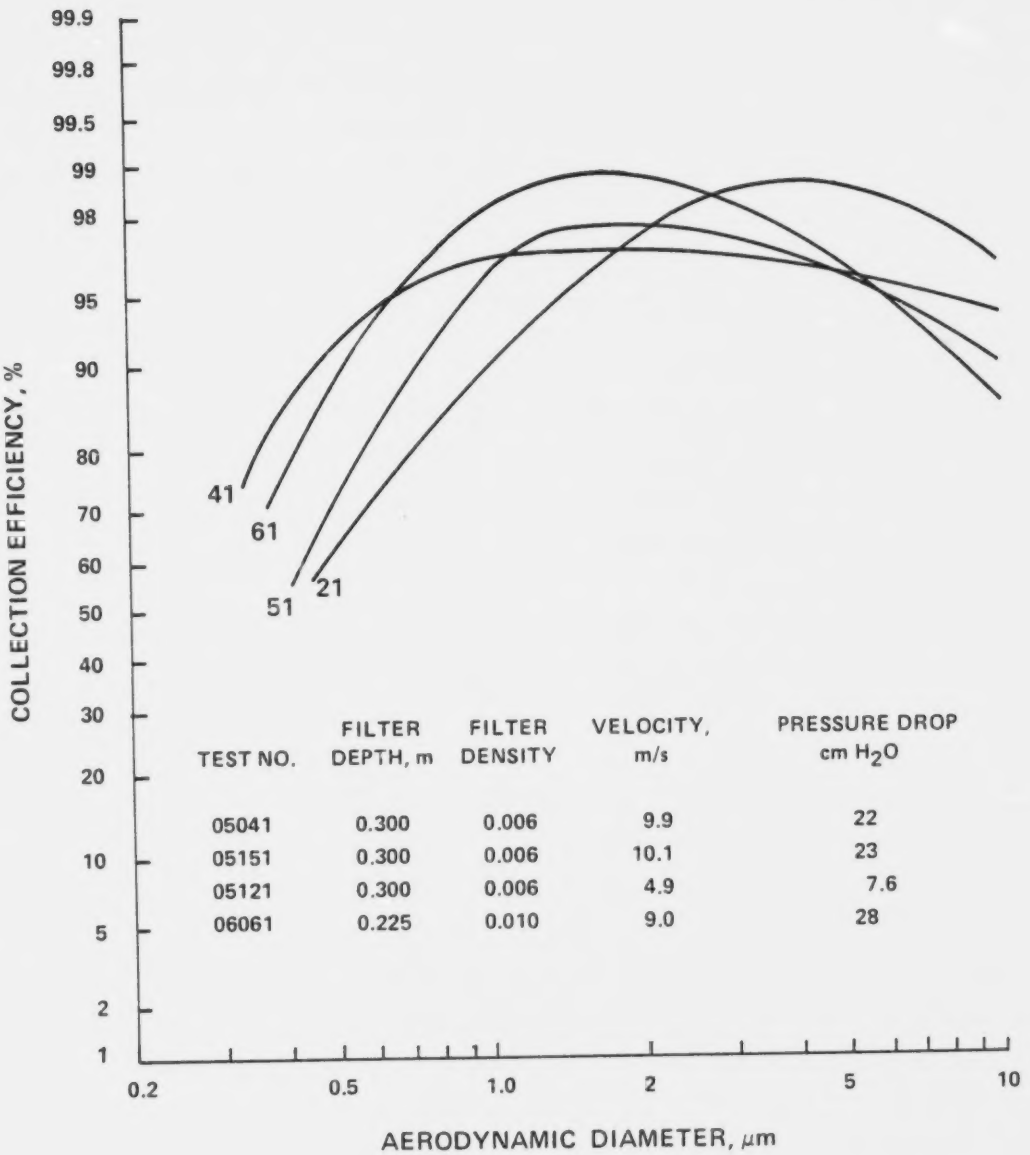

Figure 13. Results of sinter dust tests conducted in the lab pilot plant.

DEVELOPMENT OF FILTER CLEANING SYSTEM

The development of an effective filter cleaning system for the mobile pilot plant was of critical importance to the field operations. Figure 14 shows the result of simplified theoretical calculations that were conducted to evaluate the magnitude of competitive forces that would be significant in a cleaning system. The magnetic force acting on a captured particle was calculated from a simplified form of Equation (B-9); i.e.,

$$F_m = \frac{16\pi u_o \chi^* H_a^2 b^3}{3s} \qquad (3)$$

where F_m = magnetic force, N;
u_o = magnetic permeability of a vacuum, $4\pi x10^{-7}$ h/m;
χ^* = effective magnetic susceptibility, dimensionless;
H_a = applied magnetic field, ampere turns per meter;
b = particle radius, m; and
s = wire radius, m.

Equation (3) represents the maximum radial magnetic force acting on a particle at the surface of a magnetized wire. In terms of the specific magnetization

$$\chi^* = \frac{\rho_\rho \sigma}{H_a} , \qquad (4)$$

where σ = specific magnetization, emu/g; and
ρ_ρ = particle density, kg/m^3.

The magnetic force lines in Figure 14 were calculated for a particle density of 4000 kg/m^3, a wire radius of 50 μm, and an applied field of $3.98x10^5$ A/m (0.5 T). With the field off for filter cleaning, the residual force would be much smaller than that shown.

The drag force, F_d, was calculated from the expression

$$F_d = C_d \bullet \pi b^2 \bullet \frac{\rho_f V_o^2}{2} , \qquad (5)$$

where C_d = drag coefficient, dimensionless;
ρ_f = fluid density, kg/m^3; and
V_o = fluid velocity, m/s.

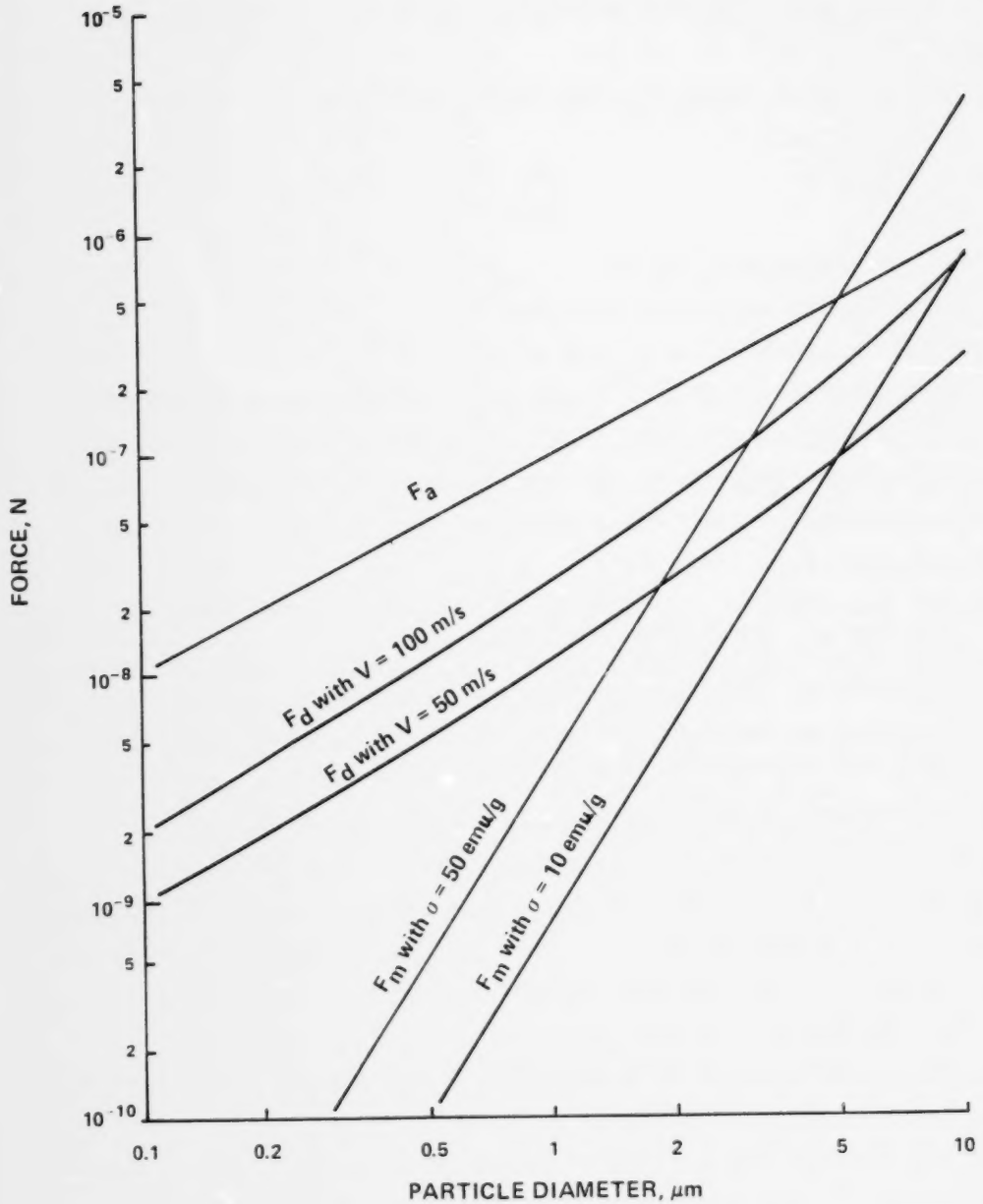

Figure 14. Comparison of forces exerted on collected particles.

The fluid was assumed to be air at 25°C and standard atmospheric pressure. The flow conditions indicated are in the transitional region above the Stokes law regime but well below the region of constant drag coefficient.

The van der Waals force, F_a, was calculated from

$$F_a = \frac{Ub}{6\ell^2} , \qquad (6)$$

where U = Hamaker constant, J; and

ℓ = equilibrium separation distance, m.

The separation distance was estimated to be 4×10^{-10} m after Krupp (1967), and a Hamaker constant of 2×10^{-19} J was used, which is appropriate for ferrous materials in air (Visser, 1972). Because of the uncertainty in estimating these two parameters, the van der Waals force must be regarded as a rough approximation, but the comparison shown in Figure 14 makes two important points:

(1) The van der Waals force is in all likelihood more important than in any residual magnetic forces holding the particles on the wires (the van der Waals force is not important to initial particle capture because it is an extremely short-range force).

(2) Flushing velocities of at least 50 to 100 m/s are most probably required to remove the particles from the wires.

The first quantitative cleaning experiments were conducted by removing a used filter from the lab pilot plant and cleaning sections of it with a small air jet. The dust accumulation was virtually unaffected by air velocities lower than 50 m/s. When higher jet velocities were applied, the dust was denuded from the wires in chunks on the order of 500 μm. The denuding action and the high air velocity requirement suggested that a pulse cleaning approach would be much more practical in application than a flush of extended duration.

A series of bench-scale filter cleaning tests was then run in the following manner. Forty samples of steel wool were placed in 10-mm diameter glass tubes,and the tubes were imbedded in a larger filter of the same length and packing density as the small samples. A collection run was then made in the laboratory pilot plant using the sinter dust.

The tubes were carefully removed and cleaned individually in a laboratory apparatus. This cleaning was accomplished by pulsing each small filter with a burst of air released from a pressurized chamber. Variations were made in the volume and pressure of the air chamber, the surge volume between the air chamber and the filter, and the orifice diameter of the quick-release ball valve. Both a baffled settling chamber and a cyclone were tested to re-collect the dust blown off the filters. The following conclusions were drawn from the tests:

(1) If a scaled-up system could be developed to release the pressurized air with dynamic pulse characteristics similar to the lab system and the pressure drop characteristics of the flow paths were the same, then the ratio of chamber volume to filter face area should be a measure of the maximum pulse velocity and thus of the cleaning potential. The lab experiments indicated that a ratio of 2 m was needed for efficient cleaning.

(2) The surge volume between the air chamber and the filter should be kept to a minimum to avoid dissipation of the air pressure. In the lab tests a surge volume of 1/3 the air-chamber volume was acceptable.

(3) A chamber pressure of at least 140 kPa gauge (20 psig) was needed for acceptable cleaning. Higher pressures gave even better results.

(4) Dynamic flow calculations led to an estimate that the test cleaning system developed a pulse velocity through the filter of 100 m/s within 0.05 seconds of the initial valve opening. To achieve this in the mobile unit would require that the quick-opening valve develop a flow coefficient of 750 in 0.05 seconds. (Valve flow coefficient is a commerical measure of the rated valve capacity. In English units of measure it has a direct physical significance in that the flow coefficient represents the number of gallons per minute of water that the valve will pass at 60°F with a pressure drop of 1 psig. For example, most 4-inch nominal butterfly valves are rated with a flow coefficient in the vicinity of 750 when in their fully-open positions, but standard pneumatic and electric actuators are not capable of opening a 4" valve in 0.05 seconds. Hence, meeting the valve requirement represented a significant design challenge.)

(5) The cyclone consistently caught over 99 percent of the material blown off the filter while the baffled settling chamber averaged 87 percent. Since a scaled-up cyclone would also require a minimal amount of space in the mobile unit, the cyclone approach was adopted.

SECTION 6

DETAILED DESIGN AND CONSTRUCTION OF THE MOBILE PILOT PLANT

The mobile pilot plant is housed in a 12.8 m (42 ft) freight van. It was designed for a nominal flow capacity of 5100 m^3/hr (3000 CFM) based on the previous experimental work. Figure 15 is a flow schematic of the portion of the system that is inside the trailer.

The dirty gas enters the trailer via a 0.317 m ID, 316 stainless steel pipe (12", Schedule 5) and passes by test ports through which samples can be drawn to determine the size distribution and concentration of the inlet dust. The gas is then directed to one of two functionally identical HGMF devices. Two filtration paths are provided so that one can be cleaned while the other is in operation. Magnet A was constructed by Magnetic Corporation of America (MCA), Waltham, MA, and Magnet B was originally constructed by Sala Magnetics, Inc., Cambridge, MA for use in the laboratory pilot plant. Magnet B was later modified by the addition of new pole pieces and stand purchased from MCA. Each of the magnetic filters consists of the iron-bound solenoid surrounding a canister that measures 0.432 m ID by 0.305 m long. The canisters are filled with an appropriate amount of magnetic stainless steel wool as dictated by the test program. Each of the magnets can be energized to provide an applied field of up to 0.5 tesla throughout the canister volume. The magnets are energized by DC modular power supplies manufactured by Controlled Power Company (Troy, MI) and purchased from MCA.

After passing through the filter, the cleaned gas travels past another set of test ports and exits the trailer. The exterior pipe size is reduced to 0.266 m ID (10", Schedule 5). The gas passes through an orifice and an induced draft blower and is then exhausted to the atmosphere through an 11 m high stack.

The filters are cleaned by backflushing with compressed air provided by a Worthington Model 7 1/2 EDBR two-stage compressor (Worthington Compressors, Inc., Holyhoke, MA) that is mounted to the underside of the trailer. The compressed air tank associated with each filter has a volume of approximately 0.28 m^3. To pulse the filter, the compressed air is

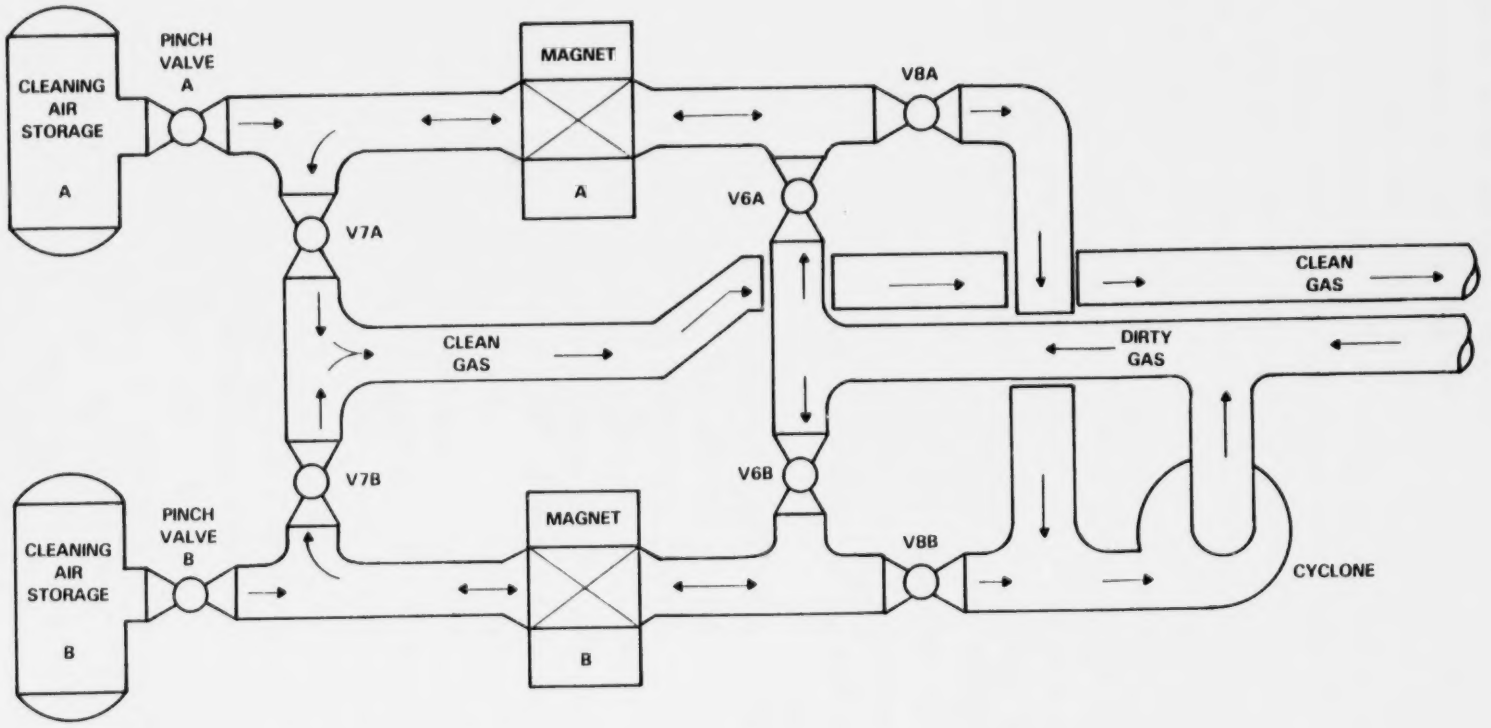

Figure 15. Flow schematic of HGMF mobile pilot plant.

released through an 8" (nominal pipe size) Galigher Delta valve (Galigher Company, Salt Lake City, UT). The Galigher valves are pneumatically actuated pinch valves with an equivalent throat diameter of approximately 20 cm and a fully-open C_v rating of 1300. Each valve consists of a pair of identical elastomeric diaphragms contained within a cast aluminum, split housing. The diaphragms are closed by introducing compressed actuator air into the chamber between the housing and the diaphragms. The valve can then be opened very rapidly by exhausting the actuator air through two large ports provided in the housing. To obtain a tight seal on the air chambers the actuator air is controlled to a pressure approximately 140 kPa (20 psi) higher than the cleaning air and is then released through 1 1/2" (nominal) Model 168S poppet valves manufactured by Kay Pneumatics (Commack, NY). Dynamic flow calculations conducted during the design phase indicated that the Galigher valves should be able to achieve the required C_v of 750 within 0.05 seconds of the initial diaphragm separation and thus release the cleaning air in a pulse sufficient to clean the filters.

The agglomerated dust that is flushed off the filer is removed from the cleaning air by a Kirk and Blum Size 6, Type C7 cyclone (Kirk and Blum Manufacturing Company, Cincinnati, OH). The exhaust from the top of the cyclone is routed back to the dirty gas stream and into the operating filter. Dust can be removed from the cyclone during operation through the double seal formed by two 6" (nominal) Norris butterfly valves (Dover Corporation/Norris Division, Tulsa, OK) that are mounted in line at the bottom of the cyclone hopper. Pneumatic vibrators are mounted on the walls of the dust hopper to aid in dust discharge.

Figures 16 and 17 are photographs taken of the interior of the trailer during the construction phase. Figure 16, taken from the rear door, shows the Galigher valves on either side with the air tanks mounted above. In the foreground is the tee that receives the outlet flow from the magnetic filters and channels it back toward the front of the trailer. The black magnets are visible behind the pipe. Figure 17 was taken from the front of the process area before the cyclone and the inlet and outlet test sections were installed. The open flange in the upper portion of the photograph connects directly to a horizontal pipe carrying the inlet gas.

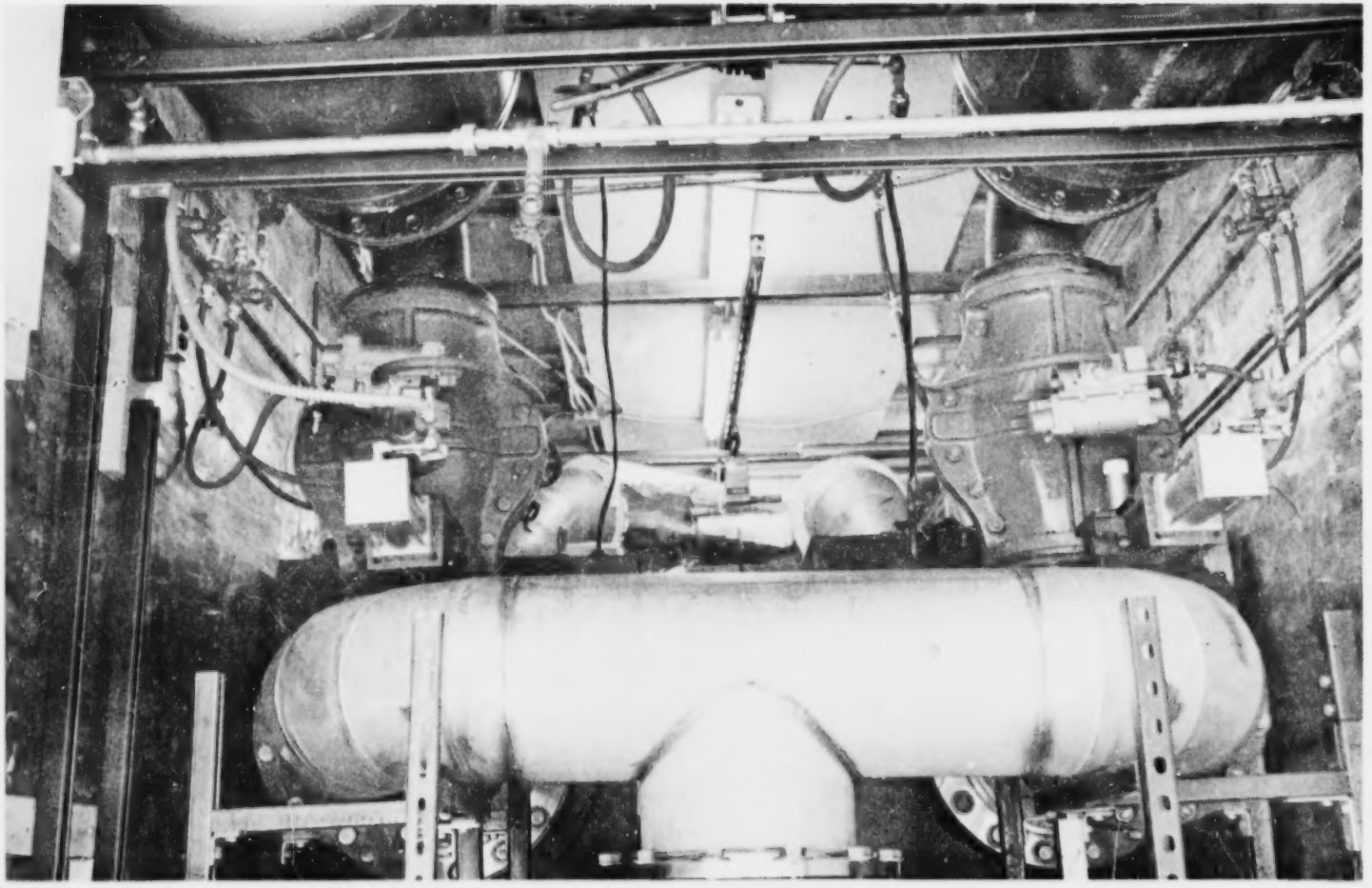

Figure 16. View of the pilot plant from the rear interior of the trailer.

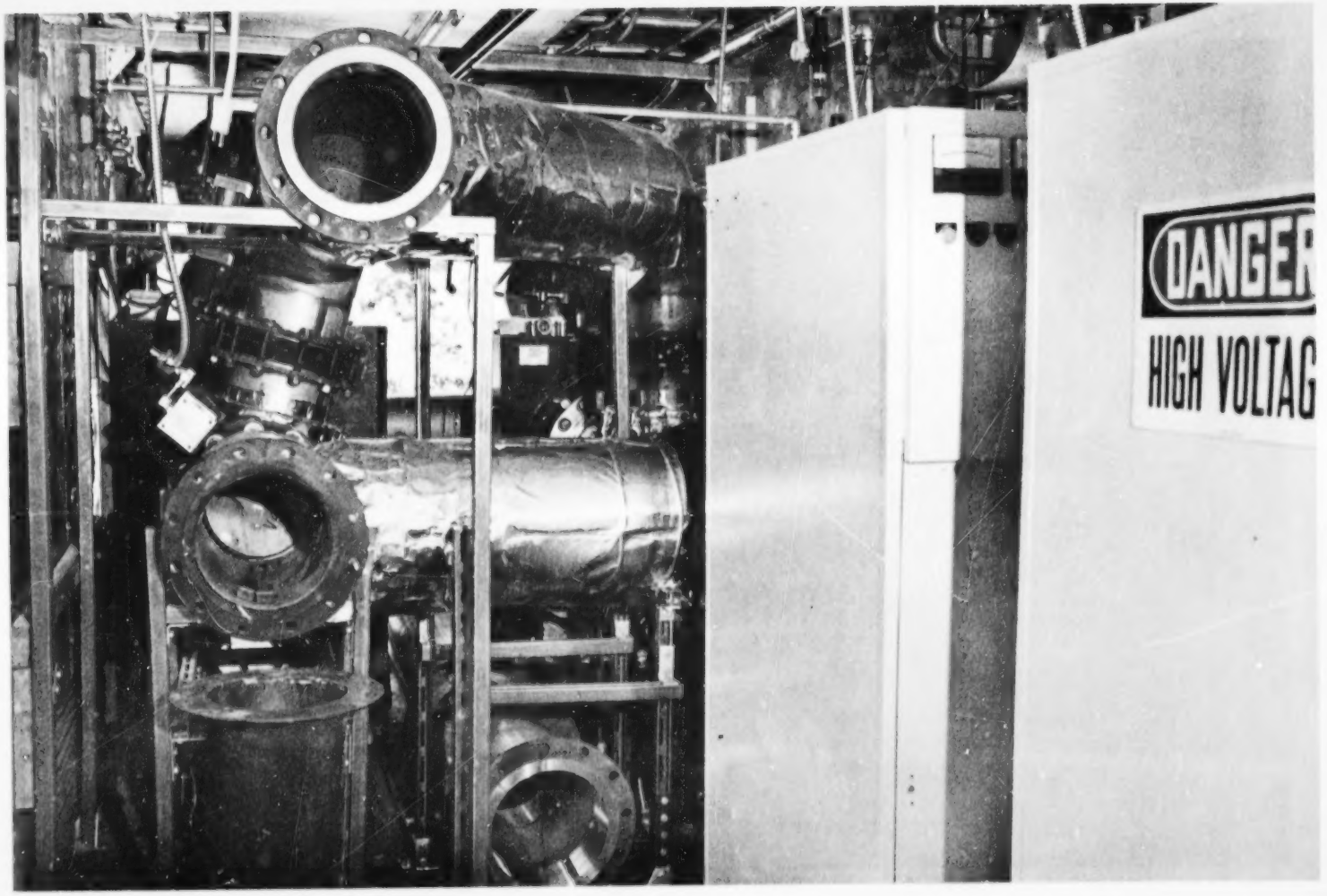

Figure 17. View of the pilot plant from the front interior of the trailer.

The inlet of the cyclone bolts to the flange below via the transition piece standing on the floor under the flange. The top outlet of the cyclone exhausts to the inlet gas pipe above. The open pipe in the lower center carries the clean outlet gas and connects to an S-shaped pipe that rises to join the outlet test section. The magnet power supplies are visible at the right.

The blower that moves the gas through the pilot plant is a Centrifan Model RB50-2 (Centrifan Company, Greenville, SC). The blower will exhaust the required 5100 m^3/hr at a suction pressure of -18.7 kPa (-75 inches H_2O) and a temperature of 150°C. With the exception of the Galigher valves, pneumatically or manually actuated Norris butterfly valves are used throughout the system. The entire system is designed to allow continuous operation at up to 200°C. The interior pipe is insulated with calcium silicate and the exterior pipe with jacketed fiber glass.

The front quarter of the trailer contains an enclosed, air-conditioned laboratory and control room. Two automated devices are incorporated to simplify operation of the pilot plant. A Xanadu Model UPT100-10-10 solid state programmable timer (Xanadu Controls, Springfield, NJ) sequences the operation of the butterfly valves, the pinch valves, and the magnets as the system cycles from one flow path to the other. The total cycle duration and the sequence of events may be changed easily in a few seconds by inserting a pencil-coded computer card and adjusting a thumbwheel switch. A Robertshaw DCM-1000 controller (Robertshaw Controls Company, Anaheim, CA) maintains constant gas flow through the pilot plant. The controller receives its signal from an orifice located in the clean gas pipe via a Robertshaw Model 117 differential pressure transmitter and adjusts a butterfly valve located on the blower exhaust. The control diagram is shown in Figure 18. The orifice pressure drop and the pressure drop across the magnetic filters are displayed and stored on two Robertshaw Model 225 strip chart recorders located in the laboratory/control room. An Omega Model 199KC digital temperature indicator (Omega Engineering, Inc., Stamford, CT) is also mounted in the control panel to display the signal from chromel/alumel thermocouples that are located in the inlet and outlet piping of the pilot plant.

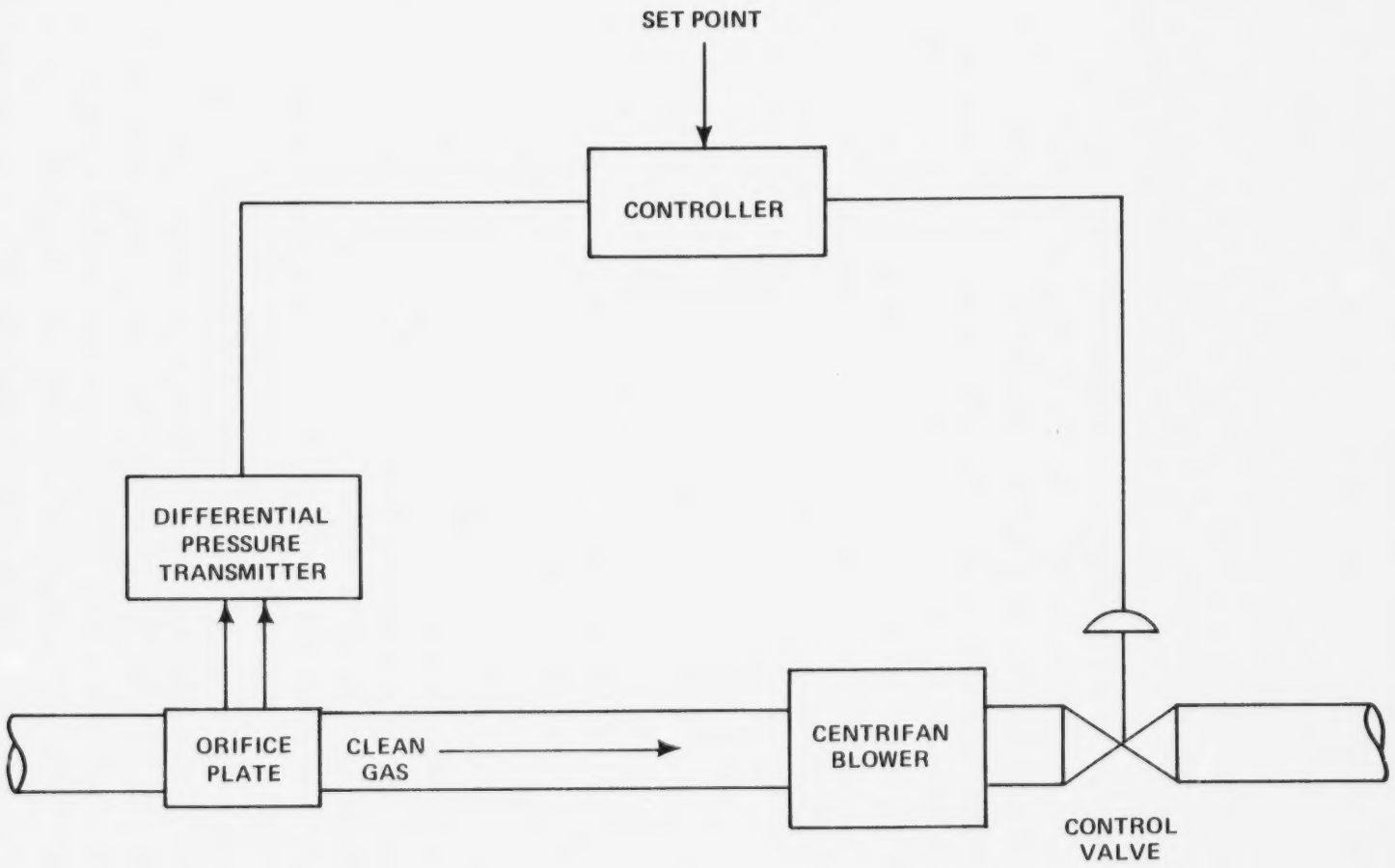

Figure 18. Flow control diagram.

The laboratory/control room also contains bench space, a wet sink, a lab oven, a solvent sink and a lab hood. MRI Model 1502 cascade impactors (Meteorology Research, Inc., Altadena, CA) are used to determine the particle size distribution and concentration. A Perkin-Elmer Model AD-2Z microbalance (Perkin-Elmer Corp., Norwalk, CT) is used to weigh the impactor substrates. A Climet Model 208A particle size analyzer with a Model 210 multichannel monitor (Climet Instruments Co., Redlands, CA) is also available to monitor transient conditions in the particle size distribution and concentration on the clean side of the magnetic filters.

The utility requirements of the pilot plant consist of electricity and water. The main power panel is breakered for 400 amperes of 480 volt AC input. The total connected load is 280 amperes, and the typical current draw is about 150 amperes. The major equipment operates off 480 VAC, and a transformer is provided to step down to 240 VAC and 120 VAC for lighting and smaller loads. Water consumption is approximately 5 m^3/hr (22 GPM) for magnet cooling plus minor usage for the compressor aftercooler and the lab sink. As illustrated later in Section 8, these utility requirements are much larger in proportion to gas flow capacity than the requirements of a full-scale HGMF system.

SECTION 7

FIELD OPERATIONS

DESCRIPTION OF THE SINTER PLANT

The sintering process is basically a scrap recovery operation developed to make the integrated steel mill more efficient. Blast furnaces require a feed material that is relatively uniform in size. In the sintering process fine, iron-bearing materials from a variety of sources are mixed and fused together to make a suitable component of the blast furnace feed.

Figure 19 illustrates the operation of the sintering process on the strand where the HGMF field tests were conducted. Ore fines, blast furnace flue dust, BOF slag, mill scale, limestone, dolomite, and coke breeze are fed to a traveling grate. The upper surface of the bed is then fired with natural gas burners, and air is drawn through the bed into a series of distribution chambers called windboxes. As the bed travels down the strand, the combustion zone moves downward through the bed, igniting, drying, heating, and fusing the mixture into a sinter. At the end of the strand, the sinter is crushed, screened, and cooled for transport to the blast furnace. Screened fines are returned to the feed.

Part of the gas drawn through the bed into the windboxes is recycled to the strand for combustion air. The remainder passes first through an inertial separator called a Lurgi Policeman where larger particles are removed. The waste gas then passes into an electrostatic precipitator for final cleanup before being exhausted through the plant stack. It should be noted that the slipstream for the HGMF pilot plant was drawn from the plant duct upstream of the plants' air pollution control devices. No testing was conducted on the plant stack; hence the data contained in this report should not be construed to contain any implications about the actual plant emissions or plant compliance with relevant emission standards at the time of the test program.

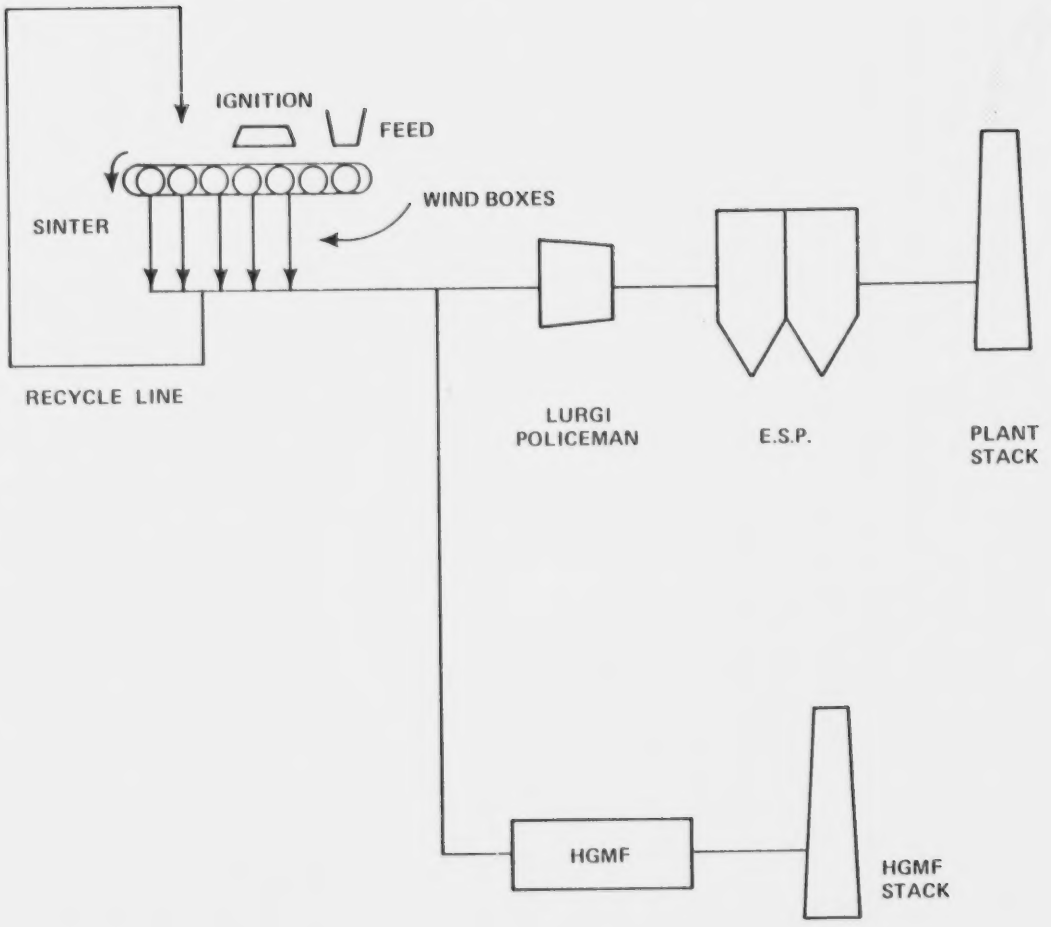

Figure 19. Layout of the sinter strand and the HGMF pilot plant.

INSTALLATION AND STARTUP OF THE PILOT PLANT

The mobile pilot plant arrived at the sinter plant on June 18, 1979, and installation of the exterior piping began. Approximately 40 m of 0.266 m ID (10" Schedule 5) pipe was run from the entrance of the pilot plant to the windbox exhaust, terminating with a 0.266 m nozzle positioned in the center of the 3.6 m diameter plant tunnel. The nozzle faced into the plant gas flow and the ratio of sizes was correct to give isokinetic flow into the nozzle at average plant and pilot plant operating conditions. (As it turned out, the effort to sample the plant gas isokinetically was futile because much of the large-particle concentration was lost in the long run of inlet pipe.) At the point from which the windbox exhaust was sampled, the typical temperature and pressure were 120°C and -9 kPa (-35 inches H_2O) gauge.

The pilot plant blower and stack were installed as planned, and all of the exterior piping was insulated. Additional sampling ports were installed in the piping leading to the pilot plant and in the pilot plant stack to allow EPA Method 5 sampling. The interior sampling ports were suitable for impactor work, but space was insufficient for the more bulky total-mass sampling apparatus.

The power and water connections were made, and initial checkout and debugging of the system began. Since the mobile system operates off a 480 VAC power source, which was not available at the fabrication site in North Carolina, most of the equipment had not been operated prior to the field startup. Operating procedures had to be established, and several problems had to be corrected before the performance characterization could begin. These activities are discussed in the next few paragraphs and are followed by photographs of the final site setup.

Temperature Control

A Universal Model 3500 FA forced-air construction heater (National-Riverside Co., Rancho Cucamonga, CA) was provided with the pilot plant to assist in cold startups. The heater burns propane gas to heat 2400 m^3/hr of air to a maximum temperature of 115°C. A tee and appropriate valving were included in the inlet line to the pilot plant so that the forced-air heater could be used to preheat the pipe coming from the plant tunnel with the assistance of the vacuum in the plant tunnel and then to preheat the interior pilot plant piping with the assistance of the pilot plant blower.

The entire preheat procedure required about 45 minutes to raise all of the piping to approximately 100°C. The flow could then be started from the sinter plant to the pilot plant without a serious drop in the gas temperature. After all of the insulation was installed, the steady state temperature drop from the plant tunnel to the inlet of the pilot plant averaged less than 10°C. From the inlet to the outlet of the pilot plant, the gas temperature normally dropped another 10°C. At the blower the temperature of the gas rose about 30 to 40°C.

Blower Noise

The noise level produced by the 3600 rpm pilot plant blower was initially unacceptable. A ventilated, double-insulated house was erected around the blower, which reduced the noise level, but the high-pitched sound emanating from the top of the stack was still far above background noise levels. A stack muffler was designed by the sinter plant superintendent, and fabricated by the plant shop. The muffler consisted of a 1-m long section of the 0.266 m diameter pipe drilled with approximately 1600 equally-spaced 1-cm holes. This pipe was then placed inside a larger-diameter cylinder, and the annular space was filled with fiber glass insulation. The ends of the internal pipe were flanged, and it was installed between the top two sections of the stack. The ends of the annular space were capped to prevent rain damage to the insulation. The muffler dramatically reduced the blower noise to an acceptable working level.

Filter Construction and Cleaning

Preliminary tests with the filter cleaning system demonstrated that the fundamental design was sound. The pressurized chambers emptied virtually instantaneously when the Galigher valves were actuated, providing the desired pulse through the filters. Operation of the system for a few hours indicated that a cycle time of 10 to 15 minutes and a cleaning air pressure of 170 kPa gauge (25 psig) should be sufficient to keep the filters clean. The cleaning pulse was so strong, in fact, that the shape of the initial test filters was found to be distorted when the magnet canisters were opened. The steel wool used in the initial tests was AISI Type 430 stainless steel as used before, but it had been donated by a new supplier for the field tests. It contained an abundance of

very fine fibers (50 μm diameter or less) that became brittle after a few hours of operation, contributing to the degradation of the filters' mechanical strength. To correct these problems, a stronger set of filter backup screens was fabricated from expanded metal, and a new supply of steel wool was obtained from the original source that had proven satisfactory in the lab pilot plant tests. Plans were also made to upgrade the density of the filter for the performance characterization since the results from the initial tests indicated an outlet dust loading of 110 to 180 mg/Nm^3, well above the desired level of 46 mg/Nm^3 (0.02 gr/DSCF).

Magnet Operation

Several minor problems were experienced initially with the magnets, but they were all corrected easily. Improper voltage indications led to the discovery of two errors in the field-wiring of the bus cables and power supply instrumentation. The safety interlock system tripped the magnets several times until this problem was traced to insufficient coolant flow. A small booster pump was added to the cooling water line. Later the differential pressure switch on Magnet B was replaced when it was found to be faulty. One of the power supplies failed after the first few hours of operation. The troubleshooting procedure in the operating manual indicated a faulty gate card (one of several internal circuit boards), which was replaced. The problem recurred later and a second gate card had to be replaced. Evidently the cards were deficient at the start or were damaged during transport of the trailer because no further problems were experienced during the several hundred hours of operation that followed.

Flow Measurement and Control

A particularly tenacious problem involved finding the source of a discrepancy between the flow indicated by the orifice and that measured with pitot tubes at the sample ports. The flow profiles at the two interior sampling points were reasonably flat and agreed with one another within about 5 percent, but the flow indicated by the orifice was 10 to 100 percent higher than the pitot flow, depending upon the flow conditions.

No significant leaks could be found in the piping system or the instrumentation lines. Finally it was observed that the orifice flanges had been welded only to the butt ends of the pipe and not to the outside of the pipe at the back of the flanges. While this construction was structurally sound, it allowed a small leakage into the flange pressure taps, which was sufficient to produce an error in the indicated orifice pressure drop when the static pressure within the pipe was significantly below atmospheric. A sealant was applied to stop the leakage and the agreement between the orifice and pitots was excellent thereafter.

Appropriate values for the proportional gain and integration constant of the flow controller were set by adjusting these parameters with the pilot plant in operation. The flow controller was capable of maintaining constant flow during the cyclic changes in filter pressure drop and withstood the filter cleaning pulse with no problems. However, occasional, unannounced fluctuations in the static pressure of the windbox exhaust caused the automatic control system to enter an unstable, oscillating condition. Since the flow varied very little with the controller in the manual model and could be corrected quickly by the pilot plant operator if necessary, manual operation was used during most of the test program.

Final Site Setup

Figures 20 through 23 show the HGMF mobile pilot plant installed on the sinter plant site. Figure 20 is a general elevation showing the front of the trailer where the laboratory/control room is located. The stack is visible at the right rear of the trailer with the muffler installed below the top section. Figure 21 shows part of the piping that leads from the windbox exhaust to the pilot plant. The gas enters the trailer via the pipe passing under the steps, turns, and flows toward the rear in the pipe visible through the open door. The clean gas pipe inside the trailer is just behind the dirty gas pipe at the same level above the floor. The interior sampling ports are located in these horizontal runs of pipe. In the left of Figure 21 is the flexible duct to which the propane heater flow was connected during startups. The exterior sampling ports on the dirty side were installed in the vertical section of pipe just above the entrance of the flexible duct.

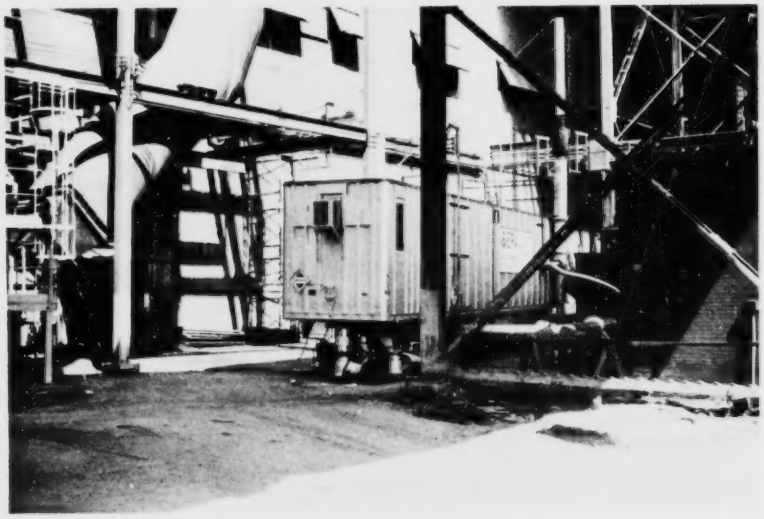

Figure 20. HGMF mobile pilot plant setup at the sintering plant.

Figure 21. Side entrance of mobile pilot plant.

Figure 22 shows closer detail of the clean side pipe, the blower enclosure, and the stack. The recycle line leading from the stack to the blower suction was used when the lowest flow rates were desired in the pilot plant. By establishing a controlled recycle flow the blower could have sufficient flow to remain in the stable operating region. Figure 22 was taken from the rear of the pilot plant and shows the dirty side piping coming over from the plant at the right. The railing around the top of the trailer was added to provide a safe working area at the Method 5 sampling ports, which were located just below the muffler.

PERFORMANCE CHARACTERIZATION

The objectives of the performance characterization were to evaluate the effects of filter density and depth, applied magnetic field strength, and gas velocity on particle collection and to identify the optimal conditions of operation for demonstration during the long-term testing period. A factorial experiment was designed with two levels of filter density, two levels of filter depth, two levels of applied field, and three levels of gas velocity. AISI Type 430 medium grade steel wool purchased from Brillo Purex Company (London, OH) was used to construct all four filters used during the performance characterization. The average equivalent cylindrical diameter of this material was calculated to be 94 μm by measuring the total length and mass of a random sampling of strands removed from the bulk supply.

The particulate sampling procedure utilized throughout the field tests was adopted from EPA guidelines for the use of cascade impactors (Harris, 1977). MRI Model 1502 cascade impactors were used with their substrates precoated with Apiezon H grease and baked at 140°C for two hours. Prior to each run, pitot traverses were run on the two 12-point perpendicular diameters along which each impactor would sample. The nozzle sizes and sample rates were then selected to establish a velocity isokinetic with the average gas velocity in the pipe. During the runs the impactor temperature was controlled to within ±20°C of the stack gas temperature, which ranged from 80 to 137°C. Two control runs conducted with the impactors at 100°C demonstrated an average substrate weight loss of

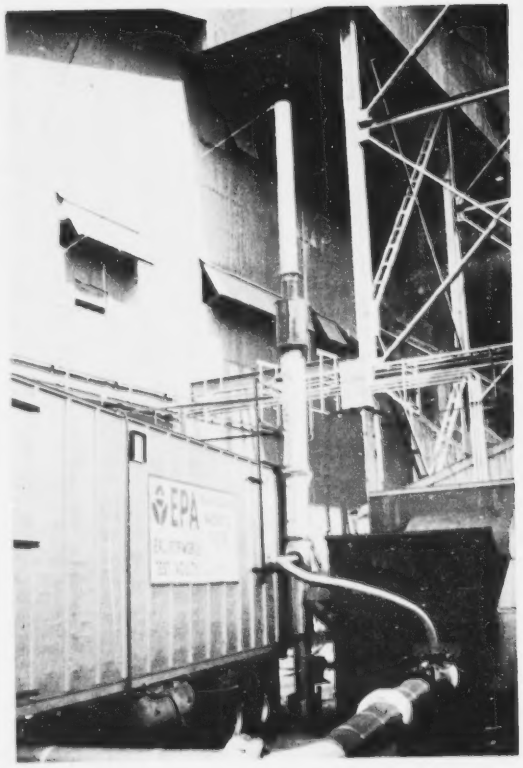

Figure 22. Clean side piping and stack.

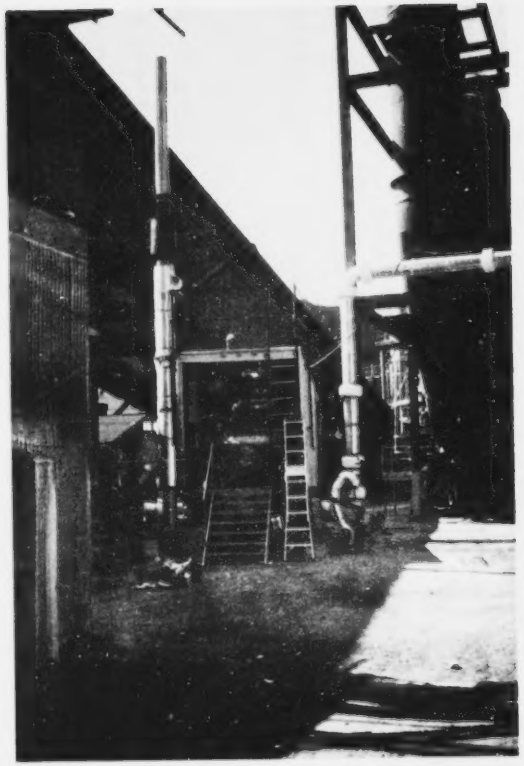

Figure 23. View from rear of pilot plant.

only 0.016 mg. In contrast, the stage accumulations during the actual runs varied from a minimum of 0.03 mg to a maximum of 31.68 mg. More typically, the stage accumulations ranged from 0.5 to 5 mg. All stage weights were determined on a Perkin-Elmer Model AD-2Z microbalance, and stage calibrations for the MRI impactors were taken from Cushing, et al. (1976).

Since the impactors were used external to the pipes, an acetone probe wash was used to recover any material that did not reach the impactors. The dried probe wash normally amounted to about 10 percent of the total catch. This mass was included in the total mass calculations derived from the impactors, but no attempt was made to assign a size to it. Hence, the fractional efficiency calculations ignored the material collected in the probe.

Suprisingly the filter catch ranged from 0.79 to 23.11 mg. In most of the runs, the filter mass dominated the total mass calculations and shifted the mass median diameter to a much lower size than was expected since sinter dust is generally regarded as a coarse material. As mentioned earlier, it is quite probable that some of the larger material dropped out in the pipe leading from the windbox exhaust to the pilot plant. The inlet concentration averaged 318 mg/Nm^3 which is about 30 percent of the value typically reported for sinter plants.

Table 3 summarizes the results obtained during the performance characterization. For additional information, Figures 24 through 29 present the cumulative particle size distributions calculated directly from the experimental data. The curves drawn through the data points were produced by a computerized data reduction scheme. Basically the scheme calculates the stage cut points and then transforms the cumulative distribution versus stage cut points to log-normal space. It then fits a natural cubic spline to the transformed data. After fitting the cumulative distribution data, the procedure differentiates the cumulative curve to obtain the differential distribution. The differential distributions of corresponding inlet and outlet data are then multiplied by the total mass concentrations (excluding the probe washes) and ratioed to obtain the fractional efficiency curve. The fractional efficiency curves of the performance characterization tests are presented in Figures 30 and 31.

Table 3. Results of performance characterization with medium grade steel wool.

Filter	Test No.	Applied Field tesla	Superficial Velocity m/s	Filter ΔP cm H_2O	Temperature °C	Collection Efficiency %	Outlet Concentration mg/Nm^3 (wet)
#1	08042	0.25	3.6	9	107	56.6	96
F=0.010	08041	0.25	4.4	11	114	51.9	107
L=0.20m	08031	0.25	5.7	18	137	0.0	166
	08062	0.50	3.8	9	121	48.7	122
	08051	0.50	3.9	11	135	46.6	126
	08061	0.50	4.9	17	120	51.1	103
	08082	0.50	7.9	32	127	66.1	134
#2	08183	0.25	3.0	89	95	94.5	29
F=0.014	08182	0.25	6.4	102	98	83.4	36
L=0.30m	08181	0.25	8.8	109	109	75.7	66
	08231	0.50	6.5	76	101	76.1	22
	08222	0.50	7.9	114	99	69.9	83
#3	08291	0.25	3.8	38	107	78.2	75
F=0.010	08282	0.25	5.9	44	100	90.5	32
L=0.30m	08281	0.25	7.7	79	104	91.2	29
	08292	0.50	3.9	31	128	81.5	55
	08301	0.50	6.0	72	106	87.2	50
	08302	0.50	6.9	114	93	87.7	86
#4	09021	0.25	3.7	18	93	85.6	62
F=0.014	09013	0.25	5.8	41	87	83.9	61
L=0.20m	09012	0.25	7.4	66	95	86.2	38
	09031	0.50	4.0	25	98	86.7	84
	09032	0.50	5.8	64	104	79.6	39
	09033	0.50	7.9	76	110	74.4	69

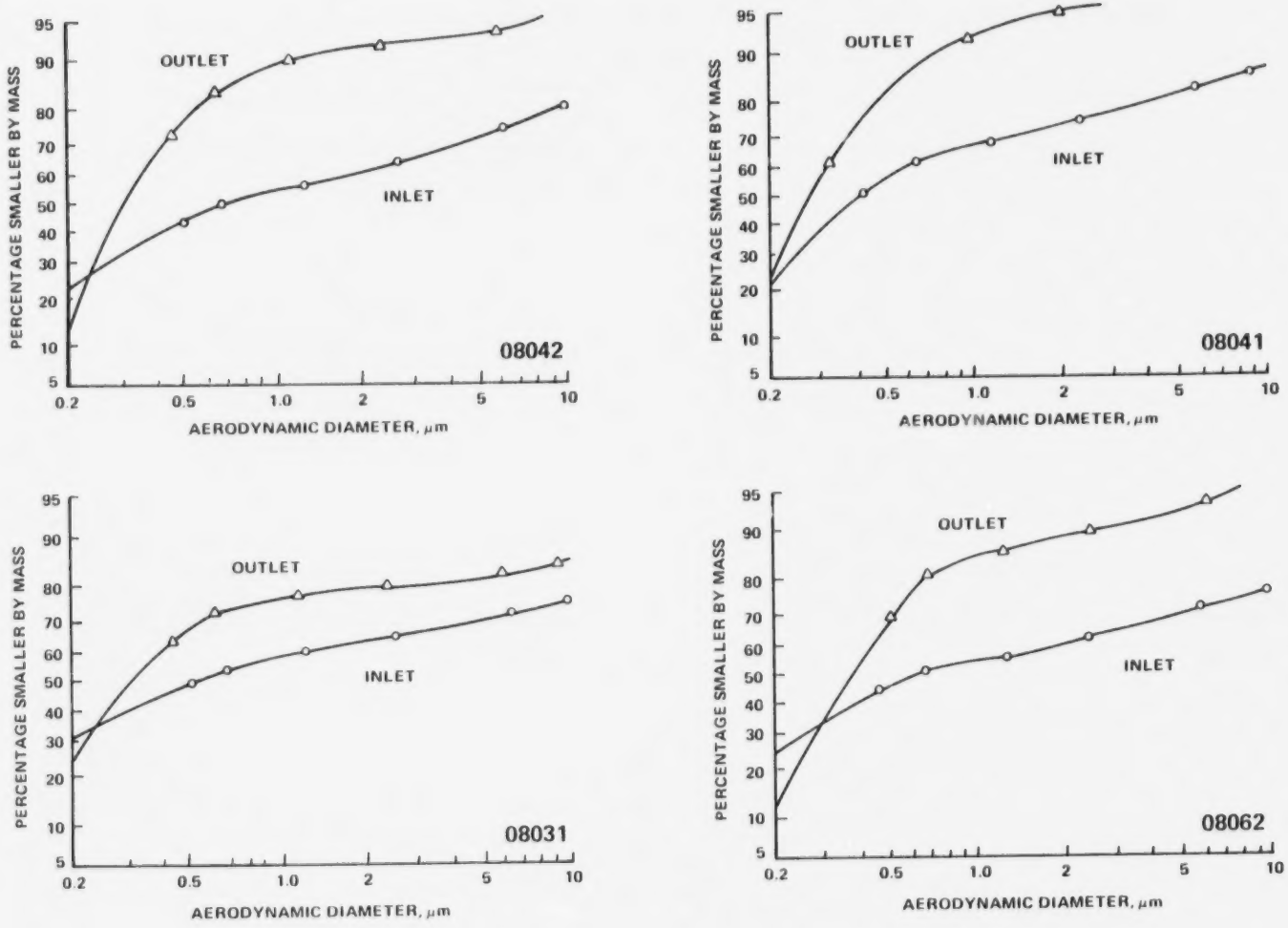

Figure 24. Size distributions from test nos. 08042, 08041, 08031, and 08062.

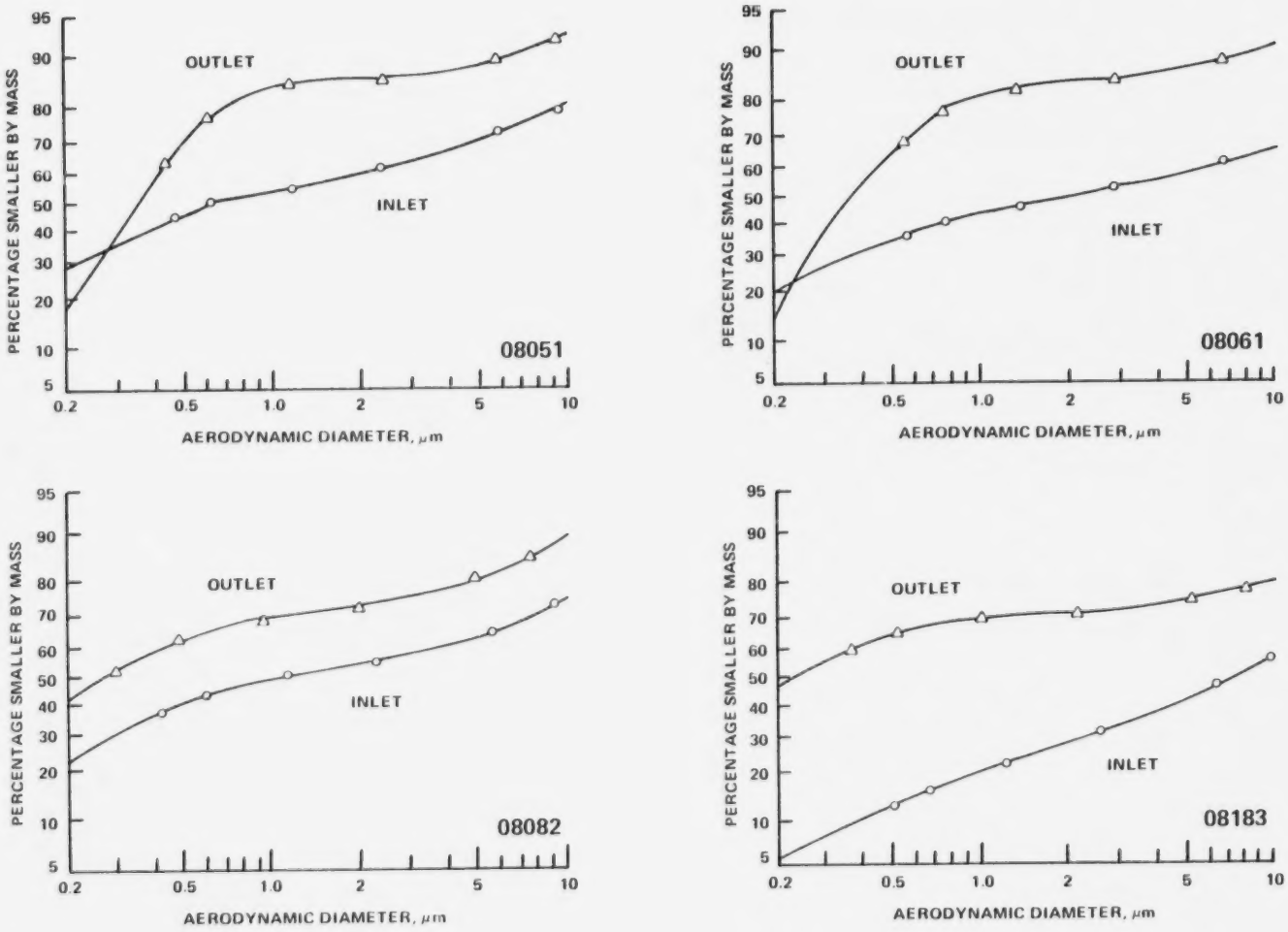

Figure 25. Size distributions from test nos. 08051, 08061, 08082, and 08183.

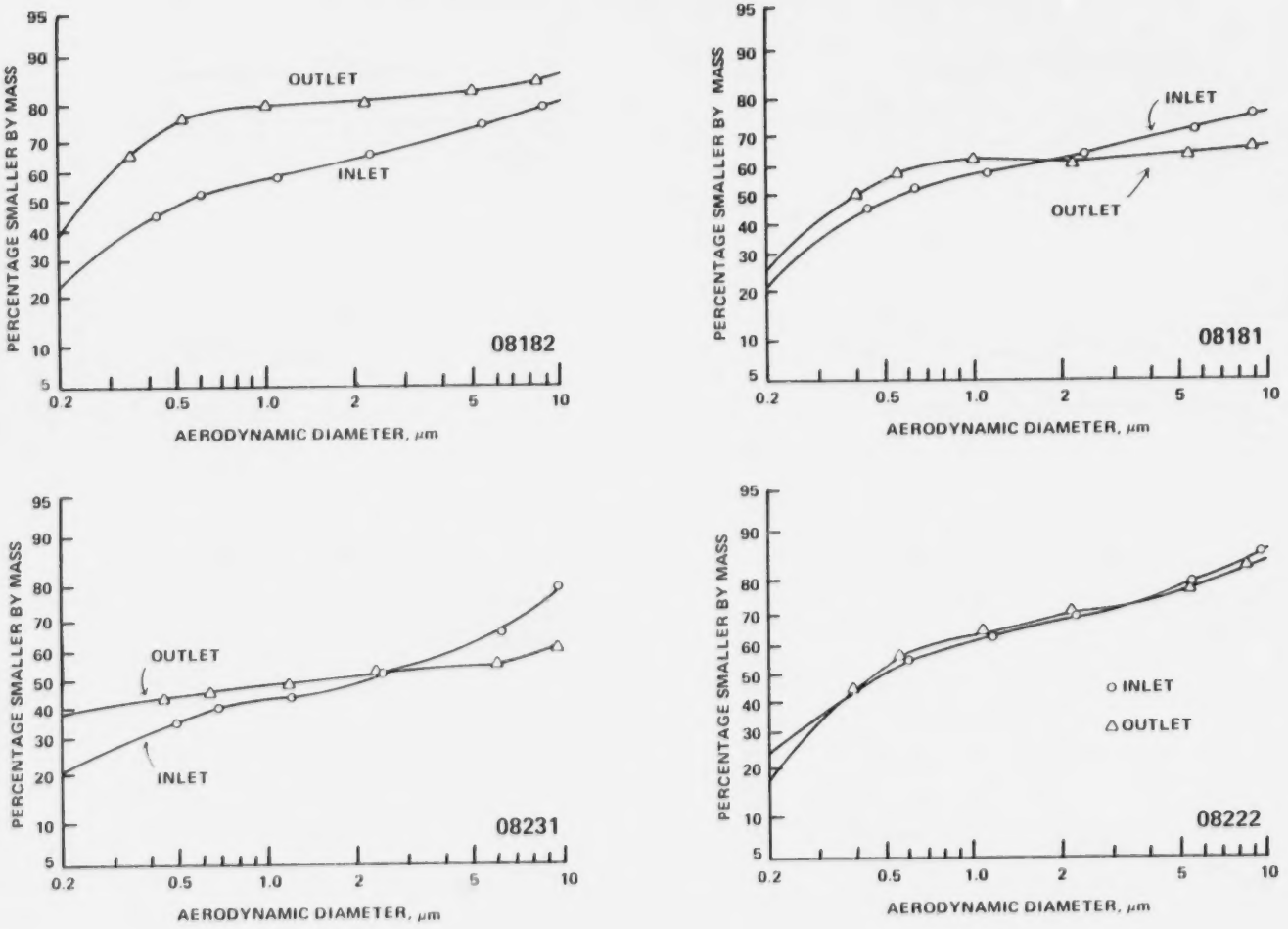

Figure 26. Size distributions from test nos. 08182, 08181, 08231, and 08222.

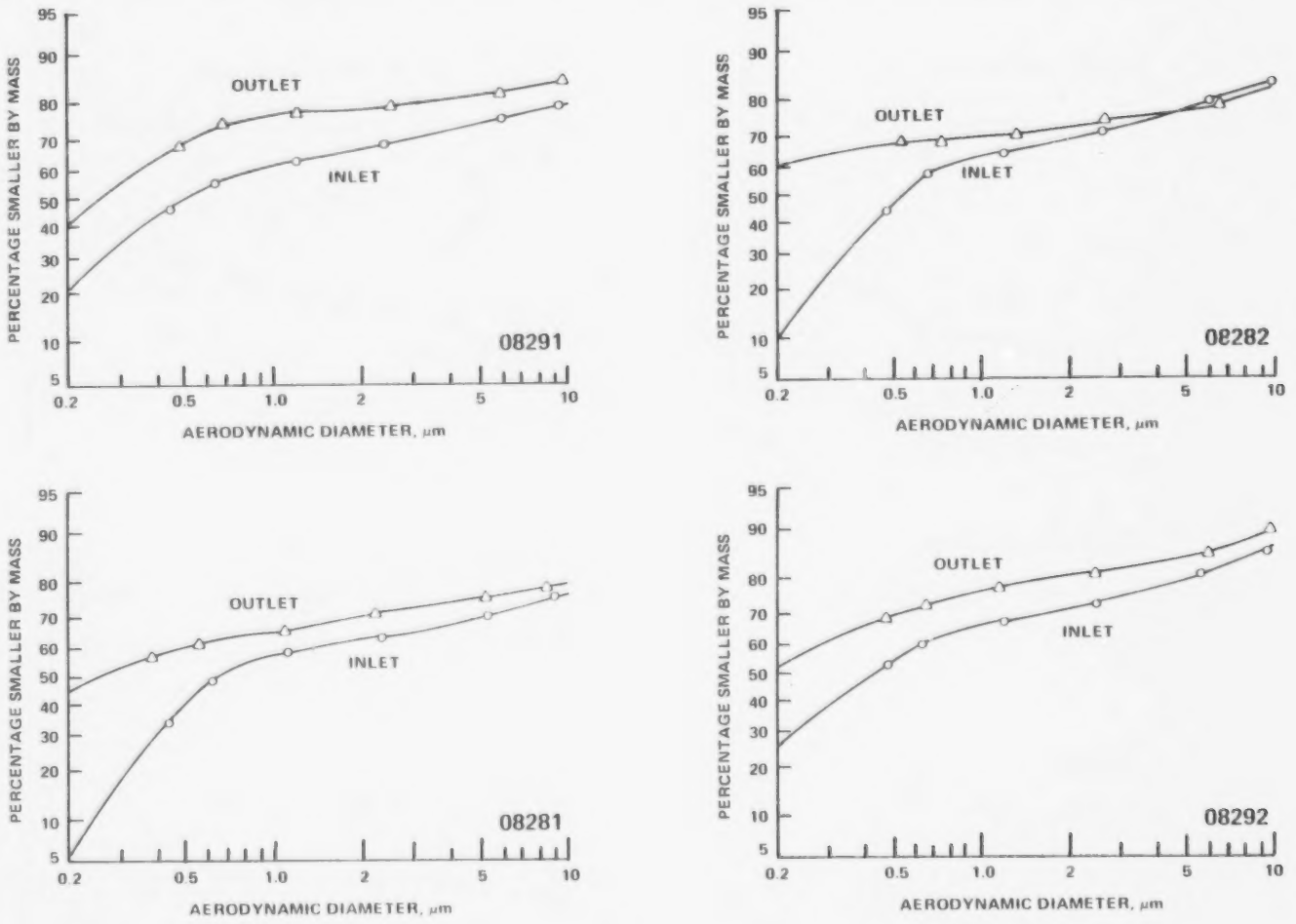

Figure 27. Size distributions from test nos. 08291, 08282, 08281, and 08292.

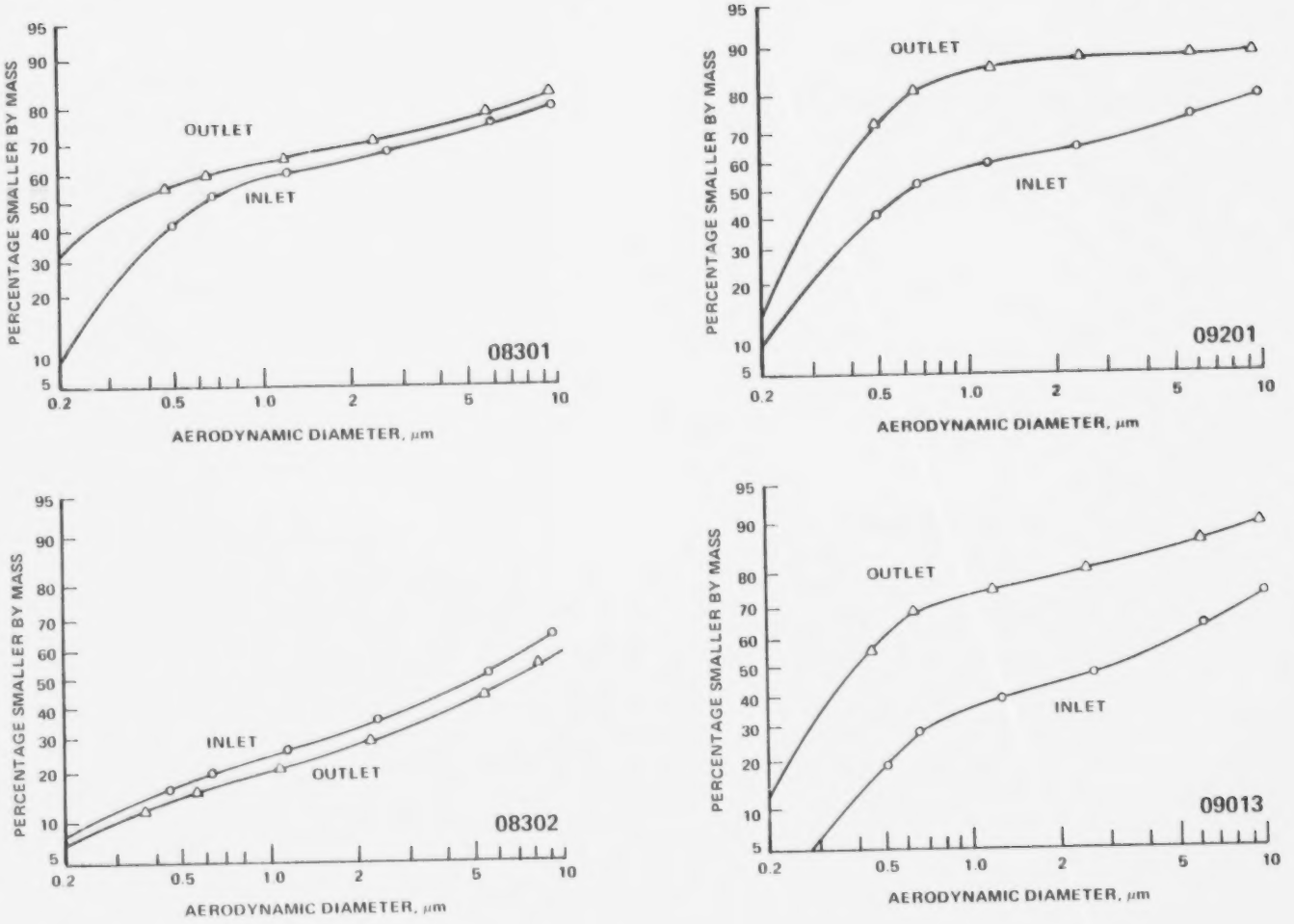

Figure 28. Size distributions from test nos. 08301, 09201, 08302, and 09013.

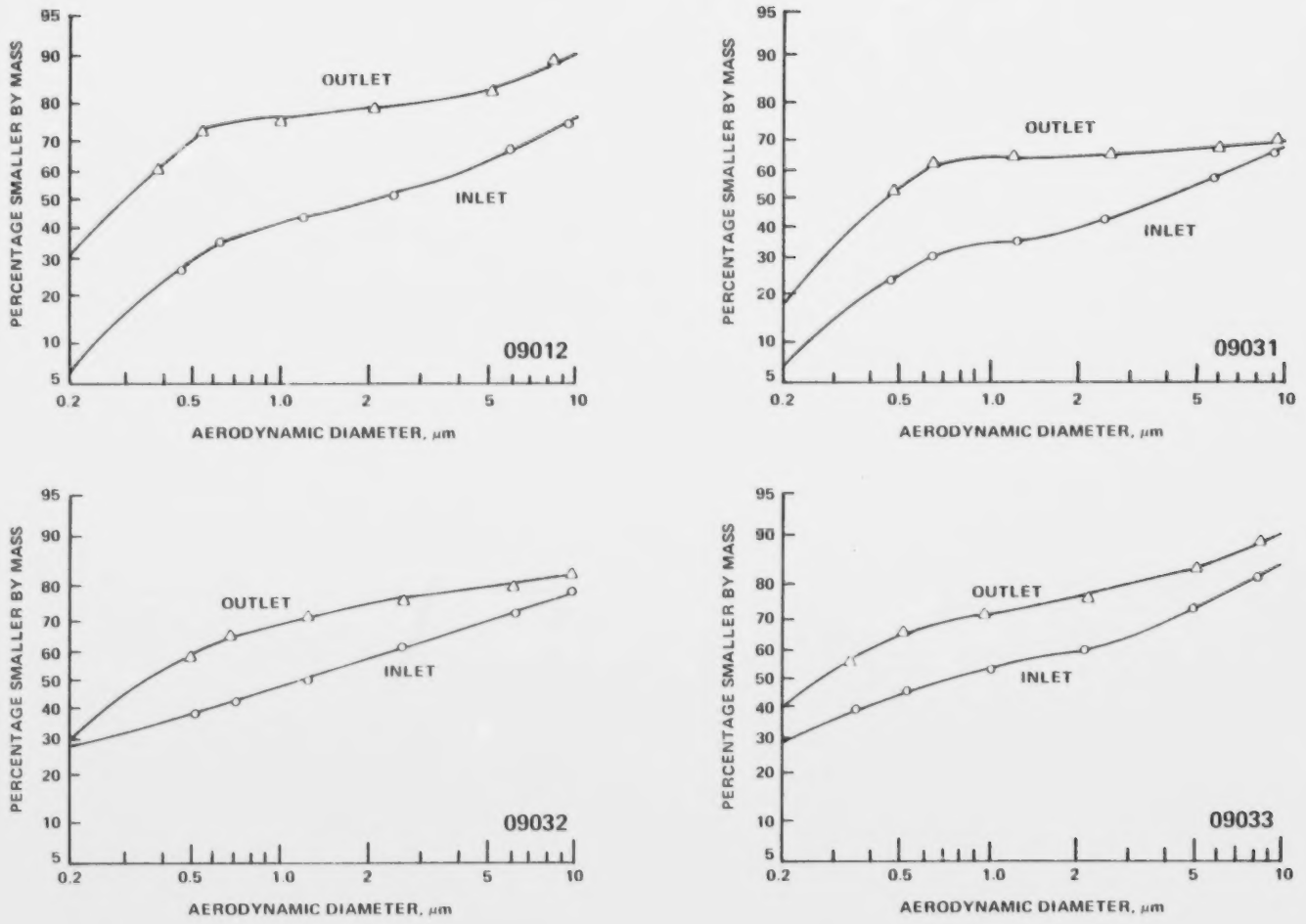

Figure 29. Size distributions from test nos. 09012, 09031, 09032, and 09033.

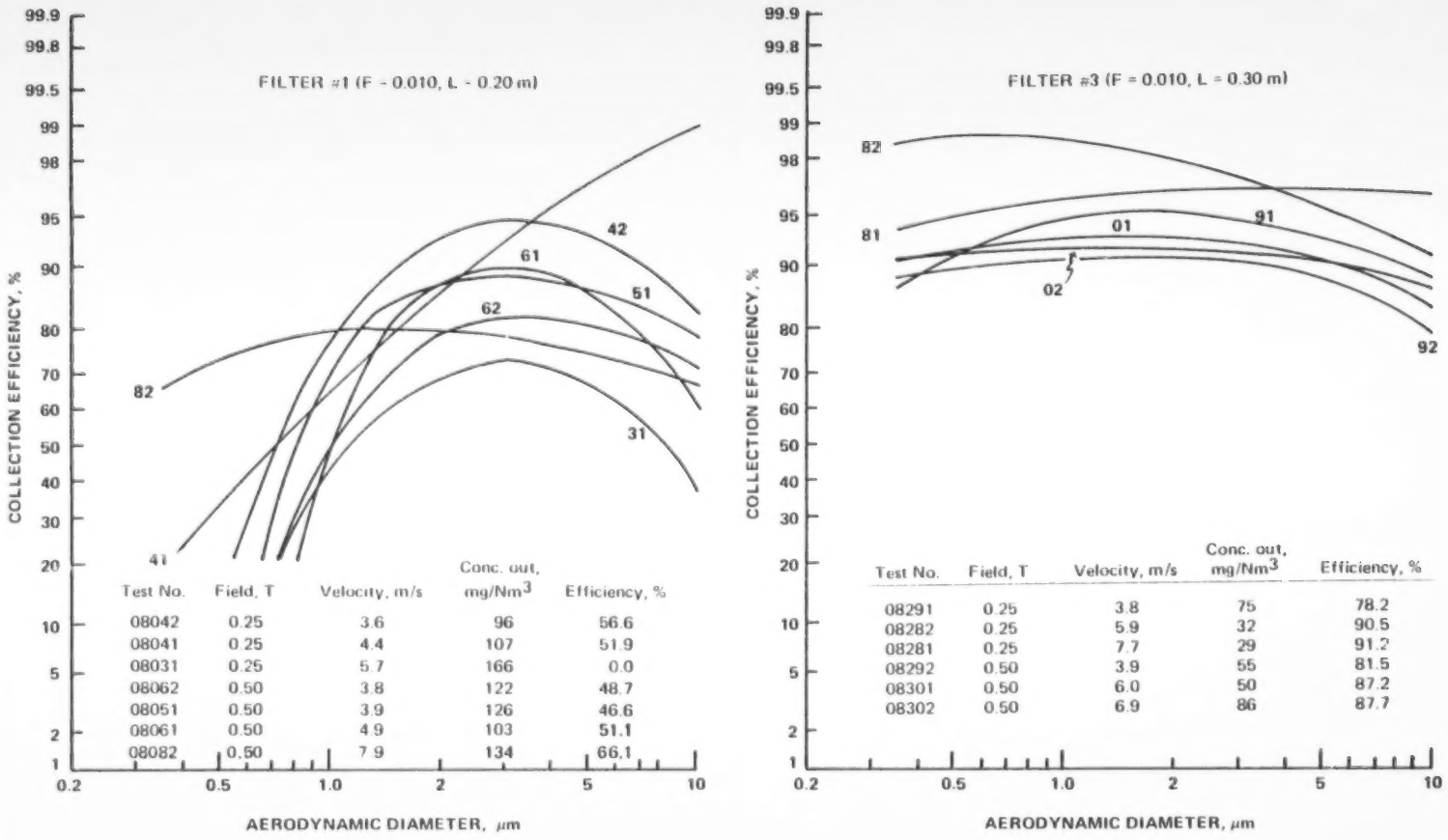

Figure 30. Fractional efficiency curves from tests conducted on filter nos. 1 and 3.

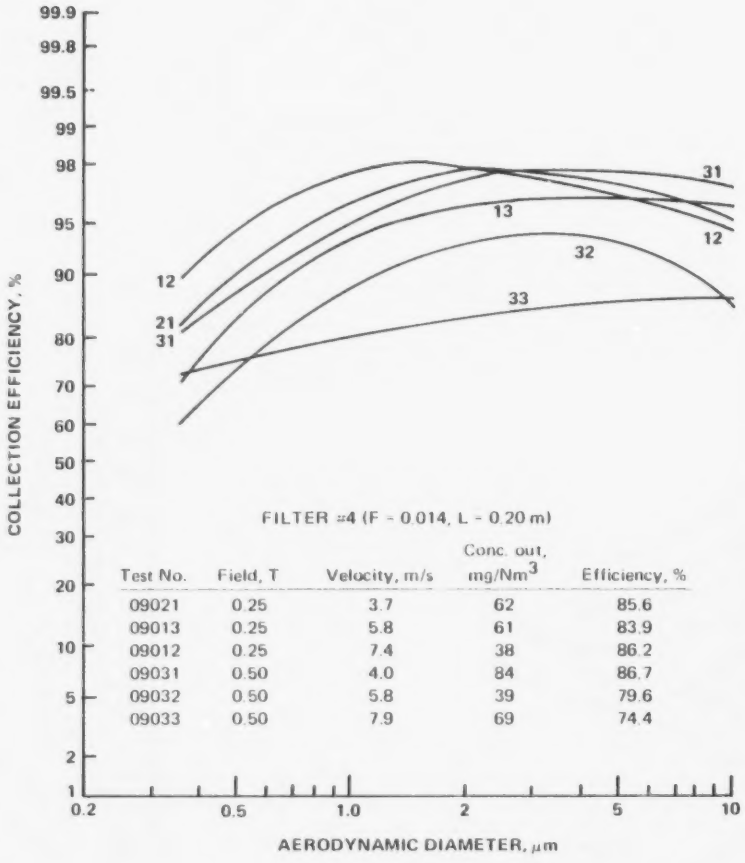

FILTER #4 (F = 0.014, L = 0.20 m)

Test No.	Field, T	Velocity, m/s	Conc. out, mg/Nm^3	Efficiency, %
09021	0.25	3.7	62	85.6
09013	0.25	5.8	61	83.9
09012	0.25	7.4	38	86.2
09031	0.50	4.0	84	86.7
09032	0.50	5.8	39	79.6
09033	0.50	7.9	69	74.4

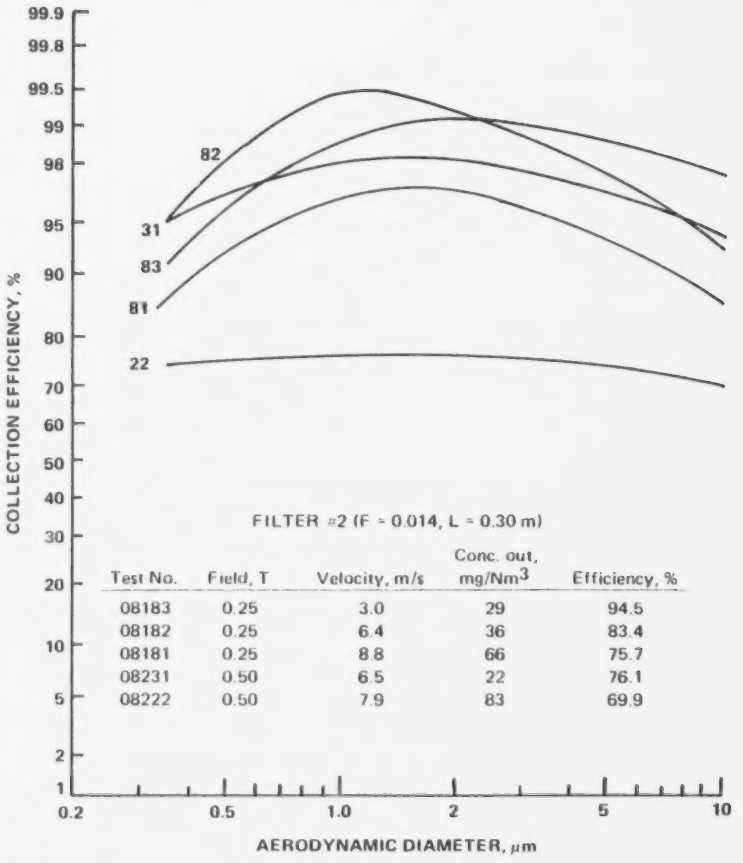

FILTER #2 (F = 0.014, L = 0.30 m)

Test No.	Field, T	Velocity, m/s	Conc. out, mg/Nm^3	Efficiency, %
08183	0.25	3.0	29	94.5
08182	0.25	6.4	36	83.4
08181	0.25	8.8	66	75.7
08231	0.50	6.5	22	76.1
08222	0.50	7.9	83	69.9

Figure 31. Fractional efficiency curves from tests conducted on filter nos. 2 and 4.

The cubic spline procedure tends to produce multimodal efficiency curves that can result from real effects of the collection device, from artifacts of the impactor, and from random error in the data. The curves shown in Figures 30 and 31 have been smoothed for clarity to show only the dominant behavior. A more complete explanation of the merits of the natural cubic spline and other impactor data-fitting procedures is given by Lawless (1978).

The goal for the outlet concentration was set at 46 mg/Nm^3 to correspond with typical regulatory requirements. Table 3 reveals that this goal was achieved in several of the tests, but the lowest filter pressure drop under which it was accomplished was 44 cm H_2O--a value that is probably too high for practical application of HGMF to particulate control. The data also show several features with respect to parametric effects. First, in Table 3 there is no consistent correlation of pressure drop with gas velocity and filter characteristics because the filters showed a tendency to plug during the test series. Thus, most of the pressure drop figures are not clean filter values, but correspond to some partially plugged state. A cycle duration of 16 minutes was used during most of the tests with a cleaning air pressure of 275 kPa (40 psig). With filter #2, which was the most troublesome with respect to plugging, the cycle time was reduced to 8 minutes, but plugging was still a problem.

The performance characterization data also show a lack of correlation of either collection efficiency or outlet concentration with gas velocity or applied magnetic field. They do demonstrate with reasonable consistency that increasing either filter depth or density increases the collection efficiency and reduces the outlet concentration. For example, direct comparison of filter nos. 1 and 3 in Figure 3 adequately demonstrates the effect of filter depth, while comparison of filter nos. 1 and 4 shows the filter density effect. During the performance characterization several observations were made:

(1) The dust passing through the HGMF was extremely fine as evidenced by the size distribution curves shown in Figures 24 through 29. Furthermore, there was a marked difference in appearance between the inlet dust and the outlet dust and between the larger dust and the finer dust. The larger inlet dust, which was collected with higher efficiency, was typically of a reddish-brown or reddish-gray color indicative of iron oxides. The finer dust that escaped was either white or light gray. Plans were made to collect samples for magnetic and chemical analyses.

(2) Although the outlet concentration goal was attained, the tendency of the filter to plug made it doubtful that this mode of operation could be sustained over a long period of time. In addition, the pressure drops experienced were impractically high. The plugging also changed, at least to some extent, the collection mechanism from HGMF to cake filtration, rendering the mathematical model of the process invalid. (The model also assumes homogeneous particle composition with size, which was clearly not true in this application.) Plans were made to try a more coarse grade of steel wool in the long-term testing period in hopes of improving the cleanability of the filter while achieving satisfactory collection.

(3) During most of the performance characterization the opacity of the pilot-plant stack plume was less than 5 percent when viewed against a blue sky in accordance with the Ringleman procedure, but when viewed against a dark background, a blue or white plume was always visible. Also the opacity increased noticeably for a few seconds each time the filter cleaning pulse was released. The Climet particle size analyzer was used to conduct a limited study of transient emission effects. The results of this work are reported in Section 8.

LONG-TERM TESTING

The overall objective of the long-term test program was to demonstrate the effectiveness and reliability of the HGMF collection process over an operating period of at least 500 hours. To have practical significance this meant that the throughput of the pilot plant should be high enough to lead to a reasonable projection of capital cost (>1500 m^3/hr); that the outlet concentration should be low enough to meet typical emission regulations (< 46 g/Nm^3); that the filter pressure drop should stabilize at a level that would project to reasonable operating costs (< 30 cm H_2O); and that all of the equipment, especially the magnetic filters and the cleaning apparatus, should function continuously without an excessive number of forced shutdowns. Table 4 is a condensed log of the 500 hours of operation accumulated during the long-term test period. The highlights are discussed in more detail below.

The long-term operations began on September 12, 1979. The first filters loaded into the magnet canisters were made of medium-grade steel wool because the coarse-grade material had not yet been received from the vendor. The filters had a depth of 0.20 m and a packing density of 0.015.

Table 4. Operating log of the long-term test period.

Time, Date	Cumulative Time of Operation, Hrs.	Observations
1615, 9/12/79	0	Start with filter #5: Medium-grade steel wool, F=0.015, L=0.20 m Applied field = 0.25 T Superficial velocity = 4.8 m/s (2550 m^3/hr) Initial ΔP = 20 cm H_2O Cycle duration = 10 min Cleaning air pressure = 275 kPa gauge Inlet gas temperature = 93°C
0100, 9/13/79	8.8	Temperature = 79°C; filter ΔP = 31 cm H_2O; reduced cycle duration to 8 min
0515, 9/13/79	13.0	Temperature = 69°C; filter ΔP = 39 cm H_2O; stopped inlet gas flow and warmed system to 100°C with hot air while operating cleaning system
0553, 9/13/79	13.0	Restarted inlet gas flow; filter ΔP = 41 cm H_2O
0750, 9/14/79	39.0	Filter ΔP has continued to be a problem, now at 34 cm H_2O; temperature = 80°C; stopped inlet gas flow and warmed system to 100°C with hot air while operating cleaning system
0850, 9/14/79	39.0	Restarted inlet gas flow; filter ΔP = 25 cm H_2O
1601, 9/14/79	46.1	Stopped system, compressor is not filling cleaning tanks to desired pressure
Sinter strand down for several days for annual maintenance		
1515, 9/22/79	46.1	Start with filter #6: Coarse-grade steel wool, F=0.015, L=0.20 m Applied field = 0.25 T Superficial velocity = 4.8 m/s (2550 m^3/hr) Initial ΔP = 9 cm H_2O Cycle duration = 8 min Cleaning air pressure = 275 kPa Inlet gas temperature = 100°C
1635, 9/23/79	71.4	Ringlemann reading 8%
1030, 9/24/79	89.4	Filter ΔP = 14 cm H_2O, running well but shut down briefly for compressor maintenance
1300, 9/24/79	89.4	System backup, Ringlemann reading 5%
0552, 9/24/79	106.2	Valve V7B not opening fully; system shut down to investigate problem
0616, 9/25/79	106.2	System back up; V7B working correctly

Table 4. (continued)

1100, 9/26/79	111.0	Tank A is filling to 210 kPa and Tank B is filling to 420 kPa; shut down to investigate; Tank B is filling via leak in diaphram of Pinch Valve B; Adjusted actuator pressure and program cycle to correct
1130, 9/26/79	111.0	System restarted; tanks filling to 275 kPa
0700, 9/27/79	154.5	Shut down for weekly maintenance on sinter strand
1705, 9/27/79	154.5	System restarted as before; filter ΔP = 11 cm H_2O; collected samples of stack particulate and dump from cyclone hopper
1345, 9/28/79	175.2	Shut down to check operation of flow controller
1400, 9/28/79	175.2	Back on line
1716, 9/28/79	178.4	Inlet gas temperature hit, highest value of 149°C; filter ΔP = 11.4 cm H_2O;
0800, 9/30/79	217.2	Shut down to change filter
1620, 9/30/79	217.2	Start with filter #7: Coarse-grade steel wool, F=0.0175, L=0.20 m Applied field = 0.25 T Superficial velocity = 6.5 m/s (3400 m^3/hr) Initial ΔP = 22 cm H_2O Cycle duration = 10 min Cleaning air pressure = 275 kPa Inlet gas temperature = 117°C
10/2/79 - 10/3/79		Steel company research team is conducting emissions tests on HGMF pilot plant; Ringlemann reading about 10%
1030, 10/3/79	273.3	Valve V7B malfunctioning again; shut down to check
1100, 10/3/79	273.3	System back up so that testing teams can finish; V7B is not functioning properly but won't affect tests
1400, 10/3/79	276.3	Stack testing completed; shut down to replace V7B with spare
1540, 10/3/79	276.3	System back up and operating as before
1110, 10/4/79	295.8	Sinter strand tripped; HGMF flow continued
1120, 10/4/79	295.8	Strand back on
2400, 10/4/79	308.5	System running well; filter ΔP = 20 cm H_2O; shutdown to give RTI operators time off and to accomodate weekly maintenance on sinter strand
1730, 10/9/79	308.5	System restarted; same filter and operating parameters as before

Table 4. (continued)

2250, 10/9/79	313.8	Filter ΔP up to 25 cm H_2O; decreased cycle time to 8 min
10/10/79 - 10/11/79		RTI team is conducting emissions tests on HGMF pilot plant; Ringlemann reading about 10%; collected dust samples for analysis
1120, 10/12/79	374.3	Sinter strand down for unscheduled maintenance; shut off HGMF
1330, 10/12/79	374.3	Sinter strand and HGMF back on line
2340, 10/17/79	504.5	Duration goal achieved; system shut down; final filter ΔP = 21 cm H_2O.

Since increasing the magnetic field strength had resulted in no significant improvement in collection efficiency during the characterization runs, the field was set at the lower value. A moderate flow rate of 2550 m^3/s was selected for initial operation.

As expected, the first filter developed problems with plugging, particularly at night when the inlet gas temperature dropped to as low as 70°C. On two occasions the sinter gas flow was stopped temporarily and the filters were flushed with hot air and backflushed with pulse air to loosen the deposits that accumulated. After 46 hours of operation, the system was shut down due to an apparent compressor malfunction that was not allowing the cleaning air tanks to fill properly.

The pilot plant remained down for 8 days while scheduled annual maintenance was conducted on the sinter strand. During this time the pressurized air problem was investigated but not completely resolved. A new filter of Purex coarse-grade steel wool was inserted, and the pilot plant was restarted on September 22 with the same operating parameters used with the first filter. In contrast to the medium-grade steel wool, which exhibited a clean filter ΔP of 20 cm H_2O at 2550 m^3/hr, the coarse-grade filter showed an initial ΔP of only 9 cm H_2O at the same flow. The equivalent diameter of the coarse fibers was determined to be 195 μm. Over 171 hours of operation the second filter experienced no significant plugging problems. Ringlemann readings taken on the pilot plant stack on two occasions were 8 percent and 5 percent. A sample of the stack dust was collected in an alundum thimble for chemical and magnetic analysis, but no quantitative stack testing was conducted.

During the operation of the second filter, the air pressure problem was traced to a leak in the diaphragm of one of the pinch valves. The leak allowed a flow of actuator air from between the housing and diaphragm of the valve into the cleaning air tank and into the clean side of the pilot plant flow. This malfunction created an imbalance in the tank pressures and also resulted in an air consumption rate beyond the capacity of the pilot plant compressor. The leakage problem was minimized and the tank pressures were balanced by adjusting the actuator pressure and by changing the duty cycle of the valves so that each would be closed (air-actuated) only when the corresponding tank needed to be filled.

The remaining deficit in air capacity was made up by tying into the compressed air system of the sinter plant.

The pilot plant was shut down on September 30 to change filters in preparation for emission testing. Since the coarse steel wool had shown no tendency to plug, the packing density of the new filters was increased to 0.0175, and the flow was increased to 3400 m^3/hr. An increase in efficiency was anticipated with the increased packing density. The flow rate was increased since the performance characterization had shown velocity to have no detrimental effect on collection, and higher flow rates naturally lead to more favorable capital cost projections.

The system was restarted on the same day with an initial filter ΔP of 22 cm H_2O. With the exception of the pinch valve and a sticky butterfly valve, all components of the pilot plant functioned perfectly for 287 more hours of operation. Four particulate concentration tests were conducted by a team from the steel company, and two were conducted by RTI personnel. The results of the tests are summarized in Table 5, which shows the mean of each measured parameter plus or minus one standard deviation. Both testing groups used EPA Method 5 on the outlet. The concentrations reported represent material collected in the probe and on the filter. The impinger filtrate proved to be negligible. The steel company used alundum thimbles for inlet sampling, and the RTI team ran two additional outlet tests with MRI impactors for comparison to the Method 5 results.

The outlet concentrations determined by the RTI sampling team are somewhat lower than those measured by the steel company team; but unfortunately even the lower values are well above the goal of 46 mg/Nm^3. Ringlemann readings on the light blue plume averaged less than 10 percent during both test periods although higher-opacity puffs occurred during each filter cleaning. The outlet size distributions determined by RTI's impactor samples are shown in Figure 32. They demonstrate that the outlet dust was extremely fine, having a mass median aerodynamic diameter of 0.2 to 0.3 μm. Comparison of the total mass results obtained from the impactors with the simultaneous Method 5 results indicate good agreement. Hence the outlet total mass concentrations obtained during the performance characterization should be valid.

Table 5. Efficiency testing during long-term operation (filter #7).

Test Team	Location	Temperature °C	Water Content %	Dust Concentration mg/Nm^3 (dry)	Collection Efficiency %
Steel	Inlet	96 ± 13	11.3 ± 1.0	550 ± 25	-
Steel	Outlet	136 ± 6	10.5 ± 0.3	260 ± 66	53*
RTI	Outlet	142 ± 9	8.3 ± 3.8	185 ± 45	66*
RTI	Outlet (MRI)	101 ± 0	-	190 ± 11	65*

*Based on ratio of indicated mean outlet concentration to the mean inlet concentration measured by the steel company sampling team.

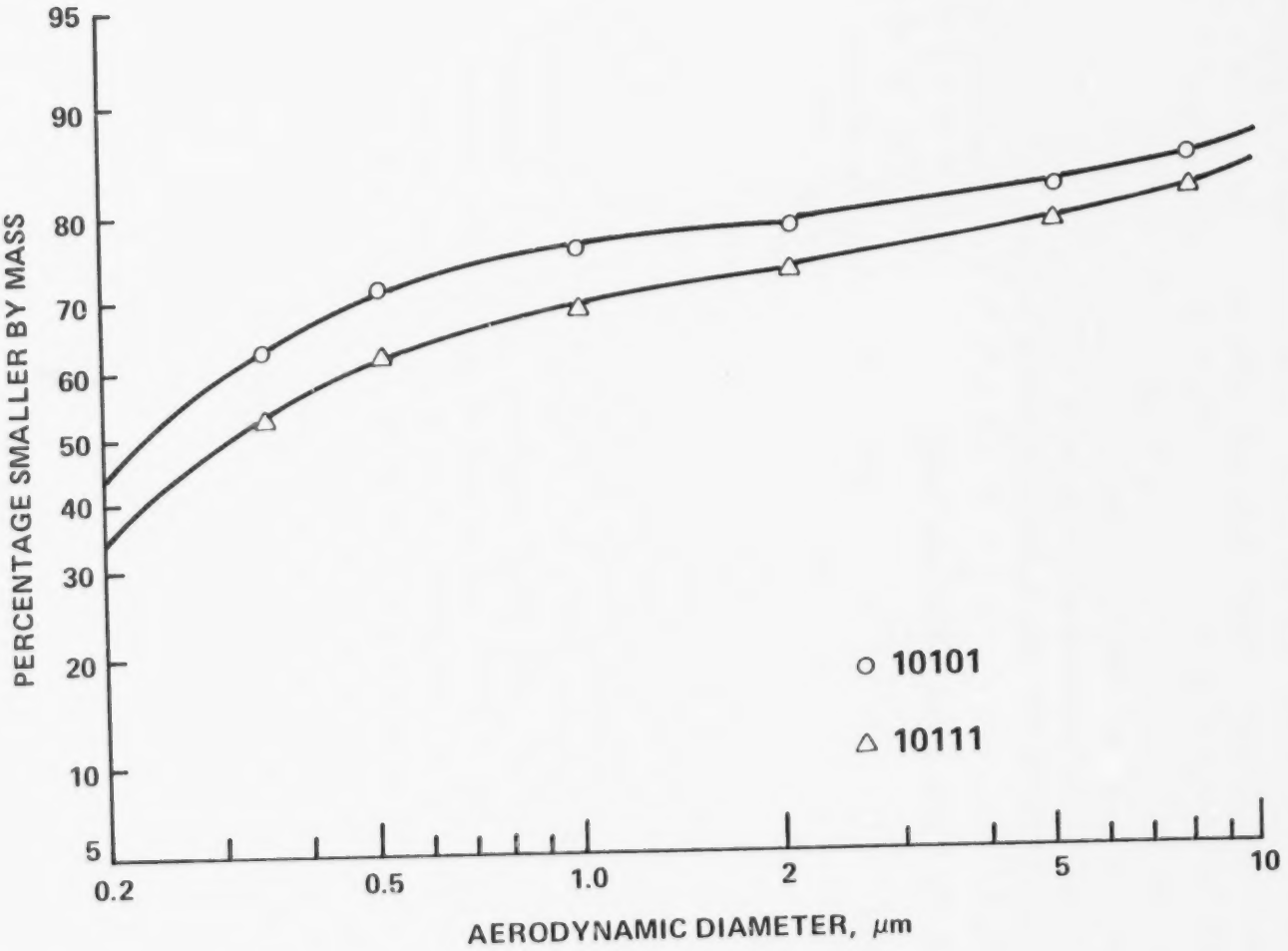

Figure 32. Outlet particle size distributions obtained during total mass sampling.

In summary, after the coarse-grade steel wool was inserted as a filter material, the pilot plant performed in a relatively trouble-free manner for over 450 hours. The pressure drop remained constant at a level lower than the pre-operational goal with a flow rate higher than the goal. But the particulate concentration tests showed that the magnetic filter could not remove a sufficient percentage of the very fine fraction of the dust while operating under these practical conditions. The reasons for the unsatisfactory collection are discussed in Section 8.

ADDITIONAL TESTS WITH COARSE-GRADE STEEL WOOL

Since a few days remained for field work at the end of the long-term operation, a brief series of additional tests was conducted with coarse steel wool. The objectives were to make a final effort at achieving low outlet concentrations under practical operating conditions and to take a second look at the effects of magnetic field strength and velocity on collection without the interference of filter plugging. The new filters were made with the same packing density as the last filter used in the long-term testing (F=0.0175) and the full available depth of the canisters (L=0.30 m). Two velocities and two fields were used and one of the four operating conditions was duplicated. Both EPA Method 5 and impactor sampling were conducted. In addition, one inlet and one outlet test were run with an alundum thimble to collect sufficient material for chemical and magnetic analysis. The results of the efficiency tests are summarized in Table 6. Cumulative particle size distributions are presented in Figure 33, and the fractional efficiency curves are shown in Figure 34.

The duplicate runs (10231 and 10271) exhibited a significant difference in the outlet concentration that was directly attributable to a similar difference in the inlet concentration. The collection efficiency of the two runs was approximately the same. Comparison of the corresponding Method 5 and outlet impactor results showed good agreement on total concentration with the exception of test no. 10241. The impactor sample of test no. 10241 showed an outlet concentration close to the established goal, but this low concentration was suspect because it was not confirmed by the corresponding Method 5 test.

Table 6. Additional testing with coarse grade steel wool (filter #8).

Impactor Tests

Test No.	Applied Field tesla	Superficial Velocity m/s	Filter ΔP cm H_2O	Temperature °C	Collection Efficiency %	Outlet Concentration mg/Nm^3 (wet)
10231	0.25	4.0	15	97	58.3	218
10271	0.25	4.4	14	80	54.1	125
10251	0.25	8.8	62	99	51.2	149
10261	0.50	3.9	13	86	41.9	185
10241	0.50	8.5	51	98	89.8	62

Total Mass Tests

Test No.	Location	Temperature °C	Water Content %	Flow Nm^3/hr (dry)	Dust Concentration mg/Nm^3 (dry)	Collection Efficiency %
10231	Outlet	133	6.1	1270	227	-
10271	Outlet----------Sampling Equipment Malfunction----------					
10251	Outlet	134	8.4	2830	187	-
10251	Outlet*	134	6.6	-	172	-
10261	Inlet*	92	7.0	-	488	54.5
10261	Outlet	129	10.8	1370	222	
10241	Outlet	135	9.1	2900	192	-

*Using alundum thimble in lieu of Method 5 filter.

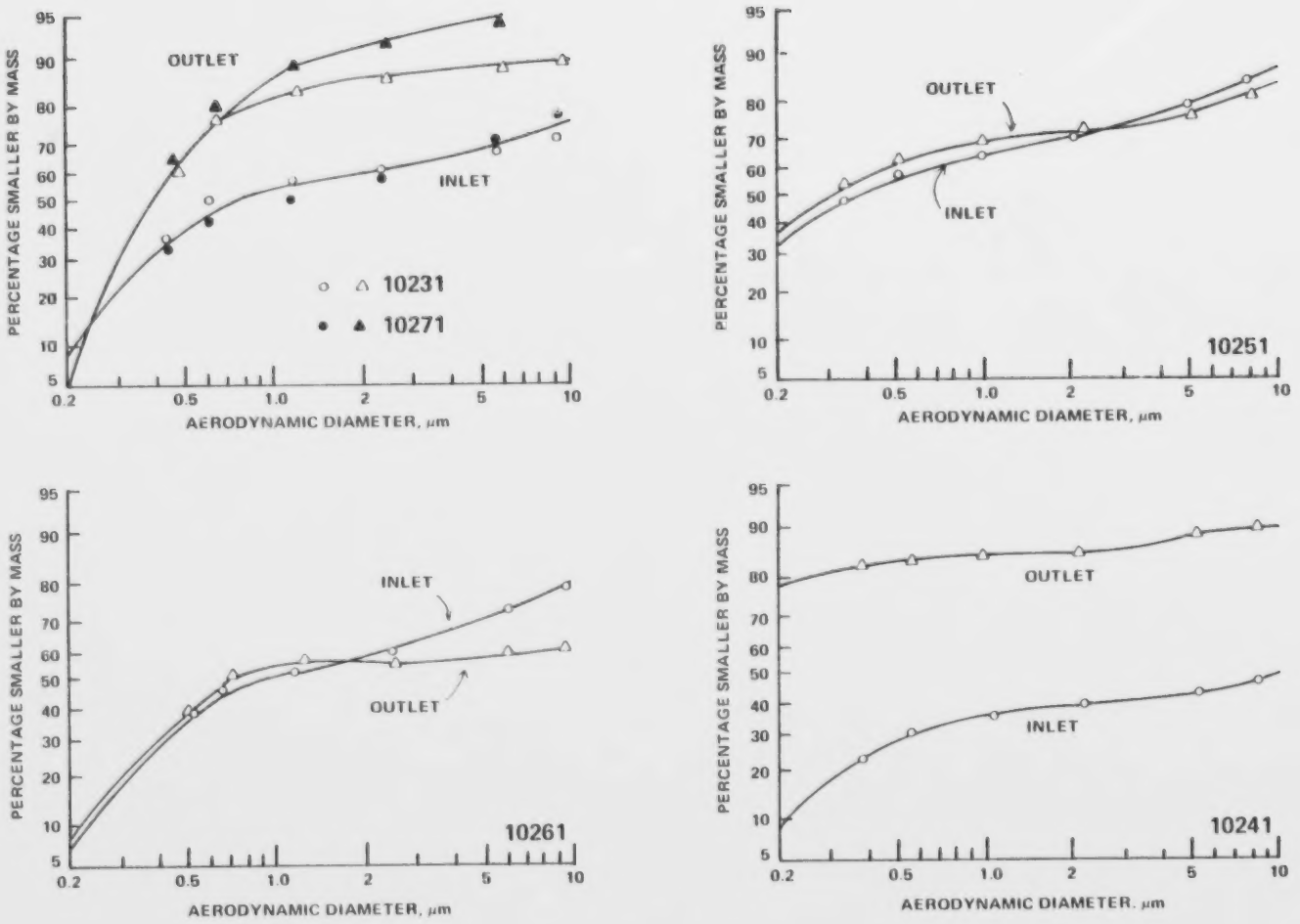

Figure 33. Cumulative size distributions for test nos. 10231 through 10271.

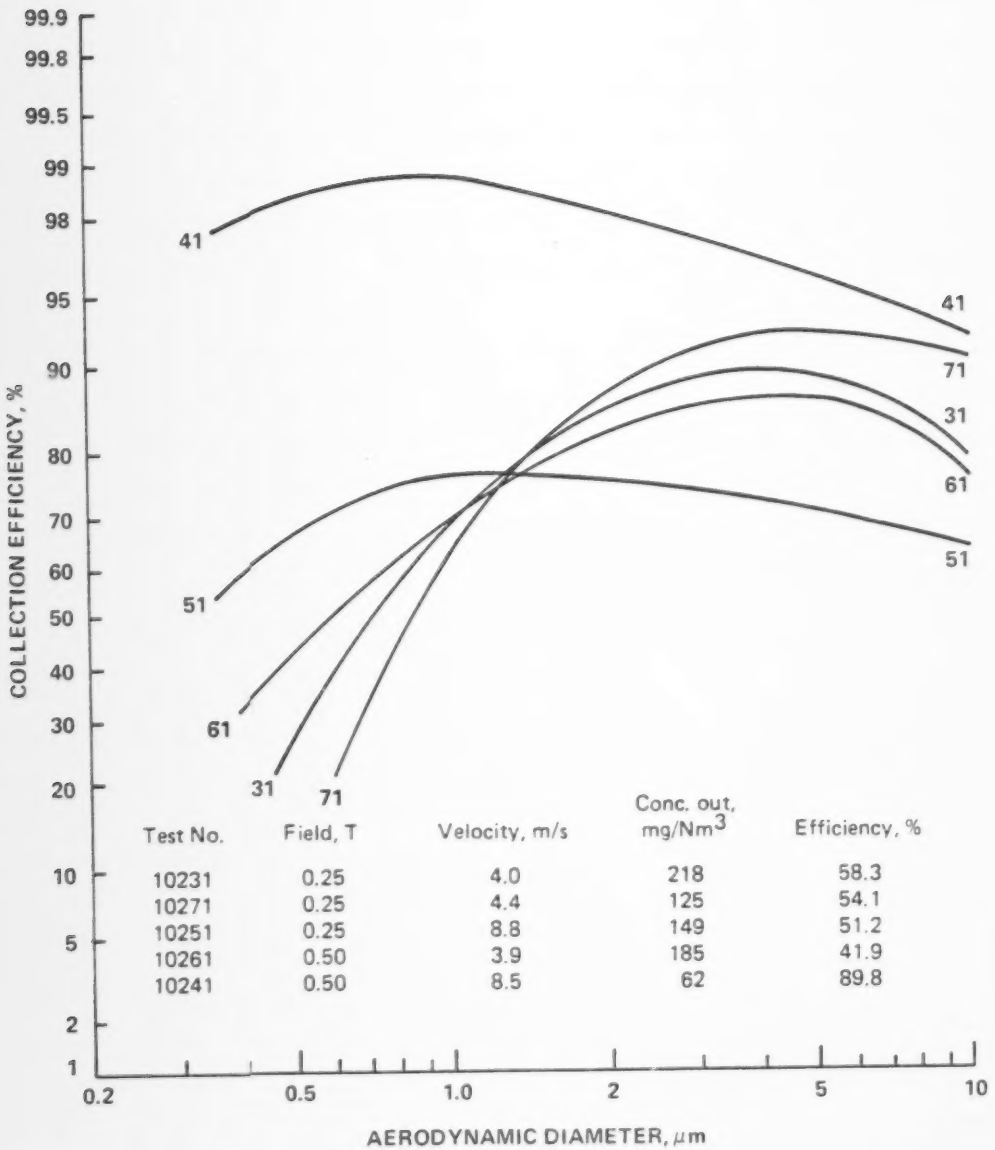

Test No.	Field, T	Velocity, m/s	Conc. out, mg/Nm^3	Efficiency, %
10231	0.25	4.0	218	58.3
10271	0.25	4.4	125	54.1
10251	0.25	8.8	149	51.2
10261	0.50	3.9	185	41.9
10241	0.50	8.5	62	89.8

Figure 34. Fractional collection efficiency curves for test nos. 10231 through 10271.

Once again the results were inconclusive on the effects of magnetic field and gas velocity. The low-field tests (10231, 10271, 10251) showed little difference in overall collection efficiency, although the fractional efficiency plots imply that increasing the velocity improved small particle collection and degraded large particle collection. This observation would be in qualitative agreement with the combined inertial impaction and reentrainment phenomena discussed in conjunction with the mathematical model. The high-field impactor data indicate that high velocity is beneficial to particle collection, but this conclusion is dependent on the questionable results of test no. 10241. The Method 5 tests showed little if any significant difference in the outlet concentrations of the four runs.

The salient conclusion from these additonal tests was similar to that of the earlier efficiency tests--that the emission rate of very fine particles was too large for the HGMF system to be applied successfully to this dust source. The reason for the high emission rate of fine particles was discovered through chemical and magnetic analyses of dust samples that are discussed in the following section.

SECTION 8

DISCUSSION AND APPLICATION OF RESULTS

This section discusses in further detail experimental data and observations that indicate why the magnetic filtration pilot plant was unable to collect a satisfactory amount of the sinter dust under practical operating conditions. Following that discussion an analysis is presented to define the criteria for successful application of HGMF to particulate emission control and to make economic estimates for applications to specific industrial processes.

CHEMICAL AND MAGNETIC ANALYSIS OF SINTER DUST

During the long-term operational period and the additional tests that were conducted with the coarse steel wool filter, samples of dust were collected for analysis from three points: (1) from the sample ports installed in the vertical section of pipe leading into the pilot plant (inlet); (2) from the sample ports installed in the pilot plant stack (outlet); and (3) from the hopper of the cyclone that acts as a secondary collector in the filter cleaning system (collected). The inlet and outlet samples were obtained by sampling isokinetically at the centerline of the respective pipes with an in-stack alundum thimble. The cyclone samples were grab samples obtained by dumping the hopper contents at designated times. Table 7 reports the results of the chemical analyses conducted on the samples. All of the metal determinations were made by flame atomic absorption. The chloride and sulfate concentrations were determined by ion chromatography.

The bottom row of Table 7 reports data on a wet, green crystalline material that was found dripping from the stack muffler. A sample was collected, and the analysis indicates that it was primarily ferrous sulfate and ferrous chloride. Both of these compounds exist in a variety of hydrated forms at the stack temperature. The material most probably originated from condensation of acid mists in the stack and muffler followed by chemical attack on the metal. The outer cylinder of the muffler was constructed of carbon steel.

Table 7. Chemical analysis of dust samples from HGMF pilot plant tests.

Sampler Description	Chemical Analysis, Reported in % by Mass								
	Fe	Ca	Mg	Al	Si	Na	K	Cl^-	$SO_4^=$
Inlet, 10/10/79	7.55	4.80	1.45	8.10	1.9	0.64	16.0	23.5	1.62
Inlet, 10/26/79	10.3	5.60	1.76	8.08	1.4	0.75	17.4	22.7	1.61
Outlet, 9/27/79	1.24	1.76	0.44	2.56	0.5	1.12	35.4	37.7	2.26
Outlet, 10/25/79	1.52	2.88	0.76	3.68	0.6	1.36	29.9	31.2	1.33
Collected, 9/27/79	12.7	6.40	1.84	10.0	2.2	0.42	11.3	14.6	1.98
Collected, 10/9/79	14.0	8.80	2.44	12.4	2.4	0.36	7.2	8.40	2.04
Collected, 10/25/79	12.3	8.00	2.32	11.8	2.6	0.42	9.4	15.8	2.96
Muffler Drippings, 9/27/79	23.3	<1	0.18	<1	0.2	0.22	<1	4.30	32.5

The inlet data in Table 7 show an average iron content of only 8.9 percent compared to the 25 to 50 percent reported in Table 2 as a generally accepted range for sinter dust. In addition, the inlet concentration of the dust averaged less than 0.5 g/Nm^3 with a mass median aerodynamic diameter of less than 2 μm compared to the generalized values of 1 to 2 g/m^3 and 10 μm. When combined, these figures indicate that a substantial quantity of larger dust particles fell out of the gas stream before reaching the pilot plant, and that the larger particles were most likely higher in iron content than the dust that reached the pilot plant. The latter contention is further substantiated by the magnetic analysis of the same seven samples that is shown in Figure 35. The specific magnetization curves of the two inlet samples are coincident and show a saturation magnetization at 3 kOe of 2.4 emu/g. In contrast, the coarser sinter dust that was obtained from the plant precipitator hoppers and tested in the laboratory pilot plant had a saturation magnetization of 9 emu/g. This partially explains the disappointing collection efficiency experienced in the field tests. The inlet dust was simply lower in magnetic susceptibility than expected.

Further analysis of Table 7 and Figure 35 reveals additional information of interest. The magnetization curves of the outlet dust are quite low because the outlet dust contained a very low percentage of iron and a high percentage of alkali chlorides. This finding is consistent with the qualitative observations made in Section 7 that the finer outlet dust was white or light gray in comparison to the inlet dust, which had a reddish-brown or reddish-gray color. In contrast to the inlet dust the collected dust had a higher iron content, a higher magnetization, and was a dark red color. Comparison of Table 7 and Figure 35 reveals, as expected, that the magnetization of each of the samples is roughly proportional to its iron content. None of the other elements or their compounds contributes significantly to the magnetic susceptibility.

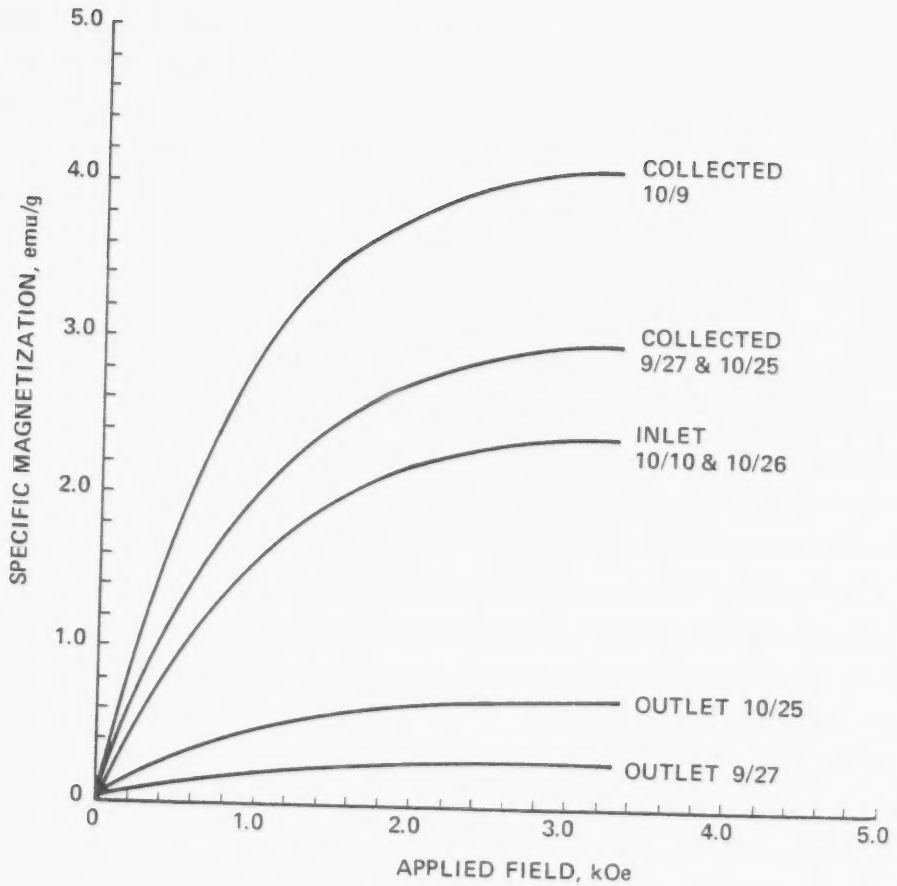

Figure 35. Magnetic analysis of dust samples from HGMF pilot plant tests.

The data in Table 7 can be utilized to construct a component mass balance that yields still more information. Although the seven samples were not collected simultaneously, the compositions of different samples from the same source are quite similar. Thus, for the sake of argument one can treat the samples from each source as if they were replicates taken during steady-state operations. The corresponding chemical analyses can then be averaged as if to minimize random error. The average analyses of the inlet, outlet, and collected dusts are reported in the first three rows of Table 8. If the three compositions of any component are treated as exactly correct, one can calculate the overall mass collection efficiency of the HGMF by constructing a mass balance on that component.

$$\text{Mass In} = \text{Mass Out} + \text{Mass Collected}; \tag{7}$$

$$M_t C_i = M_t(1-E_t)C_o + M_t E_t C_c \ , \tag{8}$$

where M_t = total mass flow rate of dust into system;
C_i = mass percentage of component in inlet;
C_o = mass percentage of component in outlet;
C_c = mass percentage of component collected; and
E_t = overall mass collection efficiency.

Solving Equation (8) for the overall collection efficiency yields

$$E_t = \frac{C_i - C_o}{C_c - C_o} \ . \tag{9}$$

The estimates of E_t obtained from each of the components are reported in the sixth row of Table 8. All of the estimates are in the range from 0.52 to 0.69 with the exception of the sulfate data, which are inconsistent. These data indicate a production of sulfate in the pilot plant, most probably due to the condensation of acid mist in the cyclone.

Table 8. Component mass balances based on chemical analysis.

Analysis	Fe	Ca	Mg	Al	Si	Na	K	Cl^-	$SO_4^=$
Avg. Inlet (C_i), mass %	8.92	5.20	1.60	8.09	1.65	0.69	16.7	23.1	1.62
Avg. Outlet (C_o), mass %	1.38	2.32	0.60	3.12	0.55	1.24	32.6	34.4	1.80
Avg. Collected (C_c), mass %	13.0	7.73	2.20	11.4	2.4	0.40	9.3	12.9	2.33
C_i-C_o, %	7.54	2.88	1.00	4.97	1.10	-0.55	-15.9	-11.3	-0.185
C_c-C_o, %	11.62	5.41	1.60	8.28	1.85	-0.84	-23.3	-21.5	0.535
E_t	0.649	0.532	0.625	0.600	0.595	0.655	0.682	0.526	-
Component Balance (based on $\bar{E}_t$ = 0.61 and average measured composition)									
Inlet Mass, kg	8.92	5.20	1.60	8.09	1.65	0.69	16.7	23.1	-
Outlet Mass, kg	0.54	0.90	0.23	1.22	0.21	0.48	12.7	13.4	-
Collected Mass, kg	7.93	4.70	1.34	6.95	1.46	0.24	5.7	7.9	-
Component Closure, %	95	108	98	101	101	104	110	92	-
Component Efficiency, %	89	90	84	86	88	35	34	34	-

When the eight estimates of total mass efficiency are averaged, a value of 0.61 is obtained. This average is quite reasonable with respect to the total mass efficiency measurements made during the same time period (see Tables 5 and 6). One can then use the estimated average total mass efficiency and the measured average component compositions to construct a mass balance for each component. For example, for iron

$$\text{Inlet:} \quad (100\ \text{kg})(0.0892) = 8.92\ \text{kg} \tag{10}$$

$$\text{Outlet:} \quad (39\ \text{kg})(0.0138) = 0.54\ \text{kg} \tag{11}$$

$$\text{Collected:} \quad (61\ \text{kg})(0.130) = 7.93\ \text{kg} . \tag{12}$$

The closure on the component mass balance is defined as

$$\text{Closure} = \frac{\text{Outlet Mass} + \text{Collected Mass}}{\text{Inlet Mass}} \cdot 100\% \tag{13}$$

Note in Table 8 that the closure on the components is distributed about 100% as expected because of the averaging procedure used to determine the total mass efficiency. It is remarkable, however, considering the time spanned by the sample collection, that the range of closure values is so small. The results show once again that the HGMF collection process was not strongly influenced by changes in the applied magnetic field or gas velocity or by minor changes in the filter density or depth.

The component collection efficiencies reported in the last row of Table 8 were calculated from the expression

$$\text{Component Efficiency} = \frac{\text{Collected Mass}}{\text{Inlet Mass}} \cdot 100\% . \tag{14}$$

The results indicate that the collection efficiency of iron was actually nearly 90 percent. A similar conclusion could be reached by conducting a "magnetics balance" on the curves reported in Figure 35. The fact that

the calculated collection efficiencies of calcium, magnesium, aluminum, and silicon are all nearly equal to that of iron suggests that these components are tightly bound together with the iron in the sintering process. In contrast the much lower calculated efficiencies of sodium, potassium, and chlorides suggest that sodium and potassium chloride appear in discrete fine particles that are collected in the HGMF primarily by inertial impaction. A credible explanation for the appearance of discrete, fine particles of sodium and potassium chloride is that these compounds are vaporized during the sintering process and reformed as a condensation aerosol in the windbox. The very fine size of the outlet dust supports this explanation. Furthermore, the fine alkali-chloride aerosol, which was emitted from the HGMF stack in a bluish-white plume, could be a major contributor to the "blue haze" that plagues many sinter plant stacks and is most often attributed to the condensation of hydrocarbons.

The component mass blances and the magnetization curves of the dusts also provide insight to the observation that increasing the applied magnetic field had no appreciable effect on dust collection. Since the magnetics are nearly saturated at 0.25 T (2.5 kOe), increasing the field would not substantially improve collection of magnetics and would have no effect on the collection of alkali chlorides.

Table 8 indicates that the collection efficiency of magnetic components was actually much higher than the total mass efficiency test results. If the larger iron-bearing particles that are characteristic of most sinter dusts had been included in the inlet, the collection efficiency surely would have been even higher. But the fact remains that the dust stream contained a concentration of non-magnetic dust sufficient to prevent successful application of HGMF. The collection of this fraction was improved only by operating under conditions conducive to filter plugging, which would not be practical for commerical applications.

TRANSIENT EMISSIONS DURING FILTER CLEANING

The Climet particle size analyzer was used to make one very revealing study of short-term transient emissions. With the pilot plant operating on a 16-minute cycle on August 29, the Climet was set up to sample from the outlet line with a 24-second counting interval synchronized to begin when the flow switched from Magnet B to Magnet A. The counting then continued through a complete cycle of operation.

The results are shown in Figure 36 for four particle size increments ranging from the smallest to the largest sizes for which valid counts could be obtained. The results show relatively constant emission rates over most of the cycle except for sharp peaks corresponding to two events--filter cleaning and flow switching. When the pressurized air is released to clean one filter, it surges through the cyclone and exhausts into the inlet line leading to the other filter. Figure 36 shows that the surge of air either knocks large particles and agglomerates off the active filter or carries large particles or agglomerates through the cyclone and through the active filter. The former explanation is more reasonable given the operating characteristics of cyclones and the fact that fine particle emissions do not rise immediately after the pulse. The emission puff subsides but is followed by a second puff of fine particles when the flow is switched from one path to another. The explanation of the second puff is more obscure. It is plausible that the cleaning pulse leaves a cloud of fine particles in the idle flow path that is then swept out when the flow is switched.

An estimate can be made of the importance of the two emission puffs to total emissions by integrating the area under each histogram. (Note that the relative concentration is plotted on a log scale so the peaks are as much as ten times the normal emission rates.) This calculation indicates that the puffs account for 16 percent of total emissions in the 0.3-0.5 μm range, 47 percent in the 0.7-1 μm range, 43 percent in the 2-3 μm range, and 51 percent in the 3-5 μm range.

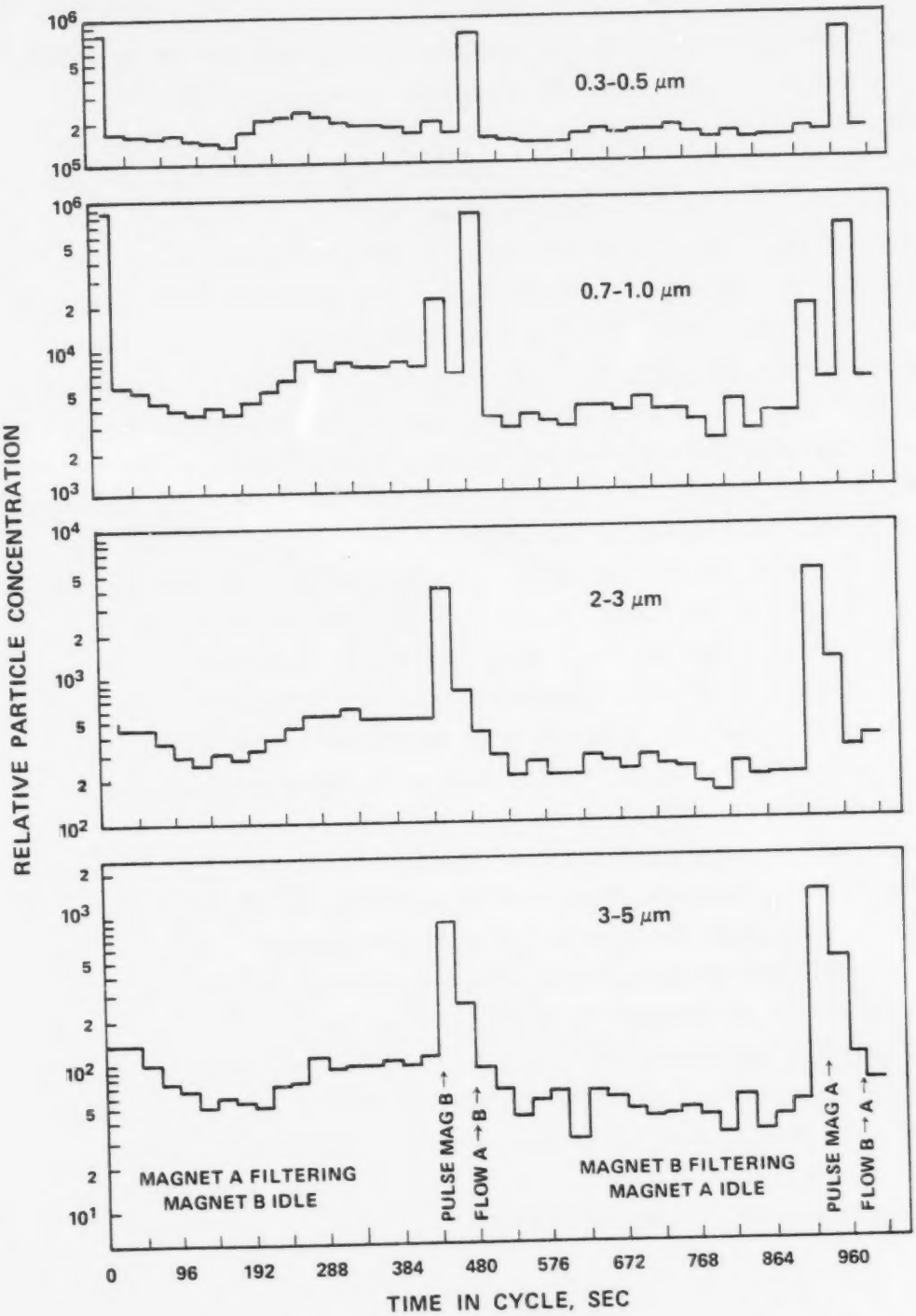

Figure 36. Transient emission levels during a single cycle of operation.

Further attempts to quantitatively evaluate the emission puffs were stymied by operating problems with the Climet. The puffs were observed qualitatively throughout the field program. An attempt was made to reduce the magnitude of the problem by changing the cycle so that the cleaning pulse occurred just after flow switching when the active filter had little dust accumulation. This would also have given the cloud in the idle path more time to settle, but the puffs persisted despite these adjustments.

Had the problem been eliminated it would not have changed the results at the sinter plant enough to make them acceptable, but the design of the cleaning system should be changed before future work is undertaken. The puff associated with the cleaning pulse could be eliminated by replacing the cyclone with a surge chamber that is vented through a single bag filter to the atmosphere or to the inlet pipe. The size of the surge chamber would not be unreasonable. For example, neglecting the surge capacity of the inter-connecting pipe, a surge chamber nine times the volume of the pressurized air tank would dissipate the back pressure to 10 percent of the original gauge pressure. In the pilot plant this would have required a surge chamber with a volume of 2.5 m^3. If the explanation of the second pulse is correct, it could be eliminated only by cleaning the filter outside of the normal flow path. This suggests the use of a continuously cleaned HGMF, which is discussed in the next subsection.

PROJECTED APPLICATIONS: ECONOMICS AND EFFECTIVENESS

The ultimate objective of EPA's support for the development of high-gradient magnetic filtration is to determine whether the process can be applied to one or more particulate emission control problems with resulting advantages over conventional control technology either in terms of economics or collection efficiency. The work presented in this report has increased the understanding of HGMF from a theoretical standpoint and has demonstrated that the process can function reliably under industrial conditions. What remains is to identify the most appropriate candidate for application and to design the proper configuration of HGMF equipment tailored to that application.

Discussion of Potential Candidates for Application

Although the collection efficiency of the mobile pilot plant was not satisfactory in the field tests with sinter dust, the previous laboratory work and the chemical analysis of the dusts from the sinter plant suggest that there are more promising opportunities for application. For example, the magnetization of basic oxygen furnace dust is roughly 20 times that of the inlet dust encountered in the field work, and the gas stream reportedly does not contain the undesirable alkali chlorides that cannot be adequately controlled by HGMF. Of the other processes listed in Table 2, the electric arc furnace has been shown in laboratory tests to be a potential candidate. One sample of scarfer fume has been obtained from an industrial source and determined to have a specific magnetization of 32 emu/g at 3000 Oe, slightly higher than the electric arc furnace dust tested. Blast furnace dust should have a very high magnetization judging from the reduced iron content, but it is also possible that the presence of discrete carbon particles could create the same problem experienced in the sinter plant field work. More information is needed on the size and composition of the dust downstream of the inertial or gravitational dust catcher that is used with most blast furnaces. Indeed, it is still possible that HGMF may be applicable to some sinter plants. Steiner (1976) reports that the characteristics of sinter dust vary widely from plant to plant. The results of the field tests indicate that HGMF can collect a large percentage of the sintered metals and flux materials. If the concentration of alkali chlorides in the gas stream is not significantly above the allowable emission level for total mass, then HGMF may be able to meet compliance codes.

Full-Scale Design Considerations

The cyclic HGMF design employed in the pilot plant must include a redundancy in magnets to achieve continuous operation. This results in a cost penalty. With dust concentrations significantly higher than the 0.5 g/Nm^3 encountered in the field tests, it is also doubtful that the cyclic version of the HGMF process can achieve operating practicality.

In the lab pilot plant work it was demonstrated that with a highly magnetic dust the HGMF filter could accumulate nearly twice its mass in dust without a decrease in collection efficiency. But pressure drop constraints and the need to insure effective filter cleaning would probably limit the accumumulation to a more conservative 10 to 20 percent of filter mass in most applications. In the latter stages of the field work the accumulation during each cycle was limited to 1 to 2 percent of filter mass to insure that plugging did not occur. Table 9 illustrates the calculated range of allowable loading times for a filter operating under typical conditions if the accumulation were limited to 10 percent of the filter mass. With the high dust concentrations that are typical to some of the processes listed in Table 2, the loading time is too short to apply a cyclic HGMF system practically.

Table 9. Illustration of filter loading times.

($F = 0.015$, $L = 0.20$ m, and $V_o = 8$ m/s)	
Dust Concentration, g/m^3	Loading Time, seconds
0.5	580
1	290
2	145
5	58
10	29

In addition to high dust concentrations, most full-scale steel industry processes involve very large gas flows. To take advantage of the economy of scale, a cyclic HGMF system would employ a number of parallel filters each much larger than that of the pilot plant. Unless a manifold system were introduced inside each flow path to sub-divide the filter into more

easily cleanable sections, the volume of the required cleaning air pulses would be proportionately larger. Not only would the tank sizes increase, the size of the release valves would increase making it much more difficult to achieve the required pulses of air.

Obviously an HGMF design that eliminates the magnet redundancy and overcomes the loading and cleaning problems discussed above would be advantageous in most applications. Several possible designs have been suggested, and at least one is commerically available for liquid applications. The SALA-HGMS® Carousel Series 480 (SMI Bulletin No. D052119-7610GB, Sala Magnetics, Inc., Cambridge, MA) is a continuous device that incorporates four magnet heads and four cleaning stations mounted on a rotating carousel (Figure 37). The magnet coils (not shown in the figure) are split into a mirrored-saddle configuration to allow the carousel to be rotated through the magnetized zone by a variable speed drive. The carousel can be loaded with filter material to a depth of 0.22 m and an active radial width of 1.5 m. Each of the magnet heads encloses an active face area of 3.4 m^2 in the direction of fluid flow. At superficial velocities of 5 to 10 m/s the total capacity of the unit would be 245,000 to 490,000 m^3/hr. With each of the magnet heads designed to provide an applied field of 0.3 T, the power dissipation is 36 kW per magnet plus a nominal amount for the carousel drive. The estimated first-quarter 1978 price of the device was $900,000 including power supplies and heat exchangers for indirect cooling of the magnets. The total cooling water requirement is 7.2 m^3/hr (32 GPM).

The carousel design is one suitable solution to the problem of scaling HGMF up to full-scale application on a high-concentration dust stream. The magnets are used continuously. A rotational speed of 1/3 rpm would satisfy the shortest loading time requirement listed in Table 9. The cleaning stations could be set up to provide pulses of air to relatively small increments of the filter at regular intervals that would be timed so that the entire filter would be cleaned after passing through each magnet. In practice, the carousel is already designed so that the filter is subdivided radially into smaller increments by solid vanes. Elastomer seals are attached to the top and bottom of each vane

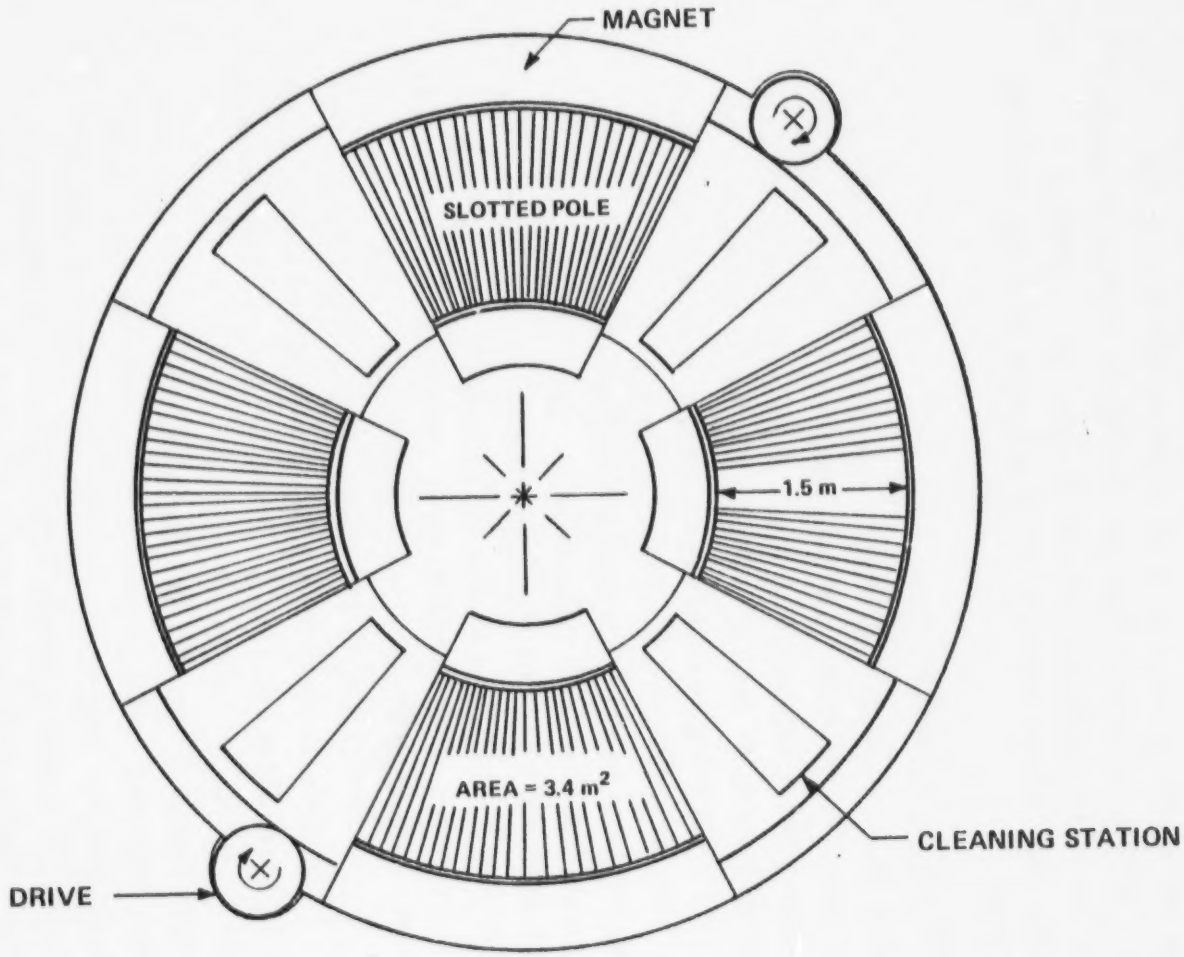

Figure 37. Schematic layout of the SALA-HGMS® 480 Series Carousel.

to provide a radial seal against leakage as the carousel passes through the magnets. Similar seals are mounted to the inner and outer circumferences of the carousel. The sealing system may require some modification (or at least careful selection of the elastomer material) before applications are proven on hot, dusty gas streams, but this is not foreseen as a serious problem. Since most particulate emission control equipment is installed at points where the process gas is under a partial vacuum, any leakage would be inward and would help the seals to be self-cleaning.

Efficiency and Economic Calculations

The design and cost of particulate emission control equipment must be evaluated carefully for each individual application, but it is instructive to consider generalized capital and operating cost figures as a basis for the evaluation of new technology. The capital investment for an electrostatic precipitator or baghouse normally runs about $2.35 per m^3/hr of gas flow ($4/ACFM), for the basic device itself. Auxiliary equipment such as ducts and fans, structures, engineering, and construction will escalate the final cost considerably. For example, a news item in the December 1978 edition of "Environmental Science and Technology" reported the turnkey installation of four electrostatic precipitators to control emissions from a basic oxygen furnace. The 510,000 m^3/hr (300,000 ACFM) system cost $5.2 million including equipment to pelletize the collected dust, which translates to $10.20 per m^3/hr ($17.33/ACFM). The initial cost of scrubbers is lower than that of precipitators or baghouses, but they usually require the addition of water pollution control equipment that drives the installed cost up to a comparable level.

Energy requirements of conventional equipment also vary. Baghouses on metallurgical processes normally operate with a pressure drop in the range of 10 to 20 cm H_2O. This translates into an energy expenditure of 1.7 to 3.4 kJ/m^3 (1.1 to 2.2 hp/1000 ACFM), assuming 60 percent fan efficiency. Bag cleaning requirements can add a significant increment. Precipitators have much lower pressure drops (typically 1 to 2 cm H_2O) but require considerable power for energization of the electrodes.

Their total energy requirement is on the order of 1.6 to 3.2 kJ/m^3 (1 to 2 hp/1000 ACFM). Scrubbers normally require much greater energy input to achieve acceptable collection efficiencies. Pressure drops as high as 150 cm H_2O are common, resulting in energy requirements of more than 25 kJ/m^3 (15.8 hp/1000 ACFM).

The projected cost of particulate emission control by HGMF is dependent on characteristics of the dust source, most notably dust size and magnetization. In applications where the effects of gas velocity and magnetic field are more readily apparent than they were in the field work, trade-offs may be appropriate between these two variables as well as filter depth and density in order to minimize costs. For example, theoretically one can keep collection efficiency constant while reducing filter density by increasing the applied field. This results in a trade-off of fan power for magnet power, which may be desirable. If gas velocity has no significant effect on collection, it can be increased at the expense of fan power in order to reduce capital costs.

The approximate capital cost and energy requirements of HGMF can be illustrated by considering one operating condition that could be suitable in a variety of applications. To take advantage of the continuous design for which cost and power requirements are available, the operating parameters listed in Table 10 are appropriate. The dust magnetizations are based on the experience gained to date and should be regarded as approximate. The predicted fractional collection efficiency for each of the three dust categories is shown in Figure 38. The curves are based on the mathematical model discussed in Section 5 and Appendix B. The model was validated for the basic oxygen and electric arc furnace dusts in the laboratory pilot plant, at least to the extent that the dusts tested were representative of emissions from their source category. The curve for σ = 2.5 emu/g corresponds roughly to sinter dust, but the model assumes the dust particles to be homogeneous in composition. In comparison to the predicted curve, sinter field tests corresponding most nearly to the conditions of Table 10 demonstrated a flatter curve with a collection efficiency of about 80 to 90 percent for larger particles and 20 to 40 percent for the smallest particles. Note that the efficiency

Table 10. HGMF operating parameters used for economic calculations.

Filter Material:	AISI Type 430 coarse-grade steel wool (equivalent cylindrical diameter = 200 μm)
Filter Depth:	0.20 m
Filter Density:	0.015
Applied Magnetic Field:	0.30 T
Superficial Gas Velocity:	8 m/s
Gas Temperature:	170°C (density = 0.8 kg/m^3; viscosity = 2.4×10^{-5} Pa·s)
Dust Magnetization:	50 emu/g (basic oxygen furnace, blast furnace (?)) 25 emu/g (electric arc furnace, scarfer) 2.5 emu/g (sinter machine)
Particle Size:	0.2 - 10 μm Stokes diameter (≈ 0.4 - 20 μm aerodynamic diameter)

is very high for the strongly magnetic dust even down into the submicron range. For lower magnetizations, lower efficiencies are indicated, but not all applications require 99 percent collection to meet emission regulations. The efficiency can be adjusted, if necessary, by varying the operating parameters as discussed in Section 5.

Filter pressure drop can be estimated from the field test results. Two valid pressure drop characterizations were run with clean, coarse filters. Since the pressure taps enclosed a considerable part of the piping network, the pressure drop was also characterized with no filter in the canister. The results are reported in Table 11. As shown in Figure 39 the ΔP data are correlated well with velocity squared as suggested by the Burke-Plummer equation for turbulent flow in packed columns (Bird, et al., 1960)

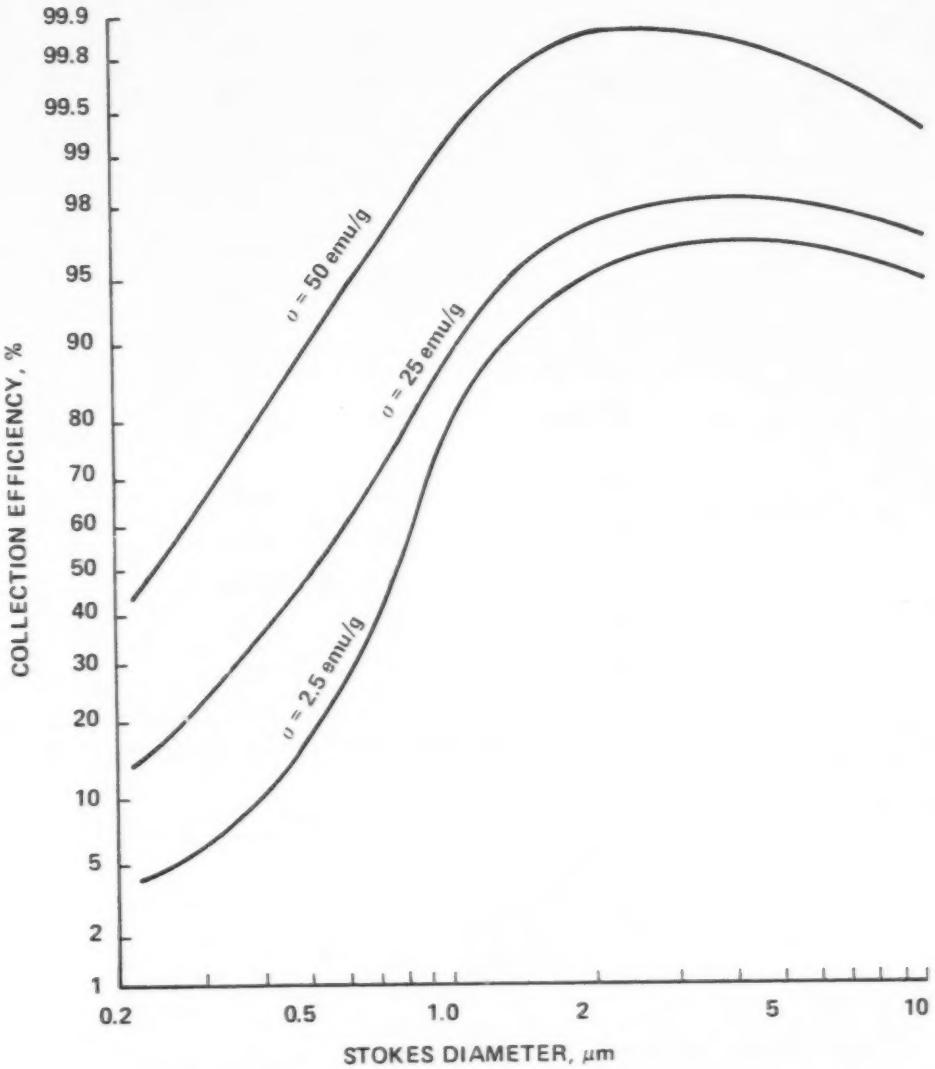

Figure 38. Predicted HGMF collection efficiency for three dust categories at typical operating conditions.

Table 11. Pressure drop characterization of coarse steel wool.

	Upstream Pressure kPa, absolute	Upstream Temperature °C	Flow* m^3/hr	Pressure Drop cm H_2O
No Filter	95.3	103	2380	2.1
	94.1	101	3090	3.7
	92.1	93	4050	5.6
	90.4	85	4880	8.5
Filter # 6 (F = 0.015, L = 0.20 m)	95.4	101	2360	7.5
	94.4	99	3090	16
	93.6	99	3790	20
	92.1	95	4590	30
	90.4	100	5390	42
Filter #8 (F = 0.0175, L = 0.30 m)	97.1	101	2480	18
	96.2	94	3210	27
	95.0	91	3770	41
	93.3	86	4470	61
	92.0	72	4950	75

*Flow corrected from orifice temperature and pressure to upstream filter temperature and pressure.

$$\Delta P = \frac{k\rho_F V_o^2 FL}{s(1-F)^3} \quad , \tag{15}$$

where ΔP = pressure drop, Pa;

k = dimensionless constant;

ρ_F = fluid density, kg/m^3;

V_o = superficial velocity, m/s;

F = filter density, dimensionless;

L = filter depth, m; and

s = wire radius, m.

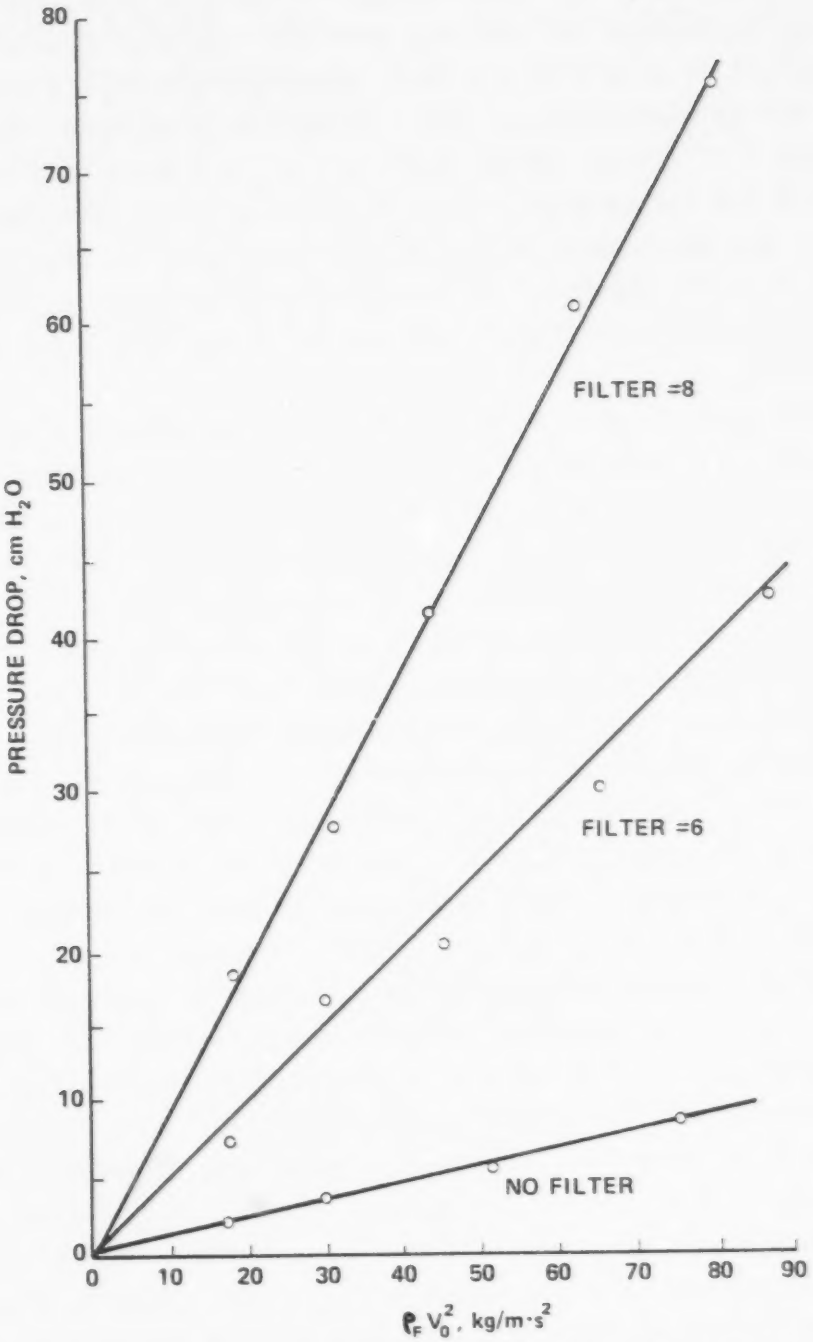

Figure 39. Pressure drop flow correlation for coarse steel wool.

In contrast, the extensive ΔP characterization conducted on medium-grade steel wool in the laboratory pilot plant showed ΔP to be proportional to $V^{1.68}$ although the Reynolds number calculations indicated turbulent flow conditions (see Appendix A). The data in Table 10 suggest a stronger dependence on F and/or L than Equation (15) indicates but the indication is uncertain because of the relatively small ranges over which these parameters were varied. In the laboratory work, ΔP was correlated with $F^{1.15}$ and L. An observation from the field work is consistent with the 1/s dependence shown in Equation (15). When coarse steel wool (equivalent diameter = 195 μm) was substituted for medium steel wool (equivalent diameter = 94 μm) in the long-term test period, the clean-filter pressure drop decreased from 20 cm H_2O to 9 cm H_2O at the same gas velocity.

Additional work is needed to better establish the pressure drop correlation across the appropriate parametric ranges. For the conditions illustrated in Table 10, however, the estimated clean-filter pressure drop can be taken directly from the data on Filter #6 shown in Figure 39. Subtracting off the contribution of the pilot plant piping, the estimated flange-to-flange filter ΔP is 19 cm H_2O. Allowing for a 10 percent increase at steady-state operating conditions, the fan energy requirement would be 3.5 kJ/m^3 (2.2 hp/1000 ACFM). With the 8 m/s velocity the Series 480 Carousel would accomodate a flow rate of slightly more than 390,000 m^3/hr (230,000 ACFM), yielding a magnet energy requirement of 1.3 kJ/m^3 (0.8 hp/1000 ACFM). Based on the conditions used in the field tests, a liberal estimate for the energy required by the cleaning system is 0.8 kJ/m^3 (0.5 hp/1000 ACFM). The combined total energy requirement is above the generalized estimates for baghouses and precipitators but well below typical scrubber energy requirements. At 8 m/s the estimated capital investment is \$2.30 per m^3/hr (\$3.90/ACFM), which is competitive with the conventional technologies.

It should be re-emphasized that the cost and energy estimates are based on a single HGMF design and are compared to generalized figures on competitive technologies. For specific applications other factors should be taken into account. The coarse stainless steel wool is relatively inexpensive and is quite durable in corrosive and hot environments.

The potential for application of HGMF in hot, combustible gas streams could lead to improved energy recovery from waste gases. Unlike many wet scrubber systems the HGMF process will not turn an air pollution control problem into a water pollution control problem. The high gas velocities and compact equipment that are characteristic of HGMF greatly reduce space requirements in comparison to baghouses and precipitators, which should produce a proportionate reduction in installed costs related to duct work, structural supports, and erection. These attractive features strongly support the continued development of the HGMF process with emphasis on field pilot plant tests to identify the most appropriate points of application and to demonstrate the application of a continuous filtration-continuous cleaning design.

SECTION 9

REFERENCES

Bird, R.B., W.E. Stewart, and E.N. Lightfoot, Transport Phenomena, John Wiley & Sons, Inc., New York (1960).

Bozorth, R.M., Ferromagnetism, D. Van Nostrand Company, Inc., New York (1951).

Clarkson, C.J., D.R. Kelland, and T.B. King, "Model for Calculation of Capture Radii of High Gradient Magnetic Separator at Moderate Reynolds Numbers," IEEE Trans. Magn., Mag-12, 901 (1976).

Cushing, K.M., G.E. Lacey, J.D. McCain, and W.B. Smith, Particulate Sizing Techniques for Control Device Evaluation: Cascade Impactor Calibrations, PB 262-849/AS, National Technical Information Service, Springfield, VA (1976).

DeLatour, C., and H.H. Kolm, "Magnetic Separation in Water Pollution Control-II," IEEE Trans. Magn., Mag-11, 1570 (1975).

Dulaney, E.L., Development Document for Effluent Limitations Guidelines and New Source Performance Standards for the Steel Making Segment of the Iron and Steel Manufacturing Point Source Category, EPA-440/1-74-024a, National Technical Information Service, Springfield, VA (1974).

Ergun, S., and E.H. Bean, "Magnetic Separation of Pyrite from Coals," Report of Investigation No. 2718, U.S. Bureau of Mines, Pittsburgh, PA (1968).

Fuchs, N.A., The Mechanics of Aerosols, Pergamon Press, New York (1964).

Gillespie, T., "On the Adhesion of Drops and Particles on Impact at Solid Surfaces. I.," J. Colloid Sci., 10, 266 (1955).

Gooding, C.H., "High Gradient Magnetic Filtration of Fine Particles from a Gas Stream," Ph.D. Thesis, North Carolina State University, Raleigh, NC (1979).

Gooding, C.H., T.W. Sigmon and L.K. Monteith, Application of High-Gradient Magnetic Separation to Fine Particle Control, PB 276-633/AS, National Technical Information Service, Springfield, VA (1977).

Hardison, L.C., and C.A. Greathouse, Air Pollution Control Technology and Costs in Nine Selected Areas, PB 222-746, National Technical Information Service, Springfield, VA (1972).

Harland, J.R., L. Nilsson, and M. Wallin, "Pilot-Scale High Gradient Magnetic Filtration of Steel Mill Wastewater," IEEE Trans. Magn., Mag-12, 904 (1976).

Harris, D.B., Procedures for Cascade Impactor Calibration and Operation in Process Streams, PB 263-623/AS, National Technical Information Service, Springfield, VA (1977).

Iannicelli, J., "New Developments in Magnetic Separation," IEEE Trans. Magn., Mag-12, 436 (1976).

IBM Application Program System/360 Scientific Subroutine Package, Version III Programmer's Manual, Program No. 360A-CM-03X, IBM Corp., White Plains, NY, 5th ed. (1970).

Jaasund, S.A., and M.R. Mazer, "The Application of Wet Electrostatic Precipitators for the Control of Emissions from Three Metallurgical Processes," Proceedings: Particulate Collection Problems Using ESP's in the Metallurgical Industry, PB 274-017/AS, National Technical Information Service, Springfield, VA (1977).

Jackson, J.D., Classical Electrodynamics, John Wiley & Sons, Inc., New York (1975).

Kelland, D.R., "High Gradient Magnetic Separation Applied to Mineral Beneficiation," IEEE Trans. Magn., Mag-9, 307 (1973).

Kelland, D.R., and E. Maxwell, "Oxidized Taconite Beneficiation by Continuous High Gradient Magnetic Separation," IEEE Trans. Magn., Mag-11, 1582 (1975).

Kolm, H.H., "The Large-Scale Manipulation of Small Particles," IEEE Trans. Magn., Mag-11, 1567 (1975).

Kolm, H.H., J.A. Oberteuffer, and D.R. Kelland, "High Gradient Magnetic Separation," Sci. Am., 223, 47 (Nov. 1975).

Krupp, H., "Particle Adhesion," Advances in Colloid and Interface Science," 1, 111 (1967).

Lawless, P.A., Analysis of Cascade Impactor Data for Calculating Particle Penetration, PB 288-649/AS, National Technical Information Service, Springfield, VA (1978).

Lawson, W.F., "The Dynamics of Paramagnetic Particles Near a Magnetized Wire," M.S. Thesis, West Virginia University, Morgantown, WV (1976).

Lawson, W.F., W.H. Simons, and R.P. Treat, "The Dynamics of a Particle Attracted by a Magnetized Wire," J. Appl. Phys., 48, 3213 (1977).

Liu, Y.A., G.E. Crow, C.J. Lin, and D.L. Vives, "A Pilot-Scale Study of High Gradient Magnetic Desulfurization of Solvent Refined Coal (SRC)," IEEE Trans. Magn., Mag-14, (1978).

Liu, Y.A., Editor, Industrial Applications of Magnetic Separation, Proceedings of Engineering Foundation Conference, Published by IEEE, Inc., 347 E. 47th St., New York (1979).

Loeffler, F., "Adhesion Probability in Fibre Filters," Clean Air, 8(4), 75 (1974).

Lyman, T., Editor, Metals Handbook, Vol. I Properties and Selection of Materials, American Society for Metals, Metals Park, OH, 8th ed. (1961).

Maxwell, E., I.S. Jacobs, and L.M. Levinson, Magnetic Separation of Mineral Matter from Coal Liquids, EPRI AF-508, Electric Power Research Institute, Palo Alto, CA (1977).

Maxwell, E., and D.R. Kelland, "High Gradient Magnetic Separation in Coal Desulfurization," IEEE Trans. Magn., Mag-14, 482 (1978).

Maxwell, E., D.R. Kelland, and I.Y. Akoto, "High Gradient Magnetic Separation of Mineral Particulates from Solvent Refined Coal," IEEE Trans. Magn., Mag-12, 507 (1976).

Melville, D., F. Paul, and S. Roath, "High Gradient Magnetic Separation of Red Cells from Whole Blood," IEEE Trans. Magn., Mag-11, 1701 (1975).

Mitchell, R., G. Bitton, and J.A. Oberteuffer, "High Gradient Magnetic Filtration of Magnetic and Non-Magnetic Contaminants from Water," Separation and Purification Methods, 4, 267 (1975).

Murray, H.H., "Beneficiation of Selected Industrial Minerals and Coal by High Intensity Magnetic Separation," IEEE Trans. Magn., Mag-12, 498 (1976).

Oberteuffer, J.A., "Magnetic Separation: A Review of Principles, Devices, and Applications," IEEE Trans. Magn., Mag-10, 223 (1974).

Oberteuffer, J.A., I. Wechsler, P.G. Marston, and M.J. McNallan, "High Gradient Magnetic Filtration of Steel Mill Process and Waste Waters," IEEE Trans. Magn., Mag-11, 1591 (1975).

Oder, R.R., "High Gradient Magnetic Separation Theory and Applications," IEEE Trans. Magn., Mag-12, 428 (1976).

Parson, T., Editor, Industrial Process Profiles for Environmental Use: Chapter 24. The Iron and Steel Industry, EPA-600/2-74-023x, National Technical Information Service, Springfield, VA (1977).

Petrakis, L., and P.F. Ahner, "High Gradient Magnetic Separations in Water Effluents," IEEE Trans. Magn., Mag-14, 491 (1978).

Steiner, B.A., "Air Pollution Control in the Iron and Steel Industry," International Metals Review, No. 209, 171 (1976).

Stenhouse, J.I.T., and D.C. Freshwater, "Particle Adhesion in Fibrous Air Filters," Trans. Inst. Chem. Engrs., 54, 95 (1976).

Trindale, S.C., and H.H. Kolm, "Magnetic Desulfurization of Coal," IEEE Trans. Magn., Mag-9, 310 (1973).

Visser, J., "on Hamaker Constants: A Comparison Between Hamaker Constants and Lifshitz - Van der Waals Constants," Advances in Colloid and Interface Science, 3, 331 (1972).

Vives, D.L., L.J. Hirth, and W.H. Summerlin, "Direct Reduction and Magnetic Beneficiation of Alabama Brown Ore with Lignite," IEEE Trans. Magn., Mag-12, 490 (1976).

Watson, J.H.P., "Magnetic Filtration," J. Appl. Phys., 44, 4209 (1973).

Whitehead, C., "Design and Operating Experience with Electrostatic Precipitators on Electric Arc Furnaces," Proceedings: Particulate Collection Problems Using ESP's in the Metallurgical Industry, PB 274-017/AS, National Technical Information Service, Springfield, VA (1977).

Whitesides, G.M., C.L. Hill, and J. Brunie, "Magnetic Filtration of Small Heterogeneous Catalyst Particles. Preparation of Ferrimagnetic Catalyst Supports," Ind. Eng. Chem., Process Des. Dev., 15, 226 (1976).

Yadidia, R., A. Abeliovich, and G. Belfort, "Algae Removal by High Gradient Magnetic Filtration," Envr. Sci. and Tech., 11, 913 (1977).

APPENDIX A

TABULATION OF EXPERIMENTAL CONDITIONS AND RESULTS FROM LABORATORY PILOT PLANT TESTS

The ranges of experimental parameters investigated during the laboratory pilot plant work are given in Table A-1.

Table A-1. Ranges of experimental parameters.

Dust Source:	basic oxygen furnace, electric arc furnace
Filter Material:	medium-grade type 430 stainless steel wool
Filter Depth:	0.075 - 0.30 m
Filter Packing Density:	0.0050 - 0.0100
Applied Magnetic Field:	0 - 0.6 T
Superficial Air Velocity:	4.9 - 11.9 m/s
Air Temperature:	24 - 46°C
Filter Inlet Pressure:	747 - 764 mm Hg
Particle Diameter (Stokes):	0.22 - 8.7 μm

The equivalent cylindrical diameter of the steel wool wires was calculated to be 108 μm by separating 50 randomly chosen strands of the material and measuring the total length and mass of the strands. Microscopic examination of the strands showed some to be roughly cylindrical while others had a more prismatic or ribbon-like appearance. Before each differently constructed filter was used, flow tests were conducted to determine the clean filter pressure drop at several velocities. The data are reported in Table A-2. A multiple regression analysis was run of the 41 observations to obtain the correlation

Table A-2. Experimental data on clean filter pressure drop.

Filter depth, m	Packing density	Air velocity, m/s	Pressure drop, kPa
0.15	0.0100	5.0	0.80
0.15	0.0100	7.6	1.22
0.15	0.0100	8.3	1.72
0.15	0.0100	10.1	2.14
0.15	0.0100	10.4	2.22
0.30	0.0050	5.0	0.62
0.30	0.0050	8.1	1.44
0.30	0.0050	10.5	2.17
0.15	0.0050	4.9	0.30
0.15	0.0050	8.1	0.67
0.15	0.0050	10.7	1.10
0.15	0.0050	4.8	0.27
0.15	0.0050	7.7	0.62
0.15	0.0050	10.7	1.12
0.225	0.0080	4.6	0.67
0.225	0.0080	6.5	1.22
0.225	0.0080	8.1	1.69
0.225	0.0080	9.2	2.14
0.225	0.0080	10.3	2.47
0.225	0.0080	10.9	2.74
0.225	0.0064	4.5	0.52
0.225	0.0064	6.6	1.00
0.225	0.0064	7.8	1.39
0.225	0.0064	9.1	1.84
0.225	0.0064	10.2	2.24
0.225	0.0064	10.8	2.39
0.15	0.0080	5.1	0.62
0.15	0.0080	7.5	1.15
0.15	0.0080	9.1	1.74
0.15	0.0080	10.5	2.19
0.15	0.0080	11.1	2.37
0.15	0.0080	6.8	0.85
0.15	0.0080	8.0	1.22
0.15	0.0080	9.0	1.54
0.15	0.0080	10.1	1.92
0.15	0.0080	10.7	2.14
0.30	0.0060	4.3	0.70
0.30	0.0060	6.2	1.25
0.30	0.0060	7.6	1.74
0.30	0.0060	9.0	2.22
0.30	0.0060	9.8	2.72

$$\frac{\Delta P}{L} = 62.7\ F^{1.15} V^{1.68}\ , \qquad \text{(A-1)}$$

where ΔP = filter pressure drop, kPa;
(1 kPa = 10 cm H_2O)

L = filter depth, m;

F = packing density, dimensionless; and

V = air velocity, m/s.

The multiple regression coefficient for Equation (A-1) was 0.990.

In contrast to Equation (A-1) the Blake-Kozeny equation for laminar flow in packed columns (Bird, et al., 1960) has the form

$$\frac{\Delta P}{L} \propto F^2 V \qquad \text{(A-2)}$$

and the Burke-Plummer equation for highly turbulent flow is packed columns (Bird, et al., 1960) has the form

$$\frac{\Delta P}{L} \propto F V^2 \qquad \text{(A-3)}$$

All of the experimental data in Table A-2 meet the Reynolds number criterion of the Burke-Plummer equation,

$$\frac{3 s \rho_f V}{\eta F} > 1000\ , \qquad \text{(A-4)}$$

where s = wire radius, m;

ρ_f = air density, kg/m^3; and

η = air viscosity, Pa·s;

but Equation (A-1) indicates that the flow was actually in the transition region between laminar and fully-developed turbulent flow. Confidence intervals were calculated on the two exponents obtained from the regression. A 95 percent confidence interval about the F exponent excluded 1.0, and a 95 percent confidence interval about the V exponent excluded 2.0. A regression analysis was also run on the data allowing the exponent on L to vary from unity. The regression exponent was 1.03, but it could not meet even an 80 percent confidence interval test, and the multiple regression coefficient was not improved.

Table A-3 lists the experimental conditions and results of the individual runs made in the lab pilot plant with BOF and EAF dusts. The experiments conducted with BOF dust are tabulated first, followed by the EAF dust experiments. Within each dust grouping the experiments are tabulated in chronological order. The data from run numbers 04191 through 07181 were reported previously (Gooding, et al., 1977), but are included here because they were used in the mathematical correlations developed as a part of this work. The notation of the operating parameters and results is as follows:

B = applied magnetic flux density, T
V = superficial air velocity, m/s
F = volumetric filter packing density, dimensionless
L = filter depth, m
T = air temperature, °C
D = particle diameter, μm
Eff = collection efficiency, %.

The particle diameter reported in Table A-3 is the Stokes diameter, which is defined as the diameter of a sphere (with the same density as the actual particle) that would behave in an impactor the same as does the actual particle. The mass median Stokes diameter of the inlet dust ranged from approximately 2 to 4 μm. Photomicrographs of each of the dusts showed that the primary particles were predominantly spheres ranging from 0.1 to 1 μm in diameter (Gooding, 1979), and larger "particles" were actually made up of agglomerates. The particle densities used in the size calculations were determined by pressurized-air pycnometer measurements to be 4.47 g/cm^3 for the BOF dust and 4.61 g/cm^3 for the EAF dust. To convert the Stokes diameter to aerodynamic diameter, one must multiply by the square root of the particle density.

In all of the lab pilot plant experiments the impactor sample rates were controlled carefully to provide equal stage cut points on the inlet and outlet sides of the HGMF filter. This allowed calculation of the fractional efficiency from a direct ratio of the fractional particle concentrations calculated from corresponding stage weights.

Table A-3. Conditions and results of laboratory pilot-plant experiments.

Run no. 04191	D, μm	Eff, %	Run no. 05041	D, μm	Eff, %
BOF dust	0.23	7.2	BOF dust	0.25	22.5
B = 0 T	0.37	39.6	B = 0.100 T	0.40	61.4
V = 5.6 m/s	0.74	80.4	V = 6.9 m/s	0.79	81.7
F = 0.0050	1.7	93.3	F = 0.0050	1.8	83.8
L = 0.150 m	3.3	96.6	L = 0.150 m	3.6	51.5
T = 31°C	7.9	91.1	T = 32°C	8.2	46.1
Run no. 04272	D, μm	Eff, %	Run no. 05042	D, μm	Eff, %
BOF dust	0.23	7.3	BOF dust	0.43	76.4
B = 0.050T	0.37	35.6	B = 0.100 T	0.85	86.6
V = 8.1 m/s	0.74	76.9	V = 10.2 m/s	1.9	75.5
F = 0.0050	1.7	74.1	F = 0.0050	3.8	74.6
L = 0.150 m	3.3	32.5	L = 0.15 m	8.5	87.5
T = 32°C	7.9	47.8	T = 37°C	---	---
Run no. 04281	D, μm	Eff, %	Run no. 05121	D, μm	Eff, %
BOF dust	0.41	33.1	BOF dust	0.23	49.0
B = 0.050 T	0.82	82.2	B = 0.200 T	0.37	82.5
V = 6.7 m/s	1.8	89.9	V = 8.0 m/s	0.73	96.3
F = 0.0050	3.6	57.8	F = 0.005	1.7	93.5
L = 0.150 m	8.3	50.0	L = 0.150 m	3.3	96.9
T = 29°C	---	---	T = 33°C	7.9	96.3
Run no. 05031	D, μm	Eff, %	Run no. 05181	D, μm	Eff, %
BOF dust	0.36	62.3	BOF dust	0.22	59.8
B = 0.100 T	0.72	84.0	B = 0 T	0.36	84.0
V = 8.5 m/s	1.6	87.1	V = 9.7 m/s	0.71	95.2
F = 0.0050	7.9	81.1	F = 0.0100	1.6	94.8
L = 0.150 m	---	---	L = 0.150 m	3.2	94.2
T = 31°C	---	---	T = 30°C	---	---
Run no. 05032	D, μm	Eff, %	Run no. 05182	D, μm	Eff, %
BOF dust	0.23	42.8	BOF dust	0.23	16.9
B = 0.100 T	0.36	51.6	B = 0 T	0.36	39.2
V = 5.6 m/s	0.72	86.6	V = 5.9 m/s	0.73	87.5
F = 0.0050	1.6	92.6	F = 0.0010	1.6	94.9
L = 0.150	3.3	85.4	L = 0.150 m	3.3	92.1
T = 35°C	7.9	62.4	T = 39°C	7.9	93.1

Table A-3 (continued).

Run no. 05191	D, μm	Eff, %
BOF dust	0.41	84.3
B = 0 T	0.81	97.2
V = 7.4 m/s	1.8	98.9
F = 0.0100	3.6	97.1
L = 0.150 m	8.3	96.8
T = 33°C	---	---

Run no. 05201	D, μm	Eff, %
BOF dust	0.36	75.1
B = 0.050 T	0.73	99.0
V = 7.8 m/s	1.6	99.0
F = 0.0100	3.3	98.6
L = 0.150 m	7.9	97.7
T = 33°C	---	---

Run no. 05252	D, μm	Eff, %
BOF dust	0.22	16.0
B = 0 T	0.35	44.5
V = 9.2 m/s	0.71	73.1
F = 0.0050	1.6	67.2
L = 0.300 m	3.2	32.7
T = 37°C	7.8	13.3

Run no. 05261	D, μm	Eff, %
BOF dust	0.42	56.2
B = 0.050 T	0.82	93.1
V = 7.5 m/s	1.8	91.2
F = 0.0050	3.7	84.4
L = 0.300 m	8.4	79.4
T = 31°C	---	---

Run no. 05272	D, μm	Eff, %
BOF dust	0.36	46.5
B = 0.050 T	0.72	92.6
V = 6.6 m/s	1.6	96.7
F = 0.0050	3.3	93.6
L = 0.300 m	7.9	87.5
T = 36°C	---	---

Run no. 06021	D, μm	Eff, %
BOF dust	0.28	41.5
B = 0.100 T	0.28	85.5
V = 10.3 m/s	2.0	91.9
F = 0.0050	3.9	89.9
L = 0.150 m	8.6	76.1
T = 32°C	---	---

Run no. 06022	D, μm	Eff, %
BOF dust	0.41	55.0
B = 0.100 T	0.81	92.7
V = 6.8 m/s	1.8	96.4
F = 0.0050	3.6	94.0
L = 0.150 m	8.3	85.7
T = 37°C	---	---

Run no. 06031	D, μm	Eff, %
BOF dust	0.42	63.3
B = 0.100 T	0.83	92.3
V = 6.8 m/s	1.9	95.8
F = 0.0050	3.7	90.0
L = 0.150 m	8.4	97.3
T = 30°C	---	---

Run no. 06032	D, μm	Eff, %
BOF dust	0.41	66.5
B = 0.100 T	0.81	94.6
V = 7.1 m/s	1.8	98.1
F = 0.0050	3.6	91.3
L = 0.150 m	8.3	93.6
T = 37°C	---	---

Run no. 06281	D, μm	Eff, %
BOF dust	0.23	66.6
B = 0.400 T	0.36	70.1
V = 8.2 m/s	0.72	96.4
F = 0.0050	1.6	98.9
L = 0.150 m	3.3	99.2
T = 35°C	7.9	99.4

Table A-3 (continued).

Run no. 10261	D, μm	Eff, %	Run no. 11211	D, μm	Eff, %
BOF dust	0.35	73.8	BOF dust	0.23	15.7
B = 0.075 T	0.69	97.3	B = 0 T	0.36	1.5
V = 5.6 m/s	1.6	99.7	V = 4.9 m/s	0.72	38.7
F = 0.0100	3.1	99.2	F = 0.0050	1.6	80.9
L = 0.150 m	7.7	98.1	L = 0.150	3.3	91.9
T = 26°C	--	---	T = 29°C	---	---

Run no. 10281	D, μ	Eff, %	Run no. 11221	D, μm	Eff, %
BOF dust	0.38	74.1	BOF dust	0.24	1.0
B = 0.90 T	0.75	94.0	B = 0 T	0.38	4.7
V = 7.7 m/s	1.7	95.2	V = 8.1 m/s	0.75	8.8
F = 0.0100	3.4	93.3	F = 0.0050	1.7	38.3
L = 0.150 m	8.0	96.8	L = 0.150 m	3.4	79.2
T = 24°C	---	---	T = 32°C	8.0	92.9

Run no. 11011	D, μm	Eff, %	Run no. 11231	D, μm	Eff, %
BOF dust	0.30	52.2	BOF dust	0.36	38.8
B = 0.100 T	0.46	84.0	B = 0.100 T	0.72	80.2
V = 10.1 m/s	0.90	93.1	V = 4.9 m/s	1.6	96.4
F = 0.0100	2.0	90.4	F = 0.0050	3.2	99.5
L = 0.150 m	8.7	90.6	L = 0.150 m	7.8	88.1
T = 27°C	---	---	T = 30°C	---	---

Run no. 11021	D, μm	Eff, %	Run no. 11281	D, μm	Eff, %
BOF dust	0.36	74.5	BOF dust	0.70	92.3
B = 0.075 T	0.71	99.0	B = 0.100 T	1.6	95.7
V = 5.0 m/s	1.6	99.9	V = 8.1 m/s	3.2	93.1
F = 0.0050	3.2	99.8	F = 0.0050	7.7	96.1
L = 0.300 m	7.8	97.3	L = 0.150	---	---
T = 27°C	---	---	T = 28°C	---	---

Run no. 11032	D, μm	Eff, %	Run no. 11282	D, μm	Eff, %
BOF dust	0.42	93.0	BOF dust	0.42	55.9
B = 0.100 T	0.33	99.3	B = 0.100 T	0.83	72.5
V = 10.5 m/s	1.9	96.4	V = 10.9 m/s	1.9	69.6
F = 0.0050	3.7	95.0	F = 0.0050	3.7	39.7
L = 0.300 m	8.4	93.8	L = 0.150 m	8.4	57.9
T = 34°C	---	---	T = 37°C	---	---

Table A-3 (continued).

Run no. 11291	D, μm	Eff, %	Run no. 12012	D, μm	Eff, %
BOF dust	0.42	67.6	BOF dust	0.23	46.6
B = 0.100 T	0.83	70.3	B = 0.400 T	0.37	71.0
V = 10.8 m/s	1.9	66.0	V = 8.9 m/s	0.74	93.7
F = 0.0050	3.7	46.9	F = 0.0050	1.7	98.2
L = 0.150 m	8.4	42.4	L = 0.150 m	3.4	97.6
T = 33°C	---	---	T = 41°C	8.0	94.4
Run no. 11292	**D, μm**	**Eff, %**	**Run no. 12021**	**D, μm**	**Eff, %**
BOF dust	0.36	38.4	BOF dust	0.37	74.5
B = 0.200 T	0.72	83.7	B = 0.400 T	0.74	95.8
V = 5.4 m/s	1.6	97.4	V = 8.6 m/s	1.7	99.4
F = 0.0050	3.2	97.7	F = 0.0050	3.3	98.8
L = 0.150 m	7.8	82.8	L = 0.150 m	7.9	91.8
T = 38°C	---	---	T = 31°C	---	---
Run no. 11301	**D, μm**	**Eff, %**	**Run no. 12051**	**D, μm**	**Eff, %**
BOF dust	0.37	67.2	BOF dust	0.42	70.3
B = 0.200 T	0.74	92.8	B = 0.400 T	0.83	93.6
V = 8.5 m/s	1.7	98.0	V = 11.5 m/s	1.9	93.0
F = 0.0050	3.3	95.8	F = 0.0050	3.7	84.6
L = 0.15 m	8.0	85.3	L = 0.150 m	8.4	89.3
T = 34°C	---	---	T = 35°C	---	---
Run no. 11302	**D, μm**	**Eff, %**	**Run no. 12071**	**D, μm**	**Eff, %**
BOF dust	0.42	66.0	BOF dust	0.36	51.5
B = 0.200 T	0.84	92.1	B = 0.600 T	0.71	90.7
V = 11.6 m/s	1.9	91.1	V = 5.6 m/s	1.6	98.8
F = 0.0050	3.7	77.8	F = 0.0050	3.2	99.6
L = 0.150 m	8.4	91.4	L = 0.150 m	7.8	95.7
T = 40°C	---	---	T = 28°C	---	---
Run no. 12011	**D, μm**	**Eff, %**	**Run no. 12072**	**D, μm**	**Eff, %**
BOF dust	0.36	48.4	BOF dust	0.37	69.3
B = 0.400 T	0.71	88.7	B = 0.600 T	0.74	95.3
V = 5.4 m/s	1.6	98.0	V = 8.5 m/s	1.7	98.9
F = 0.0050	3.2	99.0	F = 0.0050	3.4	98.4
L = 0.150 m	7.8	93.2	L = 0.150 m	8.0	97.4
T = 34°C	---	---	T = 36°C	---	---

Table A-3 (continued).

Run no. 12081	D, μm	Eff, %	Run no. 01112	D, μm	Eff, %
BOF dust	0.43	77.6	BOF dust	0.42	72.5
B = 0.600 T	0.84	94.8	B = 0.200 T	0.82	89.6
V = 11.9 m/s	1.9	96.6	V = 10.7 m/s	1.8	90.7
F = 0.0050	3.8	94.1	F = 0.0050	3.7	83.8
L = 0.150 m	8.4	97.8	L = 0.150 m	8.4	89.0
T = 35°C	---	---	T = 34°C	---	---
Run no. 01051	D, μm	Eff, %	Run no. 01121	D, μm	Eff, %
BOF dust	0.36	45.5	BOF dust	0.37	56.6
B = 0.200 T	0.72	73.2	B = 0.200 T	0.73	92.0
V = 7.9 m/s	1.6	80.7	V = 7.2 m/s	1.7	98.1
F = 0.0050	3.2	77.2	F = 0.0050	3.3	97.7
L = 0.075 m	7.8	81.5	L = 0.150 m	7.9	98.4
T = 29°C	---	---	T = 29°C	---	---
Run no. 01091	D, μm	Eff, %	Run no. 02091	D, μm	Eff, %
BOF dust	0.41	51.4	BOF dust	0.27	86.1
B = 0.200 T	0.81	73.0	B = 0.300 T	0.42	96.8
V = 11.1 m/s	1.8	66.0	V = 10.0 m/s	0.83	99.8
F = 0.0050	3.6	51.2	F = 0.0080	1.9	99.4
L = 0.075 m	8.3	51.6	L = 0.225 m	3.7	98.4
T = 29°C	---	---	T = 31°C	8.4	98.3
Run no. 011092	D, μm	Eff, %	Run no. 02101	D, μm	Eff, %
BOF dust	0.35	26.8	BOF dust	0.27	86.8
B = 0.200 T	0.70	70.6	B = 0.300 T	0.42	98.9
V = 5.9 m/s	1.6	91.3	V = 10.0 m/s	0.83	99.7
F = 0.0050	3.2	97.2	F = 0.0080	1.9	99.2
L = 0.075 m	7.8	92.5	L = 0.225 m	3.7	99.6
T = 32°C	---	---	T = 30°C	8.4	99.6
Run no. 01111	D, μm	Eff, %	Run no. 02102	D, μm	Eff, %
BOF dust	0.37	64.6	BOF dust	0.26	79.4
B = 0.200 T	0.73	95.0	B = 0.300 T	0.42	98.9
V = 7.7 m/s	1.7	99.0	V = 9.8 m/s	0.82	99.8
F = 0.0050	3.3	98.1	F = 0.0080	1.9	99.5
L = 0.150 m	7.9	96.9	L = 0.225 m	3.7	99.3
T = 27°C	---	---	T = 38°C	8.4	99.0

Table A-3 (continued).

Run no. 02211	D, μm	Eff, %	Run no. 02282	D, μm	Eff, %
BOF dust	0.23	31.2	BOF dust	0.37	80.3
B = 0.300 T	0.36	99.6	B = 0 T	0.73	84.4
V = 7.9 m/s	0.72	99.7	V = 8.5 m/s	1.7	81.5
F = 0.0064	1.6	99.8	F = 0.0080	3.3	71.5
L = 0.225 m	3.3	99.8	L = 0.150 m	7.9	59.8
T = 30°C	7.9	99.7	T = 34°C	---	---
Run no. 02231	D, μm	Eff, %	Run no. 03011	D, μm	Eff, %
BOF dust	0.23	78.7	BOF dust	0.43	47.4
B = 0.300 T	0.36	93.6	B = 0 T	0.85	84.3
V = 8.0 m/s	0.72	98.3	V = 7.0 m/s	1.9	85.1
F = 0.0064	1.6	99.1	F = 0.0080	3.8	76.6
L = 0.225 m	3.3	99.2	L = 0.150 m	8.5	59.3
T = 25°C	7.9	99.0	T = 31°C	---	---
Run no. 02232	D, μm	Eff, %	Run no. 03021	D, μm	Eff, %
BOF dust	0.23	30.1	BOF dust	0.23	60.3
B = 0.300 T	0.36	94.4	B = 0.300 T	0.36	90.2
V = 8.0 m/s	0.72	99.8	V = 8.7 m/s	0.72	98.6
F = 0.0064	1.6	99.7	F = 0.0080	1.6	99.4
L = 0.225 m	3.3	99.3	L = 0.150 m	3.3	98.0
T = 28°C	7.9	99.6	T = 29°C	7.9	97.8
Run no. 02272	D, μm	Eff, %	Run no. 03022	D, μm	Eff, %
BOF dust	0.23	0.1	BOF dust	0.43	99.3
B = 0 T	0.36	64.0	B = 0.300 T	0.85	99.7
V = 8.8 m/s	0.72	87.3	V = 6.9 m/s	1.9	99.5
F = 0.0080	1.6	83.8	F = 0.0080	3.8	98.1
L = 0.150 m	3.3	71.7	L = 0.150 m	8.5	98.2
T = 34°C	7.9	61.2	T = 36°C	---	---
Run no. 02281	D, μm	Eff, %	Run no. 03211	D, μm	Eff, %
BOF dust	0.27	51.6	BOF dust	0.36	96.6
B = 0 T	0.45	69.3	B = 0.300 T	0.72	89.9
V = 11.0 m/s	0.85	83.7	V = 7.9 m/s	1.6	96.1
F = 0.0080	1.9	73.5	F = 0.0080	3.3	95.9
L = 0.150 m	3.8	66.6	L = 0.510 m	7.9	86.0
T = 32°C	---	---	T = 46°C	---	---

Table A-3 (continued).

Run no. 03221	D, μm	Eff, %	Run no. 07122	D, μm	Eff, %
BOF dust	0.37	96.6	EAF dust	0.39	39.2
B = 0.300 T	0.73	93.5	B = 0.100 T	0.78	78.6
V = 7.5 m/s	1.6	96.8	V = 7.9 m/s	1.8	91.8
F = 0.0080	3.3	99.0	F = 0.0050	3.5	95.8
L = 0.150 m	7.9	99.2	L = 0.150 m	8.2	65.9
T = 29°C	---	---	T = 41°C	---	---
Run no. 03222	**D, μm**	**Eff, %**	**Run no. 11072**	**D, μm**	**Eff, %**
BOF dust	0.28	62.6	EAF dust	0.23	38.1
B = 0.300 T	0.43	96.7	B = 0.400 T	0.36	59.9
V = 9.5 m/s	0.85	98.4	V = 8.1 m/s	0.72	94.2
F = 0.0080	1.9	97.7	F = 0.0050	1.6	98.4
L = 0.150 m	3.8	97.1	L = 0.300 m	3.3	98.1
T = 34°C	8.5	98.3	T = 38°C	7.9	92.7
Run no. 07141	**D, μm**	**Eff, %**	**Run no. 11081**	**D, μm**	**Eff, %**
EAF dust	0.39	48.8	EAF dust	0.22	60.1
B = 0.200 T	0.77	87.6	B = 0.200 T	0.35	52.9
V = 7.6 m/s	1.8	96.1	V = 5.6 m/s	0.70	95.2
F = 0.0050	3.5	97.9	F = 0.0100	7.8	97.5
L = 0.150 m	8.1	73.2	L = 0.150 m	---	---
T = 36°C	---	---	T = 31°C	---	---
Run no. 07151	**D, μm**	**Eff, %**	**Run no. 11091**	**D, μm**	**Eff, %**
EAF dust	0.41	45.4	EAF dust	0.23	40.5
B = 0.200 T	0.81	69.8	B = 0.375 T	0.37	54.6
V = 10.8 m/s	1.8	74.0	V = 8.9 m/s	0.73	92.5
F = 0.0050	3.6	74.1	F = 0.0100	1.6	98.8
L = 0.150 m	8.3	65.6	L = 0.150 m	7.9	96.9
T = 33°C	---	---	T = 31°C	---	---
Run no. 07181	**D, μm**	**Eff, %**	**Run no. 11092**	**D, μm**	**Eff, %**
EAF dust	0.36	47.0	EAF dust	0.26	41.3
B = 0.400 T	0.71	86.1	B = 0.400 T	0.41	58.5
V = 8.2 m/s	1.6	94.6	V = 11.6 m/s	0.81	87.2
F = 0.0050	3.2	96.3	F = 0.0100	1.8	91.0
L = 0.150 m	7.8	85.2	L = 0.150 m	3.6	91.3
T = 37°C	---	---	T = 37°C	8.3	97.9

Table A-3 (continued).

Run no. 11151 EAF dust B = 0.375 T V = 7.3 m/s F = 0.0050 L = 0.300 m T = 29°C	D, μm 0.23 0.37 0.74 1.7 2.0 ---	Eff, % 55.4 62.9 97.7 99.7 99.0 ---	Run no. 11161 EAF dust B = 0.400 T V = 10.0 m/s F = 0.0050 L = 0.300 m T = 32°C	D, μm 0.26 0.41 0.81 1.8 3.6 8.3	Eff, % 29.9 63.6 84.6 86.2 98.0 85.0

APPENDIX B

MATHEMATICAL MODEL OF HGMF

The approach taken to theoretical modeling of HGMF parallels the usual treatment of conventional filtration. The particles are assumed to be spherical, uniformly distributed in the fluid stream, and moving at the same velocity as the fluid upstream of the collector. The basic element of the filter is a clean, cylindrical wire of radius s, oriented so that its axis is perpendicular to fluid flow (Figure B-1). The objective of the theoretical calculations is to determine the portion of the fluid stream from which particles are removed as the fluid flows past the wire by analyzing the trajectories of particles approaching under the influence of attendant forces. The collision radius of the wire, y_c, is defined by the initial position of the particle whose trajectory just touches the wire, as illustrated in Figure B-1.

Watson (1973) published the first trajectory model of HGMF, taking into account the magnetic and drag forces acting on a spherical particle approaching a cylindrical wire. Lawson and coworkers (1976, 1977) extended the model to include inertial and gravitational effects. The present work builds on the Lawson model to include the conditions appropriate to the magnetic filtration of particles from a gas stream.

The geometry of the system to be discussed is illustrated in Figure B-2. The fundamental equation governing particle motion is

$$w\vec{a} = \vec{F}_g + \vec{F}_d + \vec{F}_m \tag{B-1}$$

where w is the particle mass, a is its acceleration, and F_g, F_d, and F_m are the gravitational, drag, and magnetic forces, respectively. Assuming the wire to be of infinite length, the z-component of each term is neglected. In cylindrical coordinates, the inertial term becomes

$$w\vec{a} = \left[w \frac{d^2r}{dt^2} - wr\left(\frac{d\theta}{dt}\right)^2 \right] \hat{r} + \left[wr \frac{d^2\theta}{dt^2} + 2w \frac{dr}{dt} \frac{d\theta}{dt} \right] \hat{\theta}. \tag{B-2}$$

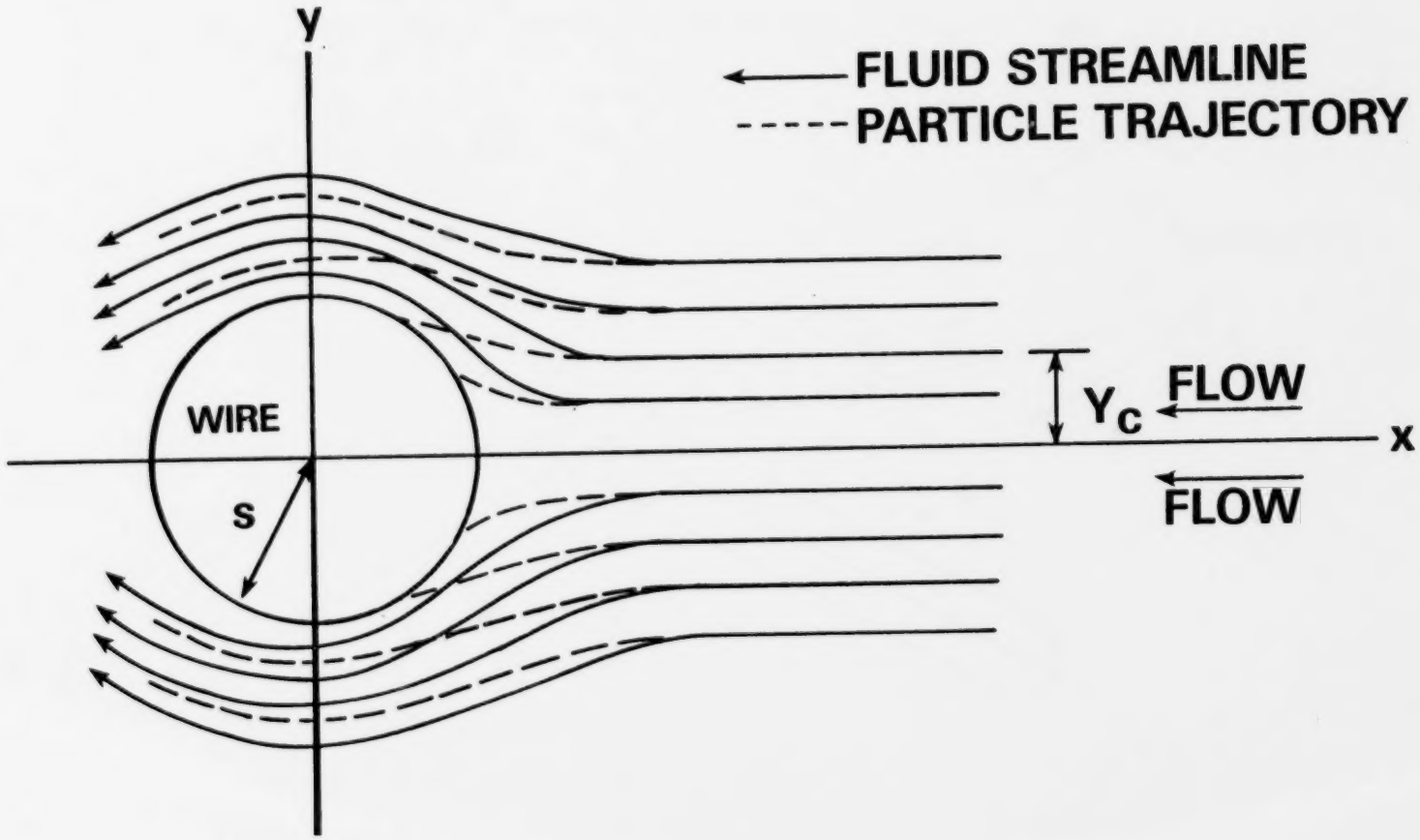

Figure B-1. Illustration of particle capture by a single wire.

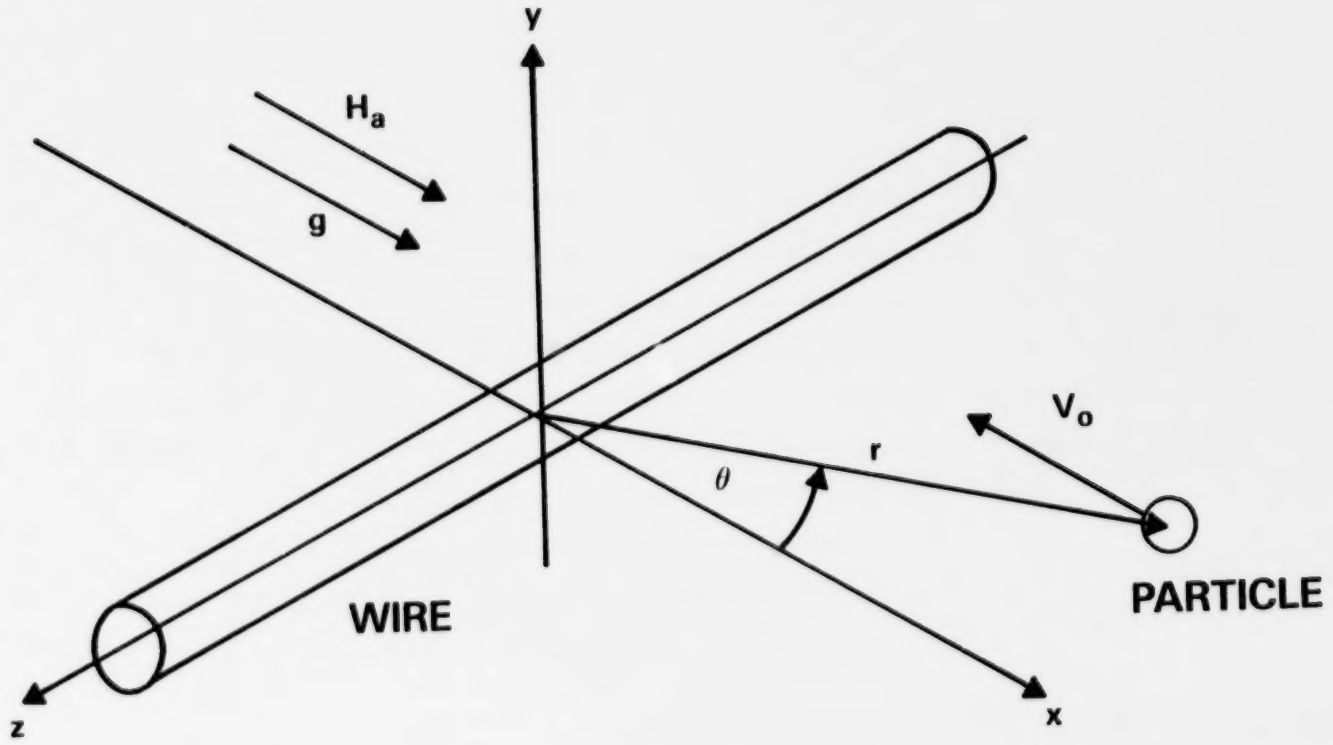

Figure B-2. Geometric basis of HGMF trajectory model.

The gravitational force acting in the x-direction is

$$\vec{F}_g = \left[wg(1 - \frac{\rho_f}{\rho_p}) \cos \theta\right]\hat{r} - \left[wg(1 - \frac{\rho_f}{\rho_p}) \sin \theta\right]\hat{\theta}. \quad \text{(B-3)}$$

Assuming potential flow about the wire and Stokes drag on the particle, the drag force is expressed by

$$\vec{F}_d = 6\pi\eta b\left[-V_o(1 - \frac{s^2}{r^2}) \cos \theta - \frac{dr}{dt}\right]\hat{r} + 6\pi\eta b\left[V_o(1 + \frac{s^2}{r^2}) \sin \theta - r\frac{d\theta}{dt}\right]\hat{\theta}, \quad \text{(B-4)}$$

where b and s are the particle and wire radii, respectively, V_o is the fluid velocity far upstream of the wire, and η is the fluid viscosity. The potential flow and Stokes drag assumptions can be satisfied concurrently provided s>>b.

The magnetization of a paramagnetic sphere immersed in a uniform field $\vec{H}_o$ is derived by Jackson (1975, p.198) in a form equivalent to the expression

$$\vec{M}_p = \chi\vec{H}_o\,(1 + \frac{\chi}{3})^{-1}, \quad \text{(B-5)}$$

where χ is the classical magnetic susceptibility, which is defined as the ratio of magnetization of a paramagnetic body to the field inside the body. The factor in parentheses in Equation (B-5) corrects for the fact that $\vec{H}_o$ is the field outside the sphere. For convenience, an effective magnetic susceptibility, χ^*, is defined as

$$\chi^* = \chi(1 + \frac{\chi}{3})^{-1}. \quad \text{(B-6)}$$

Next the particle is assumed to be small enough to be represented magnetically as a point dipole of moment $\vec{m}_p = \vec{M}_p v_p$, where v_p is the particle volume. Then from the fundamental equation for the force on a point dipole (Jackson, 1975, p.185), the force on the sphere can be expressed as

$$\vec{F}_m = \mu_o (\vec{m}_p \cdot \vec{\nabla})\vec{H}_o = \mu_o v_p \chi^* (\vec{H}_o \cdot \vec{\nabla}) \vec{H}_o. \tag{B-7}$$

In an HGMF system the field surrounding the particle at any point is determined by the uniformly applied field, H_a, and the contribution of the magnetized wire. The determination of the field surrounding a ferromagnetic cylinder immersed in a uniformly applied background field is a classical magnetostatic problem that has been solved in several theoretical developments (e.g. Lawson, et al., 1977). For the geometry shown in Figure B-2 the result is

$$\vec{H}_o = \left[\frac{s^2 M_w}{2r^2} \cos\theta + H_a \cos\theta \right] \hat{r} + \left[\frac{s^2 M_w}{2r^2} \sin\theta - H_a \sin\theta \right] \hat{\theta}. \tag{B-8}$$

Substituting Equation (B-8) into (B-7) and performing the indicated mathematical operations leads to

$$\vec{F}_m = \left[- \frac{\mu_o v_p \chi^* s^2 M_w}{r^3} \left(\frac{s^2 M_w}{2r^2} + H_a \cos 2\theta \right) \right] \hat{r} + \left[- \frac{\mu_o v_p \chi^* s^2 M_w H_a \sin 2\theta}{r^3} \right] \hat{\theta}. \tag{B-9}$$

Equations (B-2), (B-3), (B-4), and (B-9) can now be substituted into Equation (B-1). To simplify the result it is helpful to introduce one physical identity and several dimensionless quantities.

$$w = 4\pi b^3 \rho_p / 3, \tag{B-10}$$

$$R = r/s, \tag{B-11}$$

$$\tau = tV_o/s, \tag{B-12}$$

$$W = \frac{\mu_o \chi^* H_a^2}{\rho_p V_o^2}, \tag{B-13}$$

$$A = \frac{M_w}{2H_a}, \tag{B-14}$$

$$K = \frac{2b^2 \rho_p V_o}{9s\eta}, \tag{B-15}$$

$$G = \frac{sg}{V_o^2}\left(1 - \frac{\rho_f}{\rho_p}\right). \tag{B-16}$$

When these substitutions are made and Equation (B-1) is simplified, the r-component becomes

$$\frac{d^2R}{d\tau^2} - R\left(\frac{d\theta}{d\tau}\right)^2 = G\cos\theta - \frac{1}{K}\left[\left(1 - \frac{1}{R^2}\right)\cos\theta + \frac{dR}{d\tau}\right] - \frac{2WA}{r^3}\left(\frac{A}{R^2} + \cos 2\theta\right). \tag{B-17}$$

The θ-component is

$$R\frac{d^2\theta}{d\tau^2} + 2\frac{dR}{d\tau}\frac{d\theta}{d\tau} = -G\sin\theta + \frac{1}{K}\left[\left(1 + \frac{1}{R^2}\right)\sin\theta - R\frac{d\theta}{d\tau}\right] - \frac{2WA}{R^3}\sin 2\theta. \tag{B-18}$$

Two new dependent variables, $\Gamma = dR/d\tau$, and $\Omega = d\theta/d\tau$ are defined and substituted into Equations (B-17) and (B-18), with the results

$$\frac{d\Gamma}{d\tau} = R\Omega^2 + G\cos\theta - \frac{1}{K}\left[\left(1 - \frac{1}{R^2}\right)\cos\theta + \Gamma\right] - \frac{2WA}{R^3}\left[\frac{A}{R^2} + \cos 2\theta\right], \tag{B-19}$$

$$\frac{d\Omega}{d\tau} = -\frac{2\Gamma\Omega}{R} - \frac{G}{R}\sin\theta + \frac{1}{KR}\left[\left(1 + \frac{1}{R^2}\right)\sin\theta - R\Omega\right] - \frac{2WA}{R^4}\sin 2\theta. \tag{B-20}$$

Equations (B-19) and (B-20) and the definitions of Γ and Ω form a set of four first-order differential equations that can be solved numerically with the initial conditions

$$R_i = (X_i^2 + Y_i^2)^{1/2}, \tag{B-21}$$

$$\theta_i = \tan^{-1} \left(\frac{Y_i}{X_i}\right) , \tag{B-22}$$

$$\Gamma_i = \frac{X_i}{R_i} (KG - 1) , \tag{B-23}$$

$$\Omega_i = \frac{Y_i}{R_i} (1 - KG) . \tag{B-24}$$

The initial dimensionless velocities, Γ_i and Ω_i, may be obtained from a simplified form of Equation (B-1), which assumes that the steady-state particle motion far upstream from the wire is parallel to the x-axis and is determined solely by drag and gravitational forces. Equations (B-21) and (B-22) simply state the initial position of the particle at $\tau = 0$.

Specification of the initial coordinates (X_i, Y_i) and the four dimensionless parameters, W, K, G, and A provides information sufficient to determine a unique particle trajectory. Calculations for the experimental conditions used in this work showed that three of the parameters fell within the following ranges:

$$W : \quad 0 \quad - \quad 1$$

$$K : \quad 0.05 - 250$$

$$G : \quad < 2 \times 10^{-5}.$$

The fourth dimensionless parameter $A = M_w/(2H_a)$, is a measure of the relative magnitudes of the magnetic field induced in the ferromagnetic wire and the applied field. A is referred to as the near-field parameter because its effect on particle trajectory is significant only near the wire. The wire magnetization, M_w, increases with applied field until the filter is magnetically saturated. Ferritic stainless steels,

the most common materials used as HGMF filters, have saturation magnetizations ranging from 1.17×10^6 to 1.27×10^6 ampere turns per meter (Lyman, 1961). Kolm (1975) and Clarkson, et al., (1976) report that magnetic saturation of a steel wool filter occurs at an applied field of 5.6×10^5 to 6.4×10^5 ampere turns per meter, which yields a value of A ($= M_w/2H_a$) ≈ 1 at the saturation condition. With higher applied fields, M_w is constant at the saturation value and the value of A decreases.

Below saturation the magnetization of individual wires in a filter is dependent on the shape of the wires, on their orientation with respect to the applied field, and on the proximity of neighboring wires. To determine an average or characteristic value of A for a filter under these conditions, one can revert back to the analysis of Lawson, et al., (1977). The magnetization of a linear, homogeneous wire is given by

$$M_w = [(\mu - \mu_o)/\mu_o] H_{in} , \tag{B-25}$$

where μ is the magnetic permeability of the wire. The interior field of a cylindrical wire magnetized perpendicular to its axis, H_{in}, is given in terms of the applied field by

$$H_{in} = 2H_a\mu_o/(\mu + \mu_o) \tag{B-26}$$

Combining Equations (B-25) and (B-26) leads to

$$M_w = 2H_a\left(\frac{\mu - \mu_o}{\mu + \mu_o}\right) \tag{B-27}$$

In a ferromagnetic material μ is actually not constant but is dependent on the applied field and the magnetization history of the material. However, below saturation $\mu >> \mu_o$, which simplifies Equation (B-27) to $M_w = 2H_a$ or A = 1 for the idealized cylindrical wire. This result conveniently matches the experimental saturation condition with no discontinuity.

A Fortran subroutine, HPCG (IBM, 1970), which is based on Hamming's modified predictor-corrector method, was used to solve the model equations. Preliminary computer solutions showed that trajectories calculated with $G = 2 \times 10^{-5}$ were indistinguishable from the corresponding $G = 0$ trajectories, so gravitational effects were subsequently ignored. Figure B-3 shows a contour map of the dimensionless collision radius, $Y_c = y_c/s$ (see Figure B-1), as a function of W and K with $A = 1$ and $G = 0$. It is interesting to note that the contours for $Y_c < 1$ asymptotically approach vertical lines at low values of W as the magnetic attraction becomes insignificant. Solutions were obtained with $W = 0$, corresponding to no applied field, and the results were identical to those obtained by Langmuir and Blodgett for conventional inertial impaction in potential flow (Fuchs, 1964).

The single-wire results may be extended to a filter by considering a filter element of differential length dx and cross-sectional area S. A single wire of length h and radius s removes particles for an area normal to the direction of flow equal to $2hsY_c$. The volume of the differential element is Sdx, so the volume of wire is FSdx, where F is the volumetric fraction of wire in the element. The total length of wire in the element is $FSdx/\pi s^2$, and the number of segments of length h is $FSdx/\pi s^2 h$. In a randomly packed filter, the fraction of total wire length that projects on a plane perpendicular to flow, and is thus active in particle collection, is $2/\pi$. A mass balance is then formulated in a manner analogous to a plug-flow reactor analysis. For a filter of length L, the collection efficiency, E, is calculated to be

$$E = 1 - \frac{c_L}{c_0} = 1 - \exp\left[-\frac{4FLY_c}{\pi^2 s\,(1-F)^2}\right], \qquad \text{(B-28)}$$

where c_0 and c_L are the particle concentrations at the entrance and exit of the filter, respectively. Equation (B-28) implicitly assumes that there is no aerodynamic or magnetic interference between collecting wires and that every particle that collides with a wire adheres.

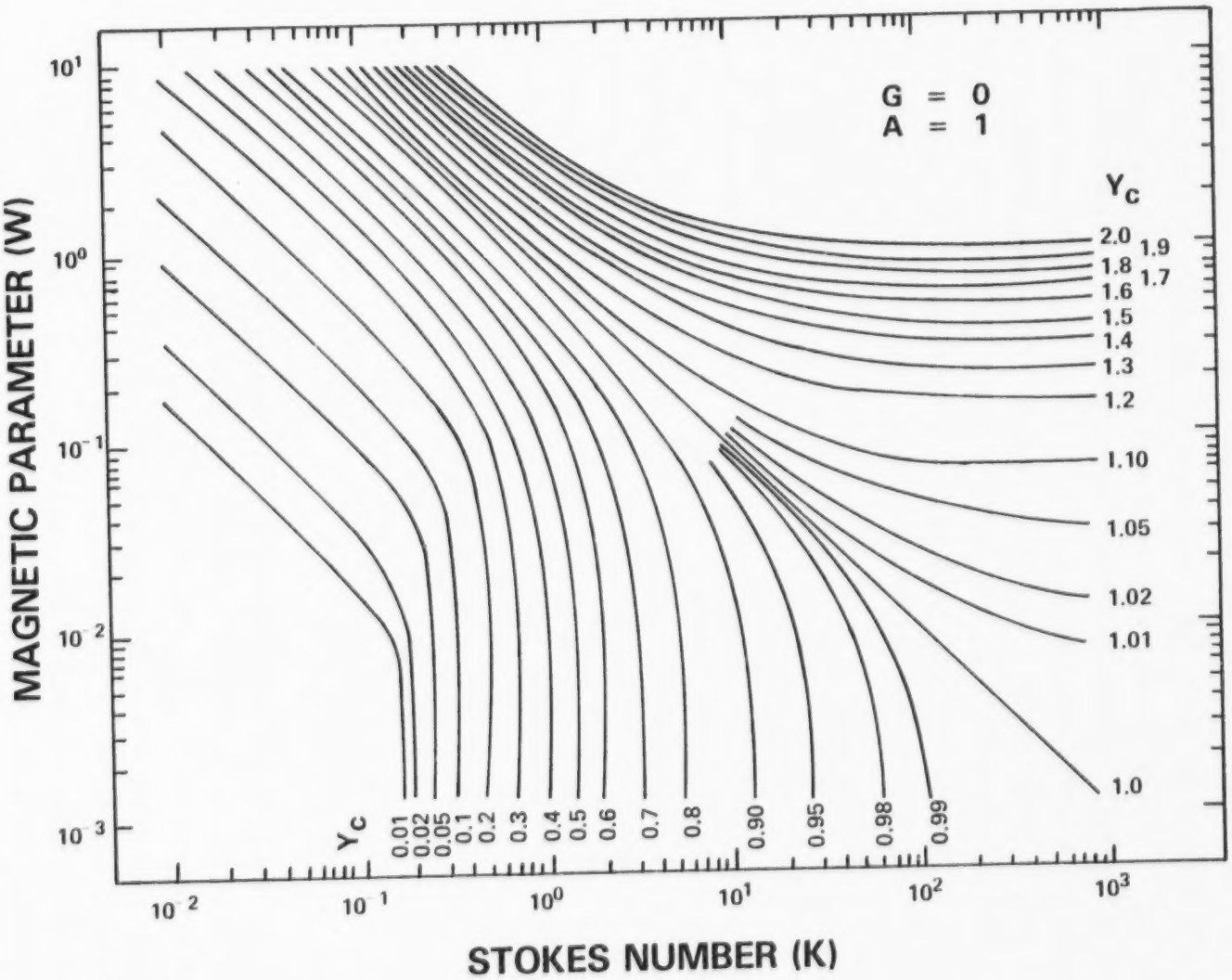

Figure B-3. Contour map of collision radius as a function of W and K (A=1, G=0).

Data from the experiments were first compared to predictions of the theoretical model as it is expressed in Equation (B-28). A typical result is shown in Figure B-4. The data and uncorrected theory agree well at small particle sizes, but the model overestimates the collection efficiency of larger particles. A reasonable explanation for the discrepancy is that larger particles may not always adhere when they strike a collecting wire. Other researchers have observed this reentrainment phenomenon in conventional fibrous filters and attributed it to a bounce mechanism or to the effect of fluid drag on the collected particles (Gillespie, 1955; Loeffler, 1974; Stenhouse and Freshwater, 1976). Both reentrainment mechanisms were considered in the subsequent analysis.

To analyze the bounce phenomenon, the physical situation illustrated in Figure B-5 was considered. To simplify the mathematics, the particle is assumed to be moving radially toward the center of the wire at the free stream velocity V_o at the instant of collision. Trajectory calculations showed this assumption to be reasonable for larger particles at moderate to high magnetic fields.

If the kinetic energy of the particle is not completely dissipated at the instant of collision, the particle rebounds radially outward from the wire with a velocity that depends on the coefficient of restitution. The rebound kinetic energy, E_{kb}, can be compared to the energy required to overcome the van der Waals attraction, E_a, plus the energy required to escape the magnetic field, E_m, to determine whether the particle will be reentrained. The residual kinetic energy, E_{kr}, is given by

$$E_{kr} = E_{kb} + E_a + E_m \qquad \text{(B-29)}$$

The model analysis consists of writing an expression for E_{kb} in terms of the coefficient of restitution of the particle; writing a van der Waals force expression for a sphere leaving the surface of a cylinder to obtain E_a, and integrating the radial component of the magnetic force $\vec{F}_m$ (from Equation (B-9) from $r = s$ to $r \to \infty$ to calculate E_m. The resulting expression for the resideual kinetic energy, E_{kr}, is set equal to zero to determine the critical value of θ (see Figure B-5) above which the impacting particle is reentrained.

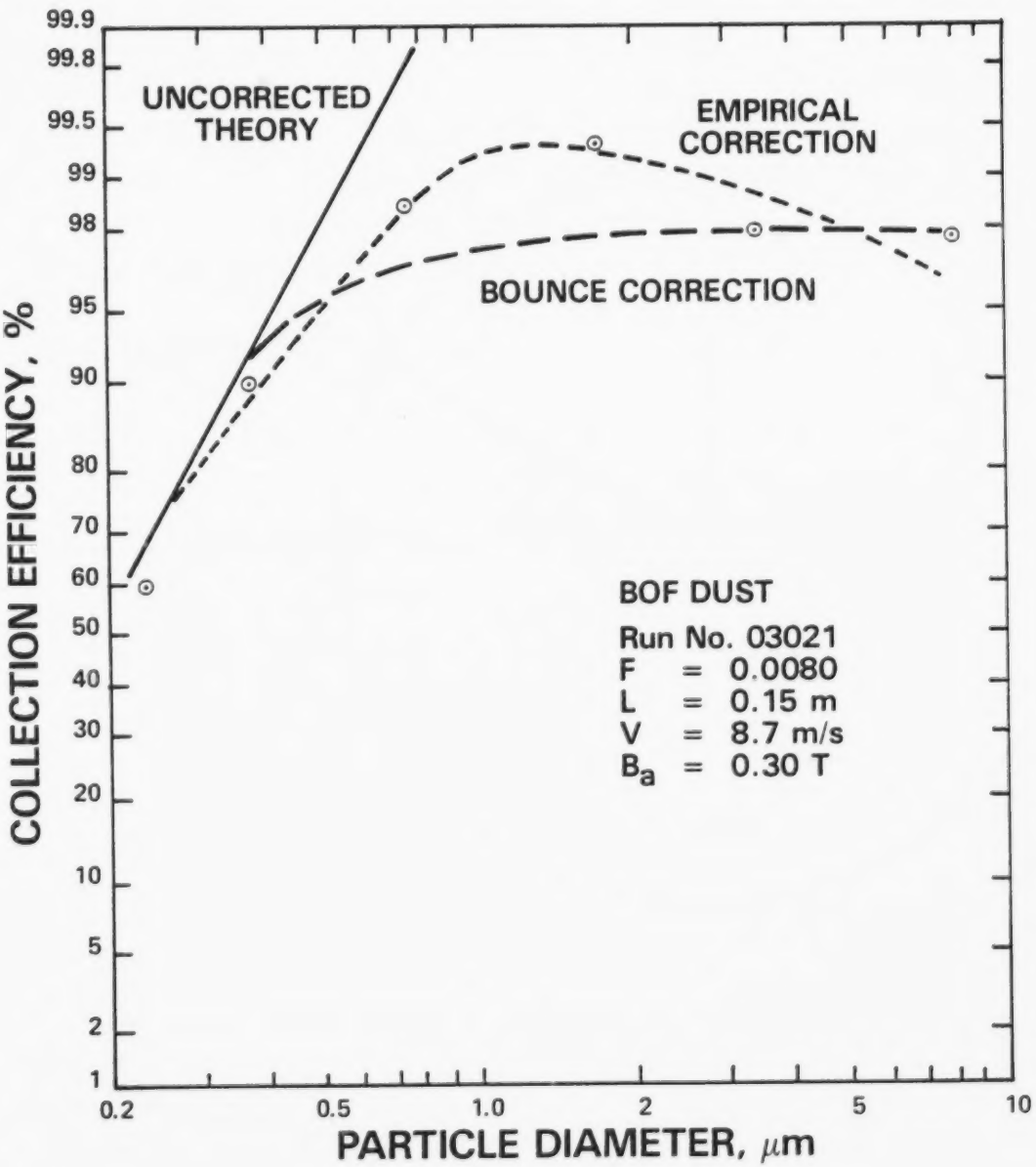

Figure B-4. Comparison of experimental data to the uncorrected theoretical prediction and to two corrected models.

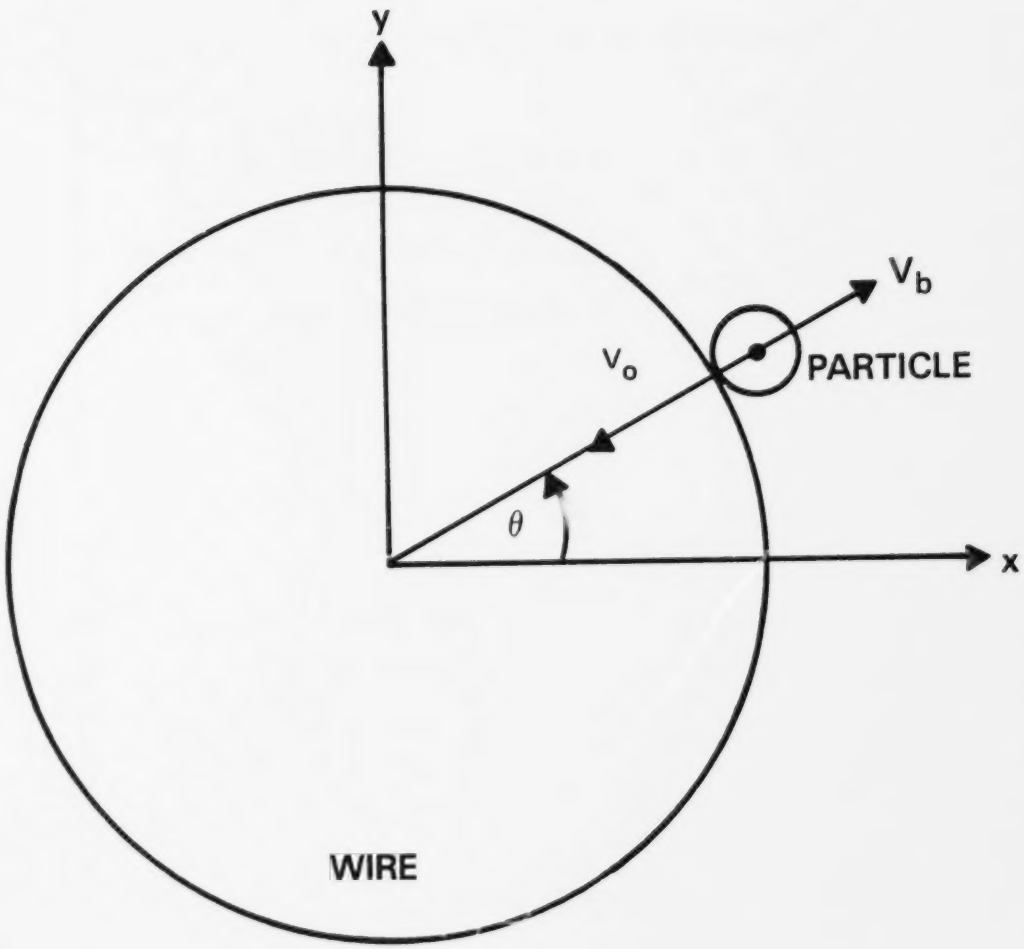

Figure B-5. Illustration of the particle bounce reentrainment model.

Details of this derivation are given by Gooding (1979). The final expression for the critical approach angle is

$$\theta_c = 1/2 \cos^{-1}\left[\frac{1}{2 \mu_o \chi^* H_a^2}\left(e^2 \rho_p V_o^2 - \frac{U}{4\pi \ell b^2}\right) - 0.5\right] . \qquad \text{(B-30)}$$

The parameters e (the particle coefficient of restitution) and U/ℓ (a quantity related to the magnitude of the van der Waals force between the particle and the wire) cannot be predicted from first principles, but may be treated as adjustable parameters within certain bounds.

A reentrainment correction to the collision radius, Y_c, may be derived in terms of θ_c. Trajectory calculations of the type that led to the construction of Figure B-3 show that the collision points are more or less equally distributed with respect to sin θ (y of Figure B-2). Thus, of the total number of collisions, only the fraction sin θ_c results in particle collection. The corrected form of Equation (B-28) then becomes

$$E = 1 - \exp\left[-\frac{4FLY_c \sin\theta_c}{\pi^2 s (1-F)^2}\right] . \qquad \text{(B-31)}$$

Analysis of the experimental data showed that Equation (B-31) could provide an acceptable correlation for isolated cases such as that illustrated by the "bounce correction" curve shown in Figure B-4; but over a broader spectrum of operating conditions, the correction proved to be too severe with respect to particle size and gas velocity. Values of the adjustable parameters that gave suitable results for low-field, high-velocity data provided almost no correction to the higher-field, lower-velocity data. Conversely, parameters fitted to the higher field data would indicate total reentrainment of larger particles at higher velocities and lower fields.

In an alternative approach that proved to be unproductive, the reentrainment phenomenon was analyzed via a force balance written for a particle that was assumed to have collided with and momentarily adhered to the wire. One can postulate that the drag force acting on a particle at the surface of the wire would tend to reentrain the particle in the gas stream. The drag force is proportional to particle radius if Stokes' Law applies, or to the radius squared at higher particle Reynolds numbers. As Equation (B-9) indicates, however, the opposing magnetic force is proportional to particle volume, or radius cubed. Hence, reentrainment caused by fluid drag would tend to diminish at larger particle sizes, rather than increasing in the manner indicated by the discrepancy between uncorrected theory and data in Figure B-4.

Since neither the bounce model nor the force-balance model could adequately predict the experimental results, an empirical reentrainment correlation was developed. Equation (B-31) was inverted to calculate a reentrainment correction from each data point; i.e.

$$p = \sin \theta_c = - \frac{\pi^2 \, s \, (1-F)^2}{4FLY_c} \, \ell n(1-E) \; . \qquad \text{(B-32)}$$

The reentrainment correction was re-labeled with the generalized symbol p, signifying the probability of a particle adhering to a wire once it collides. A multiple regression analysis was then conducted to correlate p with the previously defined dimensionless groups W and K. The results are given in Table B-1. The correlations were improved somewhat by subdividing the data into the groups indicated. For the EAF dust the exponent on W is not significantly different from zero, implying that the applied magnetic field has little effect on reentrainment. The probability of reentrainment is also higher for EAF dust than for BOF dust under equivalent conditions. The EAF data may have been biased toward lower collection efficiencies by a failure to maintain clean wire conditions throughout the impactor sampling period as indicated earlier in Figure 6.

Table B-1. Correlation of reentrainment correction.

Data	No. Data Points	Correlation	Regression Coefficient
BOF dust field-on	267	$p = 0.789 \frac{W^{0.087}}{K^{0.190}}$	0.727
BOF dust field-off	61	$p = 0.534\ K^{-0.317}$	0.669
EAF dust field-on	52	$p = 0.406 \frac{W^{0.013}}{K^{0.122}}$	0.634

The degree to which the empirically corrected model fits experimental collection data is illustrated in Figure B-4 and in Figure 7, which was presented earlier in the text. The confidence intervals in Figure 7 were calculated by first transforming the efficiency data to $\ln(1-E)$ to equalize the weight of high and low-efficiency points, and then pooling the variances calculated at the six particle sizes to get a single estimate of variance with 12 degrees of freedom. Several other fitted-data plots are presented by Gooding (1979).

The inclusion of inertial terms in the theoretical model gives gas velocity a complicated role. Referring to Equations (B-13) and (B-15), velocity appears as a squared term in the denominator of W and as a linear term in the numerator of K. Hence starting from any point on Figure B-3, an increase in velocity involves moving two units down and one unit to the right. Normally this leads to a reduction in the collision radius, Y_c, since the slope of the constant Y_c curves is between - 1 and 0 over most of the contour plot. However, in the lower left portion of the plot, an increase in Y_c can result from an increase in velocity, since the slope of the curves is less than -2. In physical terms, increasing velocity, which increases particle inertia, tends to

keep a particle moving in a straight line. If the particle is approaching in the shadow of the wire, it is more likely to collide with the wire at a higher velocity. Conversely, if it approaches from outside the projected area of the wire, it is more likely to be swept past the wire at a higher velocity. Therefore, increasing velocity increases Y_c only if $Y_c < 1$ and if inertia has a more significant effect than magnetic attraction. This combination of events is most likely to occur with weakly magnetic, submicron particles.

The effect of velocity is confounded further by the fact that the probability of reentrainment, p, is also dependent on velocity. Increasing velocity always reduces p, so the conditions under which higher velocity is beneficial are limited even more. The final result is that collection efficiency is reduced by increasing the superficial gas velocity in nearly all cases of practical interest. The magnitude of the velocity effect is illustrated in Figure 12, presented earlier in the text.